# *Active control of noise transmitted from barriers*

**Shahin Sohrabi**


# Active control of noise transmitted from barriers

by

Shahin Sohrabi

directed by

Teresa Pàmies Gómez

Jordi Romeu Garbí

A dissertation submitted in partial fulfillment for

the degree of Doctor by the Universitat Politècnica de Catalunya

in the

Universitat Politècnica de Catalunya (UPC)

January 10, 2022

Active control of noise transmitted from barriers

# *Abstract*

Escola Superior d'Enginyeries Industrial, Aeroespacial i Audiovisual

de Terrassa

Department of Mechanical Engineering

Doctor of Philosophy in Mechanical Engineering

by Shahin Sohrabi

An active noise cancellation is a unique approach that helps passive noise control in reducing sound levels at low frequencies; nevertheless, successful use of active noise cancellation necessitates performing numerous and tedious experiments together with defining several parameters properly. The locations and quantity of active control system transducers are among these parameters.

The present research provides a comprehensive framework for placing control sources and error microphones near a noise barrier in order to improve its efficiency in both narrowband and broadband noise spectra. To accomplish this, the appropriate locations for the control sources are first determined using a repetitive computation method, and then the optimizations are completed by determining the best position for the error microphone.

Several alternative transducer locations near the barrier are incorporated in the repetitive computation, and the optimal sites for the control sources and error microphones are found using two-step optimization methods as well as the genetic algorithms approach.

The findings reveal that the best places to put the control sources are on the incident side, below the barrier's edge, and the best locations to place the error microphones are on the shadow side, as close as possible to the target area. The effect of ground reflection on the

efficiency of the active noise control system is also investigated, and it is discovered that while ground reflection has no significant effect on the performance of the active noise control system for broadband frequency ranges, it does reduce the control system's efficiency at tonal noises.

In order to optimize more parameters, further calculations are performed based on the genetic optimizer. The output of the GA calculations found new configurations for the control units that result in higher noise level reduction at the target area.

In addition to the active noise barrier, the application of active noise cancellation for open windows as a particular case of the barrier is explored as a particular case of the barrier. Two arrangements are studied for the control units close to the open windows, including boundary and planar control arrangements. The control units in a boundary configuration are positioned on the opening's edge, while in the planar control, they are located on the opening’s surface. In a boundary configuration, the control units are placed on the opening's edge, whereas in a planar design, they are placed on the opening's surface.

The effect of several parameters such as the incident angle of noise waves, the distance between error microphones and the opening, and the number of control units are investigated. The results demonstrate that the active noise control system with planar configuration has higher performance than the boundary control. Furthermore, when the frequency and incident angle increase, the effectiveness of active noise reduction decreases.

# Acknowledgments

It is my pleasure to acknowledge the roles of several individuals who were instrumental in the completion of my Ph.D. research. First of all, I would like to express my sincere gratitude to my supervisors Prof. Teresa Pàmies Gómez and Prof. Jordi Romeu Garbí for their continuous support during my Ph.D. study and research, and for their patience, motivation, and immense knowledge. Their guidance helped me in all the time of research and writing this thesis. Muchas gracias!

Also, I would like to acknowledge the valuable input of Prof. Peter Svensson, who contributed to many discussions that helped to shape this project. Also, he gave me the opportunity to join his research group at the Norwegian University of Science and Technology (NTNU) and I learned many aspects of Acoustics from him.

I would also like to express my appreciation to all the members of the LEAM research group, especially Dr. Robert Arcos, Dr. Andreu Balastegui, and Dr. Arnau Clot. Without their valuable opinions and ideas, this research would not have been accomplished. These acknowledgments would not be complete without mentioning my colleagues: Milad, Kenny, Guiemro, Javad, Victor, Behshad, Pablo, Jay, and Salvatore. It was a great pleasure working with them and I appreciate their ideas, help, and good humor.

Special thanks to Hamid (Khosravi), Milad, Mahsa, Pouya, Sepideh, Hamidreza, Rezvan, Hamid (Ghorbani), and Neda for being real friends for me. They are my second family. Thank you for all the good time made for me, taking care of and worrying even a little bit.

Finally, I want to express my deepest gratitude to my parents and siblings. There are no words to express how grateful I feel for all your support. The goals were achieved so far because

you always believed me and motivated me to move forward. Thank you for encouraging me to follow my dreams.

# Contents

# List of Figures

# List of Tables



Therefore, the optimizations are attempted with different numbers of error microphones from $Ne = Ns$ to $Ne = Ns + 2$. The results reported in Table 4.4 show the best outcome of

*To my family*

# *Chapter 1* : *Introduction*

### 1.1. Background of the research

Noise is defined as an unpleasant sound [1] and it is recognized as one of the most problematic environmental issues in the world. The environmental noise could easily interfere with human sleep, work, and life activities and in intense conditions, the high amplitude noise may cause damage to the human auditory organs [2]. World health organization (WHO) developed guidelines to provide recommendations to protect human health against environmental noise arising from a variety of sources, including transportation (road traffic, train, and aviation) noise, wind turbine noise, and recreational noise [3]. In the last decades, many researchers studied the impact of environmental noise pollution on human health [4–8]. On the other hand, many investigations have been conducted to reduce the noise level in an area by the means of different noise control techniques. Generally speaking, the noise control techniques divide into two categories, passive and active noise control methods. In the following sections, these noise control strategies together with their applications are described.

#### 1.1.1. Passive noise control

The passive noise control technique is the effort to reduce the noise propagation by partially or completely blocking or absorbing the sound waves with noise-insulating materials such as sound-absorbing tiles [9], and noise barriers [10–12]. Passive materials achieve noise reduction either through absorption, diffusion, or reflection of sound. However, the penetration of noise depends on the density or thickness of materials and the acoustic wavelength. The passive noise control strategy is more efficient at high frequencies with short-wavelength [13].

The noise barrier which is considered as another application of passive noise control is a solution to reduce the noise level at an area behind the barrier by blocking the direct propagation of sound between source and receiver. Over the last decades, numerous studies investigated different aspects of noise barriers and their impacts on the noise cancellation behind the barrier [12,14–19]. In these investigations, the diffracted field is recognized as the most important phenomenon that should be considered when noise barriers are utilized to create an acoustic shadow region behind the barrier.

Diffraction is the ability of sound waves to bend at the edge of obstacles. Diffraction occurs when an acoustic wave encounters the edge of an object along its path [20]. The lectures provide three main theories for the diffraction, namely the Huygens–Fresnel theory, the Helmholtz–Kirchhoff theory, and the geometrical diffraction theory (GDT) to estimate the behavior of sound waves around finite and infinite obstacles [21–26], in time [27] or frequency [28] domains. These theories were established based on wave optics which have small wavelengths in comparison with the size of the obstacles. However, with the same system geometry assumptions, they can be used in acoustics [20]. In the present study for estimating the diffracted field behind a barrier the Macdonald's solution [29] will be used. This solution is the extension of Sommerfeld's approach [30] which is based on Fresnel integrals.

The previous studies show that regardless of which theory is used to estimate the edge diffraction, the amount of diffraction increases with wavelength [31], and therefore the passive barriers fail to decrease noise levels in the shadow zone when low-frequency sounds are encountered. The effectiveness of noise barriers depends on their height, length, continuity, and distance to the noise source [13]. Plenty of investigations have been conducted to design or optimize the functionality of the passive barrier by considering the

shape [32], thickness [33], and other physical parameters of the barrier [34–38]. However, these solutions may increase the project costs and above that, there are some limitations due to aesthetic, and safety reasons. On the other hand, the active noise control technique is recognized as a wide-spreading solution for the barriers which expands their application in a wider range of noise frequencies. In the next subsection, the active noise control and its applications for the noise barriers are described.

### 1.1.2. Active noise control

The main difference between passive and active noise control is that the latter achieves attenuation by introducing energy in the system or plant. This technique employs electro-acoustic or electromechanical devices to lower the noise pressure level in an acoustic primary field, based on the concept of superposition. The control system generates a noise of similar amplitude and opposite phase, which is mixed with the primary noise and result in the cancellation of both fields. The amount of noise cancellation depends on the precision of the system to create the amplitude and phase of the noise generated by the control sources. Lueg [39] in 1936 was the pioneer in the study of noise control by proposing the concept of reducing the noise level by destructive interference of acoustic waves in a duct. The concept is presented in Fig. 1.1.

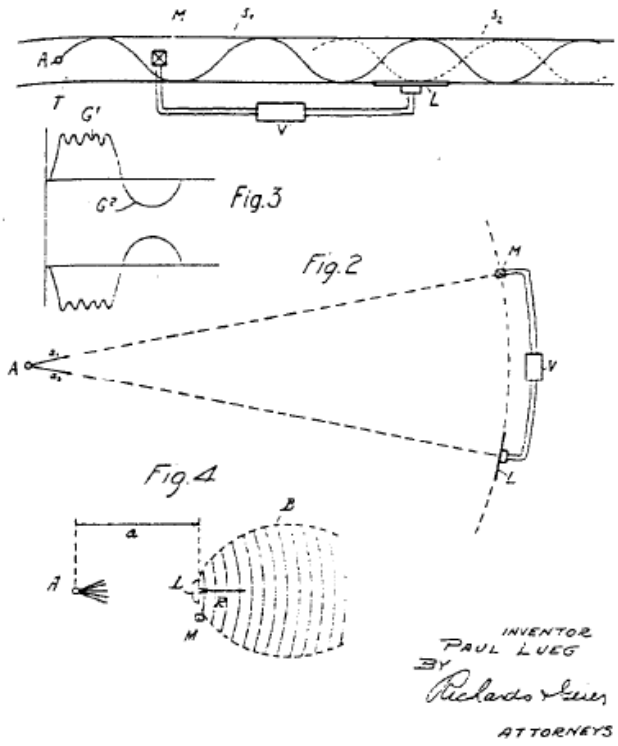


Fig. 1.1: The active noise control system proposed by Lueg [39] in a duct.

However, because of the limitation in hardware and signal processing equipment at that time more investigation was postponed until the eighties when the advancement of technology in the creation of fast digital signal processors has made active sound control a viable option for a variety of applications [40–42]. More recently, many investigations studied the applications of active noise control systems for the outdoor [43–49], and indoor [50–54] noise cancellations, and also for the transferred noises from the road [55,56] and engines [57–61].

As expressed in the previous section, passive barriers have poor performance at low frequencies. Therefore, the active noise barrier is introduced as a successful example of hybrid approaches of passive and active noise cancellations, which increase the performance of noise barriers by minimizing the diffracted waves over the top of the barrier [62]. This

reduction of diffracted noise is equivalent to a virtual increase in the effective height of the noise barrier [31]. The active noise barriers are commonly used for traffic noise [45] and construction sites [63].

Generally, two types of active noise control approaches are available: feedforward and feedback [64]. The feedforward strategy uses a coherent reference input which is sensed before it propagates past the secondary source. This signal is sent to a controller which generates the optimum signal to cancel the primary noise. Thus, the control system could change the control signal according to the changes made by the primary noise. On the other hand, in feedback control, the active noise controller attempts to cancel the primary noise without the anticipation benefit of a reference input. In general, feedforward control is more used than feedback control due to its robustness. Whatever the strategy, the unit control is usually a digital adaptive filter [8]. Those filters alter the spectral content (magnitude and phase in frequency domain) of an input signal in a specified manner and send it to the loudspeakers. The loudspeakers are electroacoustic transducers that convert electrical audio signals into corresponding sound waves. All the required signals for the unit control are collected by microphones which convert the sound waves to a small electrical current when they hit the diaphragm of the microphones. In an active noise control system, the error microphones use to create a localized zone of quiet at the physical position of these microphones by minimizing the acoustic pressure with the secondary sources [65].

In the present Thesis, the application and mechanism of noise cancellation by an active noise barrier are studied. The performance of the active noise barrier is optimized by searching the proper locations for the actuators (e.g. secondary loudspeakers and error microphones) at low-frequency noises. The “Introduction” of the following chapters provides a comprehensive history of prior investigations that are conducted on the active noise barriers.

## 1.2. Objectives

Regardless of the applications of the active noise control or the type of controller, the performance of the system plays a significant role in the implementation of the active noise control technique, specifically at the low-frequency range. The performance of the active noise barrier as a successful hybrid model of passive and active strategies has been investigated recently [37,66]. However, some issues remained uninvestigated regarding the position of the transducers and their effects on the performance of the active noise barriers.

The aim of the present thesis is to introduce a guideline for the locations for the control units around a barrier and also an aperture. The aperture can be considered a particular case of the barrier as it is a composition of four finite edge barriers. The guideline attempts to find and propose those locations of the transducers where the active control system performs more efficiently. To this end, the suitable geometric parameters of the active control units that minimized the square pressure in a target area are searched. Such purpose is accomplished by the development and implementation of a comprehensive acoustic model that makes it feasible to use the optimization based on repetitive calculations and the genetic algorithms (GAs) optimizers. As a result, the following objectives are proposed:

- Development of an acoustic model for an infinite barrier and then implement the active noise control system to improve its performance. Such implementations must consider not only the achieved reduction at the target area but also the feasibility of the installation of control units in a real application.

- Defining the suitable regions for the installation of control sources and error microphones around the barrier. The active noise barrier should perform more efficiently when the transducers are placed in these regions.
- Exploring the mechanism of noise cancelation for those transducers that are located in suitable regions. These analyses may help to introduce a general rule for the placement of transducers.
- Investigating the influence of different parameters such as frequency range on the optimization outputs.
- Finding the optimal values for those parameters that affect the performance of the active noise barrier. In order to accomplish this objective, the parameters could optimize by optimization algorithms such as Genetic Algorithms. The general rule that is proposed by studying the cancellation mechanism could help to limit the upper and lower boundaries of the parameters which consequently reduces the calculation efforts.
- Finding a suitable arrangement for the transducers of an active noise control system close to an open window. For this objective, the extra attenuation obtained by different arrangements should be investigated.

### 1.3. Outline and development of the Thesis

The content of the present thesis is divided into six chapters. All chapters except Chapter 1 and Chapter 6, Introduction and Conclusion, and further work, respectively include their state of the art within the introduction. The chapters of the thesis are organized as follows:

- Chapter 1 presents a general background of the research and introduces passive and active noise control as strategies to reduce the noise, together with their applications. Finally, the objectives and the outline of the thesis are defined.
- Chapter 2 proposes a strategy based on the repetitive calculation to define the suitable locations of control sources and error microphones close to the barrier to obtain the maximum reduction at a target area in the shadow zone of the barrier. Furthermore, the mechanisms of noise cancellations for different locations of active control units are described.
- Chapter 3 complements the proposed repetitive calculation in the previous chapter to determine the best locations of active control means to maximally reduce the noise level at the shadow zone of the barrier and on the façade of a tall building behind the barrier. In this chapter, the overall reduction achieved at the third-octave band from 63 Hz to 1 kHz is considered to determine the optimum locations.
- Chapter 4 introduces briefly the previous studies that were used the GA-optimizer to improve the efficiency of different applications of active noise control techniques. Then the general algorithm and different optimization approaches to enhance the performance of an active noise barrier are expressed.
- Chapter 5 shows the application of the active noise control system for an opening. First, the outputs of Macdonald's and Svensson's models for computing the diffracted waves from finite and infinite edges are compared. Then the suitable position of control sources and error microphones are defined based on the two-step approach. Finally, the performance of the proposed configuration is compared with the

conventional placement of control sources and error microphones for an active noise window.

- Finally, Chapter 6 presents the general conclusions of the study as well as the possible research lines that could be followed in the future.

# *Chapter 2 : Proper locations of transducers for an active noise barrier*

## 2.1. Introduction

The use of acoustic barriers to reduce undesired propagated noise in the shadow zone is a fairly widespread solution. However, it offers rather limited results in low-frequency ranges. During the past two decades, several studies have been carried out to improve the performance of acoustic barriers. Among those, the application of active noise control (ANC) gives appreciable results, specifically for low-frequency noise [62,67,68]. The efficiency of an active noise barrier (ANB) largely depends on the number and location of error microphones and control sources; a key factor that has been the focus of previous studies.

As the efficiency of the active noise barrier is always measured by the increase of attenuation at some receivers in the shadow zone, the best performance should be achieved when error microphones are deployed within the receiver zone [69], but in the real world, this configuration basically could be applied in reduced environments [70], because deploying error microphones throughout the shadow zone can require considerable hardware and can also interfere with the activity in that area. Moreover, great outdoor distances between control sources and the receivers could lead to a degradation in the coherence of the error and reference signals, causing a loss in performance [43]. It is therefore convenient to seek a configuration for the active noise barrier with transducers close to the barrier itself. With the aim of avoiding the diffraction of the sound waves, error microphones can be tentatively deployed at the edge of the barrier, where the diffracted waves are originated, and thus, a reduction of sound pressure at the shadow zone is expected [67]. For instance, Omoto et al. [49,71] placed the error microphones on the barrier edge, and the secondary sources were located on the same side as the primary source, but with different angles and radii to the top edge. Their results revealed that the distance between error microphones should be less than

half of the wavelength to achieve a noticeable attenuation. Guo et al. [72] studied a similar configuration and concluded that the optimal distance between secondary sources and error microphones depends on the distance between error microphones and the frequency, as it does for free field cancellation [73].

For a quite similar configuration, Borchi et al. [46] found that the lower the distance between secondary sources and error microphones, the poorer is the attenuation achieved. Fan et al. [67] investigated quite similar configurations of transducers but for a T-shaped barrier by locating the secondary sources in the incident region (on and off the path between the primary source and the edge of the barrier) and on the first edge of the T-shaped barrier. The error microphones were deployed on the first and second edge and in the shadow zone, close to the top. The best results are achieved when the error microphones were on the first edge and the secondary sources were in the incident region.

The diffracted wave can also be tentatively canceled when secondary sources instead of error microphones are placed on the edge of the barrier. Niu et al. [74] carried out an investigation placing the secondary sources on the top of the edge instead and explored the efficiency of the active noise barrier for three different arrangements of error microphones placed near the edge. Their observations showed that better results are achieved when the error microphones were placed above the secondary sources and that attenuation depends on the distance between control sources and error microphones. Liu et al. [75] proposed an arrangement including two rows of eight control sources on the barrier's top edge, one row at the incident region and the other at the receiver region. The error microphones are placed 8 cm above the edge. Each row of the control system could work either separately or together. Their results showed that the maximum efficiency was attained when both rows of the control system were

working simultaneously, given that the row of the receiver zone was the one that gave poorer results when acting alone.

Other investigations seek configurations of transducers placed not on the edge of the barrier but near it: Han et al. [76] placed three secondary sources at the bottom of the incident side of the barrier and three error microphones at three different positions close to the edge, getting a similar performance for all three positions as a result. Hart and Lau [77] examined the performance of an active noise barrier, with three control sources and three error microphones linearly arranged above the top edge, each array normal to the other. The variable was the orientation of the array system. Their results showed that the angular orientation of the control sources and error microphones is a weak factor for acoustic pressure reduction at the shadow zone when the distance between the control sources and error microphones is less than a quarter wavelength of the primary noise.

Other alternative arrangements consider the secondary sources in the receiver zone [78,79] or include the secondary sources and error microphones vertically along with the receiver side of the barrier [80], giving these configurations generally poor results, although only one position was tested in each case. But, in general terms, the new design of secondary sources [81], practical applications [82], or theoretical studies of the cancellation mechanisms [83] place secondary sources or error microphones at the top of the barrier.

To summarise the investigations done on the active noise barriers, a very limited set of secondary sources and error microphones placed on or around the top of the barrier are used. As a result, neither an optimal design nor a general rule for good practice designing an active noise barrier has been established. However, a recent development by the authors [63], applying a two-step optimization procedure for the location of both sets of transducers close

to the barrier for a typical construction environment, showed that there is a different suitable configuration of the microphones which gives a similar cancellation at the receiver zone far from the barrier.

The objective of this chapter is to identify general criteria for the location of transducers close to the barrier, where the active control achieves its maximum ability to mitigate the primary sound field in the shadow zone. To achieve this configuration, the current study follows a computational procedure, for both narrowband and broadband noise, that calculates the reduction at the shadow zone for different candidate positions of transducers in a region close to the barrier itself and with different soil conditions and frequencies.

## 2.2. Theory

### 2.2.1. Diffraction model

There are several methods to model the diffraction of wavefronts, but an analytical model is preferable in the case of a repetitive calculation method due to its low computational requirements. Although various analytical models have been proposed for calculating diffraction, the one developed by Macdonald [29] for general sound diffraction around a wedge due to incident spherical waves is widely used for the barrier's calculations, and it is the one that is used throughout this study.

Given one receiver, one sound source, and one semi-infinite barrier, three different regions are found depending on the relative locations of these elements, see Fig. 2.1. Those receivers that are located at Region III (incident zone) receive direct, reflected, and diffracted wavefronts from the source. The reflected wavefront disappears in Region II and only the diffracted wavefront remains in Region I or the shadow zone.

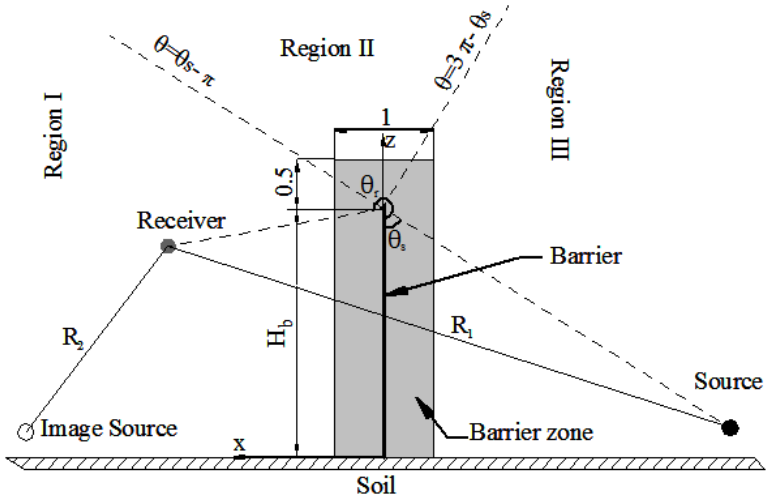


Fig. 2.1: Schematic diagram of the barrier and different regions around it.

In this study, the acoustic pressure field of diffracted wavefront ($P_D$) is calculated using Macdonald's solution, Equation 2.1, for a cylindrical coordinate system along the barrier edge.

$$P_D = \frac{k^2 \rho\, c}{4\pi} q_0 [\mathrm{sgn}(\zeta_1) \int_{|\zeta_1|}^{\infty} \frac{\mathrm{H}_1^{(1)}(kR_1 + s^2)}{\sqrt{s^2 + 2kR_1}}\, ds \qquad 2.1$$

$$+ \mathrm{sgn}(\zeta_2) \int_{|\zeta_2|}^{\infty} \frac{\mathrm{H}_1^{(1)}(kR_2 + s^2)}{\sqrt{s^2 + 2kR_2}} ds]$$

where $k$ is the acoustic wavenumber, $q_0$ [$\mathrm{m^3\ s^{-1}}$] is the source strength, and $\rho$ and $c$ are the air density and speed of sound in air, respectively. $\mathrm{H}_1^{(1)}(\,)$ is the Hankel function of the first kind, $R_1$ and $R_2$ are the distances from the source and its barrier image to the receiver, respectively, illustrated in Fig. 2.1. The second term of Equation 2.1 can be ignored for the barriers with the acoustically absorptive surface at the source's side. $s$ is the variable of the contour integral and the limits of the two contour integrals in Equation 2.1 are determined according to:

$$\zeta_1 = \mathrm{sgn}(|\theta_s - \theta_r| - \pi)\sqrt{k(R' - R_1)} \quad 2.2$$

$$\zeta_2 = \mathrm{sgn}(\theta_s + \theta_r - \pi)\sqrt{k(R' - R_2)} \quad 2.3$$

where sgn() is the sign function and $\theta_s$ and $\theta_r$ are the source and receiver angles to the barrier's face, respectively. $R'$ is the shortest path from the source to the receiver through the edge. Direct and reflection acoustic pressures are calculated as follows,

$$P_d = (-\frac{\mathrm{i}k\rho\, c}{4\pi} q_0)\frac{e^{\mathrm{i}kR_1}}{R_1} \quad 2.4$$

$$P_{ref} = (-\frac{\mathrm{i}k\rho\, c}{4\pi} q_0)\frac{e^{\mathrm{i}kR_2}}{R_2} \quad 2.5$$

The effect of the soil's reflection can be considered based on the image method [84]. Thus, the total pressure ($\boldsymbol{P_T}$) at a receiver is the superposition of all wave paths from the source to the receiver. For a receiver in the shadow zone, $\boldsymbol{P_T} = \boldsymbol{P_1} + Q_r\boldsymbol{P_2} + Q_s\boldsymbol{P_3} + Q_rQ_s\boldsymbol{P_4}$, where $\boldsymbol{P_1}$ is the diffracted wavefronts and $\boldsymbol{P_2}$, $\boldsymbol{P_3}$, and $\boldsymbol{P_4}$ refere to those diffracted pressure paths that are reflected from the ground, illustrated in Fig. 2.2. In this equation $Q_s$ and $Q_r$ are the spherical wave reflections at the source and receiver sides, respectively, and depend on the acoustical characteristic of the ground and the source/receiver geometry [85,86].

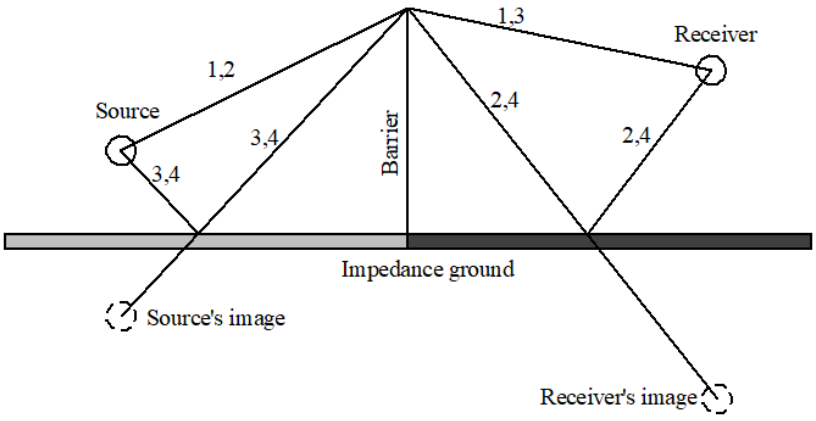


Fig. 2.2: Reflected and diffracted wave paths from a source to a receiver in the shadow zone of the barrier [14].

### 2.2.2. Active noise control for barriers

The overall objective of adding active sources to a barrier is to increase its performance in the shadow zone of the barrier. The best procedure to increase the attenuation in the shadow zone is to define a set of receivers in that area so that the active control aims to reduce the pressure in that set of receivers. However, the practical design of an active noise barrier is that both control sources and error microphones are located close to the barrier itself. In this study, the "barrier zone", shown in Fig. 2.2, is used to call the domain in which the transducers could be located close to the barrier.

The procedures of finding the suitable locations for the transducers of an active noise barrier are followed by two steps [63,87,88]: the first step is to determine the proper position of the control source that ensures the minimum acoustic pressure level at a set of receivers placed in the shadow zone. This location is selected from those candidate positions that are located inside the barrier zone. Once the position of the control source is determined, the second step is to seek the suitable position of the error microphones. It should be noted that the best position selected for the error microphones is not the one giving maximum attenuation at the error microphones, but the one which maximally minimizes the acoustic pressure at receivers in the shadow zone which is far from the location of the error microphones. With this setup, the active noise barrier thus achieves the greatest attenuation at the shadow zone

#### 2.2.2.1. Location of the secondary sources

Equation 2.6 describes the total acoustic pressure ($\boldsymbol{P}_r$) obtained at a finite number of receivers in the shadow area with respect to primary and control sources,

$$\boldsymbol{P_r} = \boldsymbol{Z}_{Pr} q_P + \boldsymbol{Z}_{sr} \boldsymbol{q}_{sr} \qquad 2.6$$

where $\boldsymbol{Z}_{Pr}$ is the vector of complex impedances for the primary source with strength $q_P$ at receiver points. $\boldsymbol{Z}_{sr}$ is an $M \times N$ impedance matrix, corresponding to $N$ control source at $M$ receiver points, and $\boldsymbol{q}_{sr}$ is the vector for secondary source strength. Equation 2.7 shows the total squared pressure at the receiver points,

$$\boldsymbol{J}_{pr} = \boldsymbol{P}_{\boldsymbol{r}}^{\boldsymbol{H}}\boldsymbol{P}_{\boldsymbol{r}} = \left|q_p\right|^2 \boldsymbol{Z}_{Pr}^{\mathrm{H}}\boldsymbol{Z}_{Pr} + q_p^{*}\boldsymbol{Z}_{Pr}^{\mathrm{H}}\boldsymbol{Z}_{sr}\boldsymbol{q}_{sr} + \boldsymbol{q}_{sr}^{\mathrm{H}}\boldsymbol{Z}_{sr}^{\mathrm{H}}\boldsymbol{Z}_{pr}q_P + \boldsymbol{q}_{sr}^{\mathrm{H}}\boldsymbol{Z}_{sr}^{\mathrm{H}}\boldsymbol{Z}_{sr}\boldsymbol{q}_{sr} \qquad 2.7$$

where the symbol H denotes the complex conjugate of the vector and matrix transpose. This equation is a quadratic function with an optimal vector for the control sources' strengths. The unique minimum value is specified by [89],

$$\boldsymbol{q}_{sr} = -(\boldsymbol{Z}_{sr}^{H}\boldsymbol{Z}_{sr})^{-1}(\boldsymbol{Z}_{sr}^{H}\boldsymbol{Z}_{pr}q_P) \qquad 2.8$$

which is the set of secondary source strengths that guarantee the maximum reduction at the receiver points for a given position of the secondary sources.

The efficiency of the active noise control system at a single tonal noise is measured by the average insertion loss, $\bar{IL}_r$, calculated at the receiver points placed at the shadow zone,

$$\bar{IL}_r = 10log_{10}\left(\frac{\sum_j^M \left|P_j^{OFF}\right|^2}{\sum_j^M \left|P_j^{ON}\right|^2}\right) \qquad 2.9$$

where $P_j^{ON} = Z_{Pj}q_P + \boldsymbol{Z}_{\boldsymbol{sj}}\boldsymbol{q}_{\boldsymbol{s}}$ is the total pressure corresponding to the primary and control sources at $j$th receiver, when the active noise cancellation is "*ON*" and $Z_{Pj}$ and $Z_{sj}$ are respectively the complex impedance matrice of the primary and control sources at the $j$th receiver. Also, $P_j^{OFF} = Z_{Pj}q_P$ is the pressure at $j$th the receiver point when the control system is "*OFF*".

In addition to Equation 2.9 which defines the average insertion loss at a single frequency, Equation 2.10 is used to compute the overall insertion loss, $IL_o$, of active noise control at broadband spectra rather than only one single frequency,

$$IL_o = 10\ log(\frac{\sum_{i=1}^{i=13}\sum_{j=1}^{M}\left|\boldsymbol{P}_{ij}^{OFF}\right|^2}{\sum_{i=1}^{i=13}\sum_{j=1}^{M}\left|\boldsymbol{P}_{ij}^{ON}\right|^2}) \quad 2.10$$

where $\boldsymbol{P}_{ij}$ is the pressure at the central frequency of the 1/3 of octave band between 63 Hz and 1 kHz, at the *j*th receiver points in the shadow zone.

In this study, the best position for the set of secondary sources within the barrier zone is the one that gives a maximum $\overline{IL}_r$ or $IL_o$, depending on whether the primary noise is narrowband or broadband, respectively.

#### 2.2.2.2. Location of the error microphones

For a compact active noise barrier, the error microphones are aimed to be placed in the barrier zone as well. The cost function is therefore not the same as the one previously used for the location of the secondary sources. $\boldsymbol{P_e}$ in Equation 2.11 describes the total pressures at the position of the error microphone.

$$\boldsymbol{P_e} = \boldsymbol{Z}_{Pe}q_P + \boldsymbol{Z}_{se}\boldsymbol{q}_{se} \quad 2.11$$

The $\boldsymbol{Z}_{Pe}$, $\boldsymbol{Z}_{se}$, and $\boldsymbol{q}_{se}$ have the same definition as described in Equation 2.6 but for the error microphones close to the barrier instead of the receivers at the shadow zone. Equation 2.12 is the vector of the control sources' strength while the squared pressure at the error microphones' position is minimized.

$$\boldsymbol{q}_{se} = -(\boldsymbol{Z}_{se}^H\boldsymbol{Z}_{se})^{-1}(\boldsymbol{Z}_{se}^H\boldsymbol{Z}_{pe}q_P) \quad 2.12$$

This is obviously a different result from that of Equation 2.6. In this case, however, the performance of the active control system is monitored through the average insertion loss at receiver points by Equation 2.9 and Equation 2.10, and the best position for the error microphones within the barrier zone is the one that gives the maximum $\overline{IL}_r$ or $IL_o$ at the receivers placed in the shadow zone, (Equation 2.10), but using $\boldsymbol{P}_j^{ON} = \boldsymbol{Z}_{Pr}q_P + \boldsymbol{Z}_{sr}\boldsymbol{q}_{se}$ .

## 2.3. Method

This study considers a thin, rigid, and infinite barrier with a practical height of $H_b = 2.5$ m between a primary source and the zone where it is intended to reduce the primary noise (see Fig. 2.3). The mass of the barrier is considered sufficient to avoid noise transmission through the barrier itself for the entire frequency range studied in this work. The barrier zone, where transducers are intended to be deployed, is a parallelepipedic volume within 0.5 m of the barrier's surfaces. This zone is intentionally selected close to the barrier to be feasible for the installation of transducers in real applications. For this study, the soil is considered to be either totally absorbent ($Q_s = Q_r = 0$), or a perfectly reflecting surface ($Q_s = Q_r = 1$).

The noise source is fixed at the point (- 7, 0, 0.3) m, with a power output of 1 W at each frequency. The frequency spectra through this study are formed by the center frequency of every 1/3 of the octave band from 63 Hz to 1 kHz. The shadow zone of the barrier is covered with 15 receiver points that are fairly distributed in a horizontal plane of $10 \times 8$ m$^2$ at a height of 1.65 m (Fig. 2.3). These points are used to calculate the average insertion loss at the shadow zone by the active noise barrier according to Equation 2.9 and Equation 2.10.

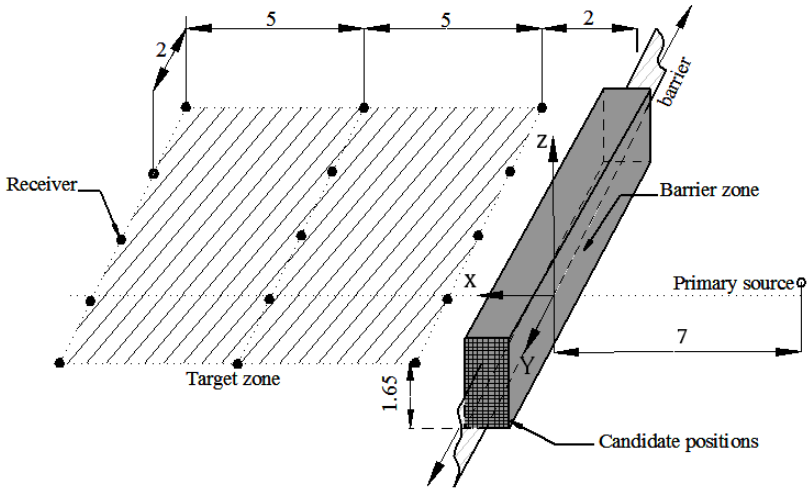


Fig. 2.3: Schematic diagram of an infinite barrier with 15 receiver points in the shadow zone. The grid of the candidate positions shows the location of pre-selected positions for the arrays of transducers. (Units are in meters)

The control sources are defined by an array of $N_s$ =10 units that are arranged linearly along the *Y*-direction and distributed symmetrically with respect to the *X*-axis. The space between adjacent control sources in the *Y*- direction is $d_s = 0.2$ m, which is close to half of the shortest wavelength at 1 kHz, the maximum distance between secondary sources. This space ensures the best performance for an array of secondary sources [90,91].

A suitable location for the control sources is found among 341 candidate positions that are located inside the barrier zone. The barrier zone is defined by a grid of candidate points with 0.1 m steps in both the *X*- and *Z*-direction, presented in Fig. 2.3. The best location of control sources is where the maximum attenuation is achieved at the shadow zone. For this purpose, the strengths of the secondary sources are calculated at all candidate positions and for each 1/3 of the octave band, using Equation 2.9.

Once the best location of the secondary sources is identified, attenuation at the receivers in the shadow zone is attempted by using a set of error microphones. For this purpose, an array of error microphones is arranged linearly along the *Y*-direction. The error microphones are

distributed symmetrically with respect to the *X*-axis and with the interval of $d_e = 0.2$ m between them. This distance is close to half of the shortest wavelength and ensures the best performance in terms of attenuation at the shadow zone [71,90]. The quantity of error microphones is $N_e = 41$ to cover the width of the receivers' area in the shadow zone in the *Y*-direction.

With the control sources fixed at the best position of each frequency, the strength of the control sources is calculated to minimize the squared pressure at the error microphones in all candidate positions inside the barrier zone. The position that gives the maximum attenuation at the receivers in the shadow zone, calculated by Equation 2.9, should provide the best configuration of control sources and error microphones within the barrier zone. This two-step approach is repeated for the overall spectra to define the appropriate configuration of all desired frequency range.

## 2.4. Results

### 2.4.1. Location of the secondary sources

Table 2.1 presents the best locations of the control sources and their corresponding active control attenuations calculated by Equation 2.9. This table also shows the noise level reduction achieved by the passive barrier at each frequency, which is the difference of the average pressure level at receiver positions with and without the barrier.

Table 2.1: $\overline{IL}_r$ [dB] at the best positions of control sources, at different frequencies.

| | Absorbent soil | | | Hard soil | | |
|---|---|---|---|---|---|---|
| Freq. [Hz] | $(X_S, Z_S)$ [m] | $\overline{IL}_r$ [dB] | $\overline{IL}_{passive}$ [dB] | $(X_S, Z_S)$ [m] | $\overline{IL}_r$ [dB] | $\overline{IL}_{passive}$ [dB] |
| 63 | (0.5, 2.3) | 31.7 | 7.7 | (-0.5, 1.0) | 28.3 | 8.4 |
| 80 | (-0.1, 0) | 38.2 | 8.3 | (0.1, 0.6) | 34.1 | 9.4 |
| 100 | (-0.2, 0.2) | 34.5 | 8.9 | (-0.1, 0) | 29.1 | 8.9 |

Table 2.1 (continue): $\overline{IL}_r$ [dB] at the best positions of control sources, at different frequencies.

| | Absorbent soil | | | Hard soil | | |
|---|---|---|---|---|---|---|
| Freq. [Hz] | $(X_S, Z_S)$ [m] | $\overline{IL}_r$ [dB] | $\overline{IL}_{passive}$ [dB] | $(X_S, Z_S)$ [m] | $\overline{IL}_r$ [dB] | $\overline{IL}_{passive}$ [dB] |
| 125 | (-0.3, 0.1) | 33.2 | 9.6 | (-0.5, 2.2) | 28.4 | 8.4 |
| 160 | (-0.5, 0.4) | 33.5 | 10.4 | (-0.5, 1.7) | 26.2 | 9.8 |
| 200 | (-0.4, 0) | 37.3 | 11.1 | (-0.5, 2.4) | 22.4 | 15.2 |
| 250 | (-0.5, 0) | 32.1 | 11.9 | (-0.5, 1.1) | 23.6 | 12.1 |
| 315 | (-0.5, 0) | 26.2 | 12.7 | (0.5, 2.2) | 23.9 | 12.5 |
| 400 | (-0.5, 0) | 22.3 | 13.6 | (-0.5, 2.5) | 19.7 | 14.6 |
| 500 | (-0.5, 2.7) | 19.8 | 14.4 | (-0.5, 2.2) | 15.1 | 20.0 |
| 630 | (-0.5, 0.9) | 15.7 | 15.4 | (-0.5, 0.2) | 14.7 | 21.6 |
| 800 | (-0.5, 0.5) | 11.7 | 16.4 | (-0.2, 2.7) | 16.1 | 34.1 |
| 1000 | (-0.5, 2.1) | 11.7 | 17.4 | (-0.5, 1.8) | 10.6 | 24.1 |
| Overall | (-0.5, 0) | $(IL_o)$ 21.6 | 11.2 | (-0.5, 1.8) | $(IL_o)$21.3 | 11.4 |

Those positions in Table 2.1 are the best locations for the array of control sources at each frequency and overall spectra. However, there are probably more suitable locations that get comparable attenuations in the shadow zone. In order to seek these locations, Fig. 2.4 represents the average insertion loss at the receivers in the shadow zone ($\overline{IL}_r$) for all 341 candidate positions of the control source by color maps for 63, 125, 250, 500, and 1000 [Hz], and also the overall position calculated by Equation 2.10 for both types of soil.

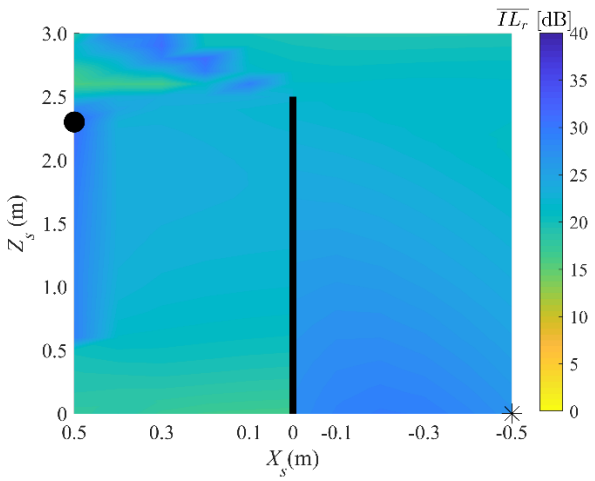


(a-i)

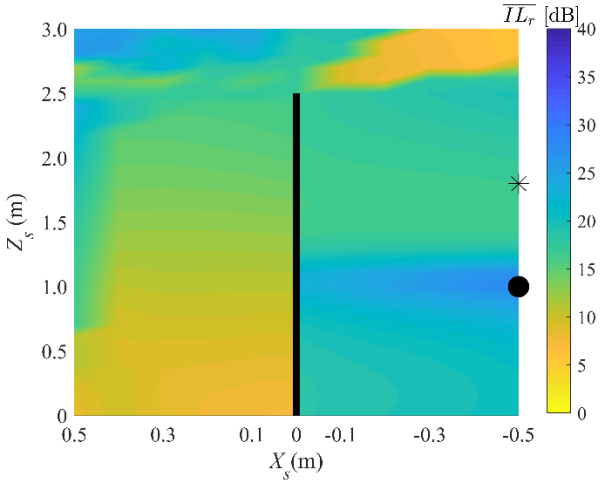


(a-ii)

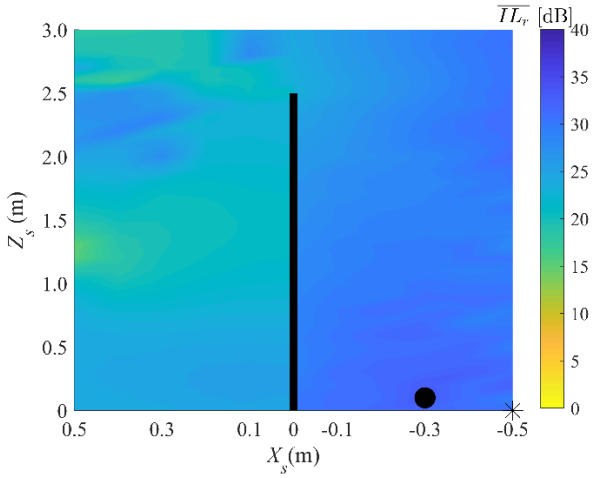


(b-i)

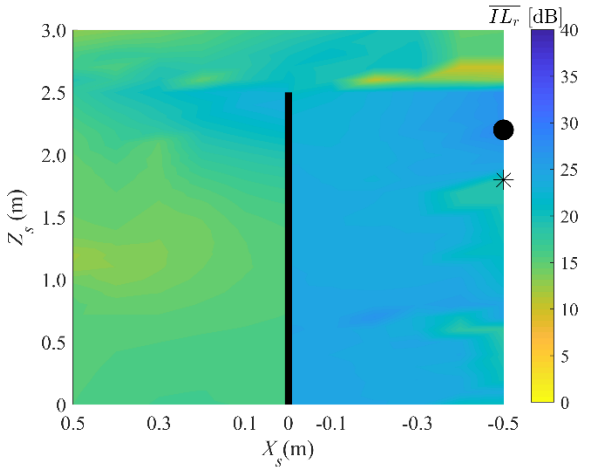


(b-ii)

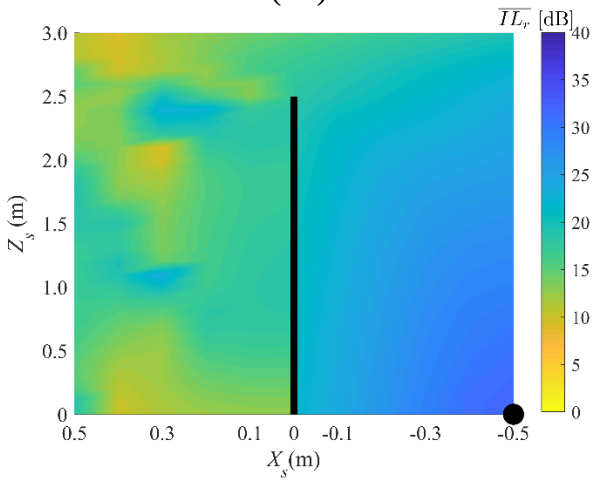


(c-i)

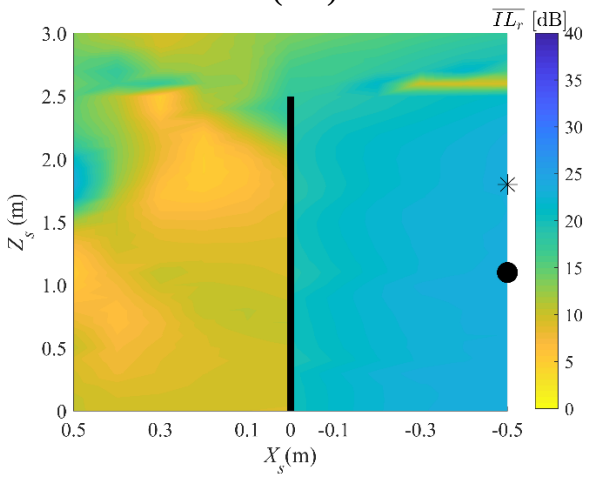


(c-ii)

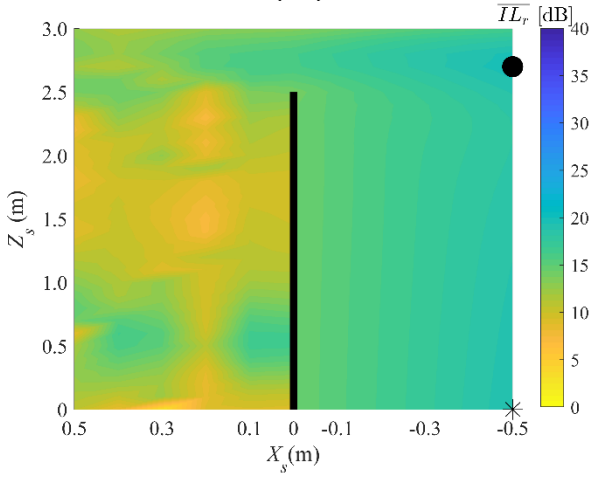


(d-i)

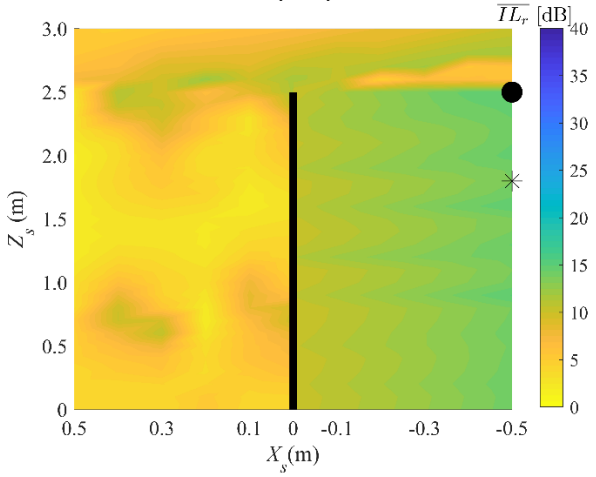


(d-ii)

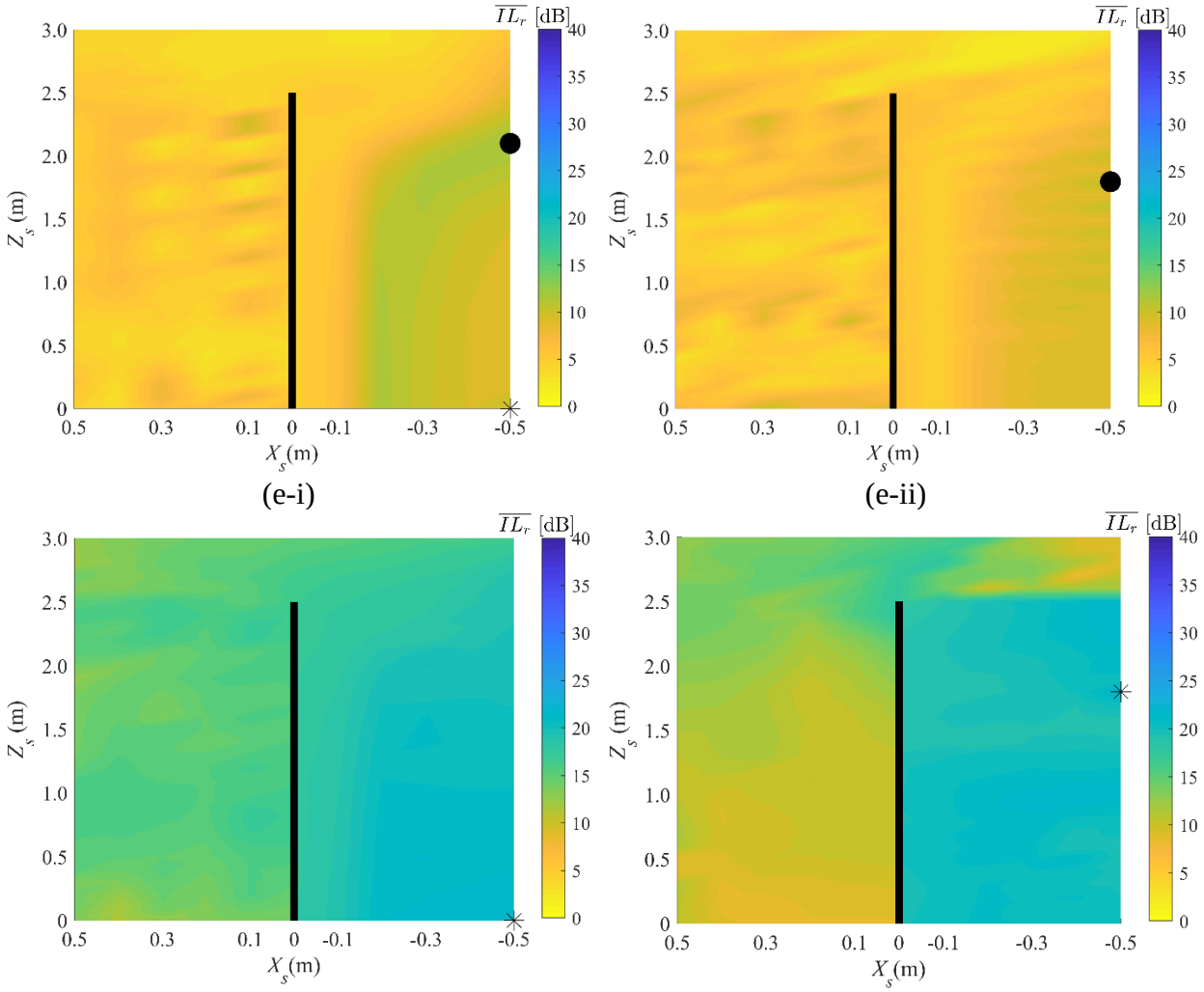


Fig. 2.4: $\overline{IL_r}$ [dB] of all candidate positions of the control sources. (i): absorbent soil, (ii): hard soil. The barrier is represented by a black bar in the middle. ● is the best position of the control sources. (a): 63 Hz, (b): 125 Hz, (c): 250 Hz, (d): 500 Hz, (e): 1 kHz, (f) overall, and * is the overall position of the control sources.

### 2.4.2. Location of the error microphones

Table 2.2 defines the best locations for error microphones among all 341 candidate positions when the control sources are located at the positions presented in Table 2.1. The error microphones at these positions achieve the maximum attenuation at the shadow zone.

Table 2.2: $\overline{IL}_r$ [dB] at the best positions of error microphones with secondary sources at the positions presented in Table 2.1.

| | Absorbent soil | | | Hard soil | | |
|---|---|---|---|---|---|---|
| Freq. [Hz] | $(X_e, Z_e)$ [m] | $\overline{IL}_r$ [dB] | $\overline{IL}_{passive}$ [dB] | $(X_e, Z_e)$ [dB] | $\overline{IL}_r$ [dB] | $\overline{IL}_{passive}$ [dB] |
| 63 | (0.5, 1.5) | 5.9 | 7.7 | (0.5, 2.7) | 14.9 | 8.4 |
| 80 | (0.5, 1.2) | 15.3 | 8.3 | (0.5, 0.8) | 9.7 | 9.4 |
| 100 | (0.5, 1.9) | 13.9 | 8.9 | (0.2, 0.9) | 13.6 | 8.9 |
| 125 | (0.5, 2.1) | 14.1 | 9.6 | (0.5, 0.4) | 18.8 | 8.4 |
| 160 | (0.5, 2.2) | 13.5 | 10.4 | (0.5, 0.1) | 15.4 | 9.8 |
| 200 | (0.5, 2.1) | 13.3 | 11.1 | (0.5, 0.4) | 8.2 | 15.2 |
| 250 | (0.5, 2.3) | 12.6 | 11.9 | (0.4, 2.0) | 7.1 | 12.1 |
| 315 | (0.5, 2.2) | 11.9 | 12.7 | (0.1, 2.5) | 2.5 | 12.5 |
| 400 | (0.5, 2.2) | 9.0 | 13.6 | (0.3, 0.2) | 4.8 | 14.6 |
| 500 | (0.5, 0.5) | 2.7 | 14.4 | (0.5, 0.7) | 4.5 | 20.0 |
| 630 | (0.1, 0) | 3.6 | 15.4 | (0.5, 1.8) | 3.4 | 21.6 |
| 800 | (0.5, 2.4) | 3.3 | 16.4 | (0.2, 2.8) | 1.6 | 34.1 |
| 1000 | (0.4, 2.5) | 2.5 | 17.4 | (0.2, 2.5) | 3.8 | 24.1 |
| Overall | (0.5, 2.0) | $(IL_o)$ 9.1 | 11.0 | (0.4, 0.2) | $(IL_o)$ 9.3 | 11.4 |

Fig. 2.5 shows the achieved attenuation at the shadow zone when error microphones are located in all 341 candidate positions in the barrier zone. The control sources are placed in the best positions given in Table 2.1.

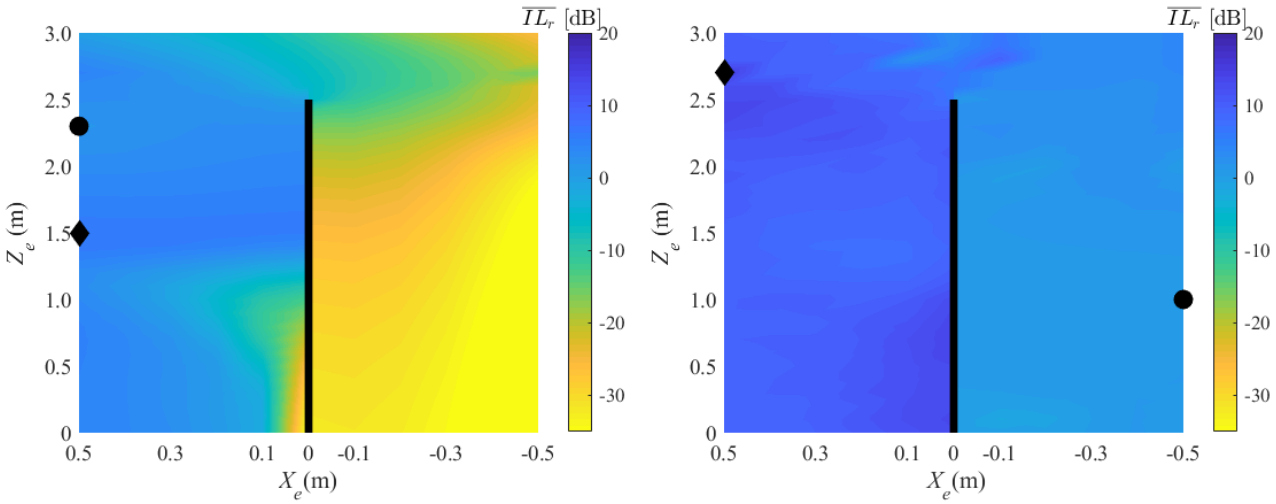


(a-i) (a-ii)

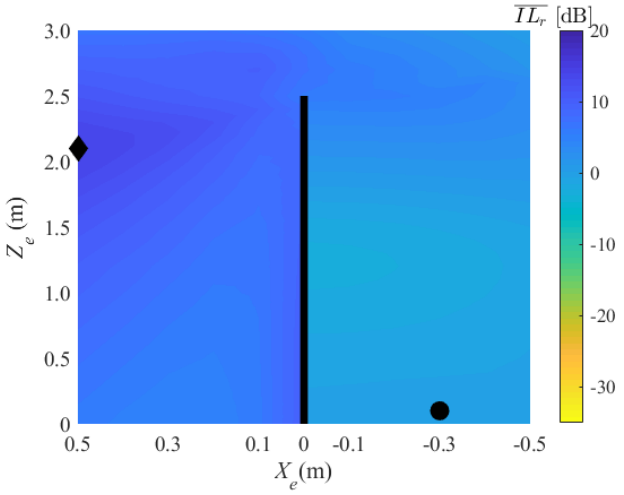


(b-i)

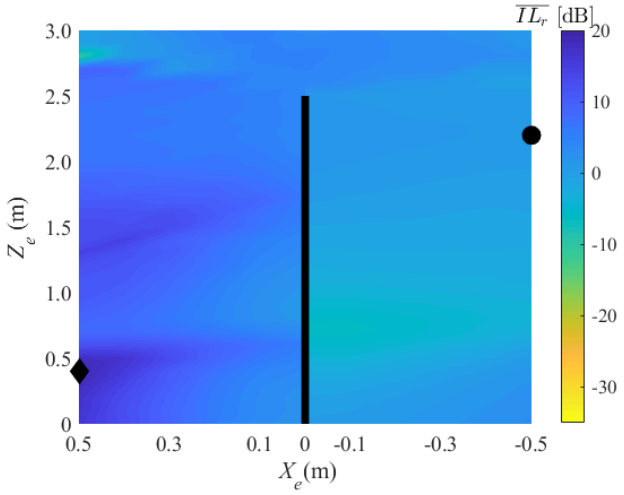


(b-ii)

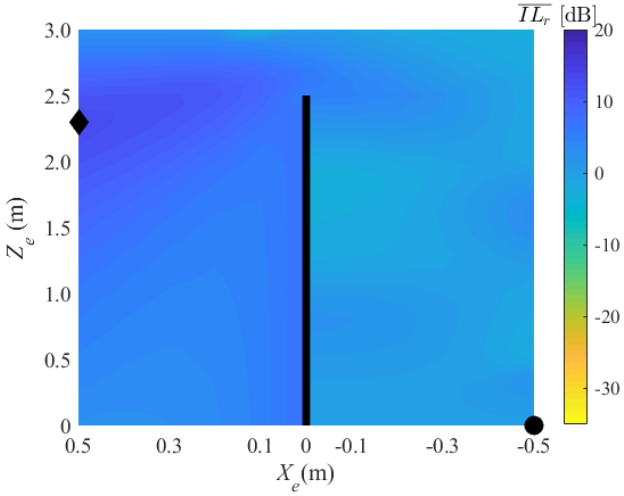


(c-i)

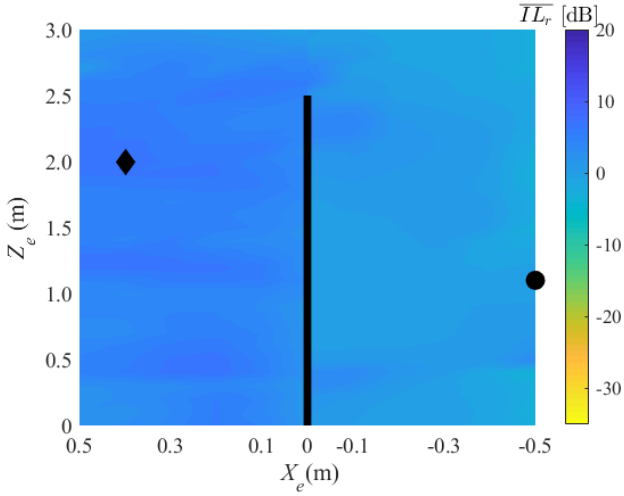


(c-ii)

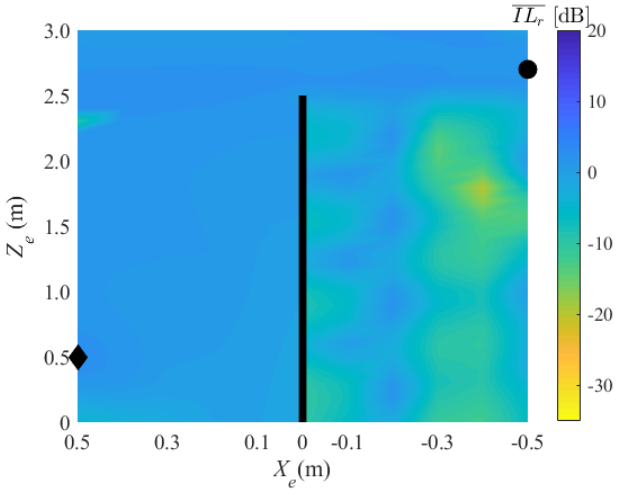


(d-i)

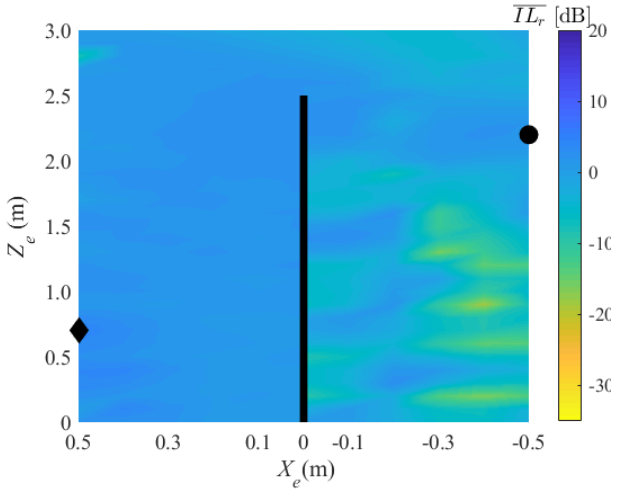


(d-ii)

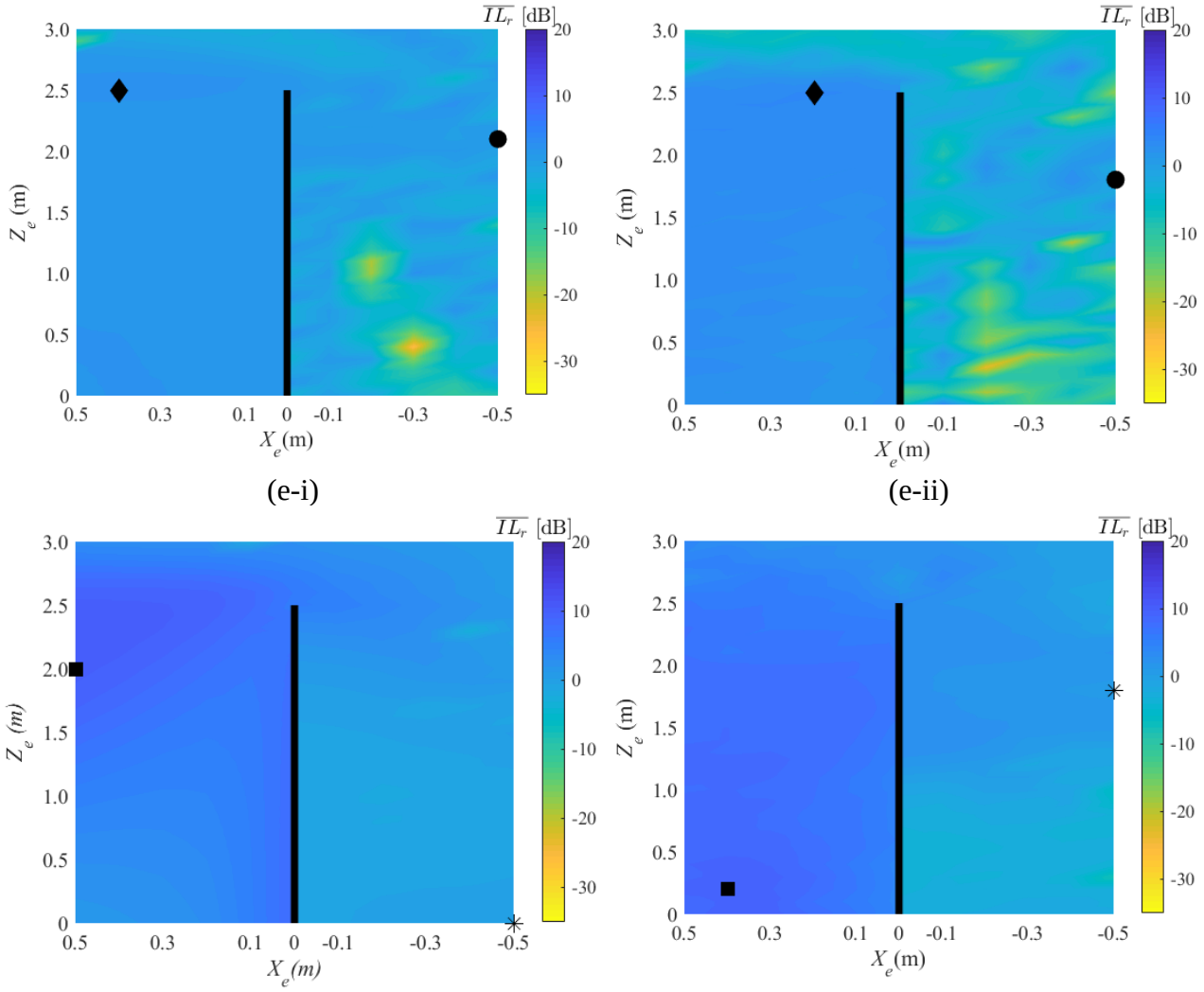


Fig. 2.5: $\overline{IL_r}$ [dB] of all candidate positions of the error microphones in the barrier zone, (i) absorbent soil, (ii) hard soil. (a): 63 Hz, (b): 125 Hz, (c): 250 Hz, (d): 500 Hz, (e): 1 kHz, (f) overall. ● is the position of control sources at each frequency, ◆ is the best position of error microphones, * is the overall position of control sources, and ■ is the overall position of error microphones.

## 2.5. Discussion

### 2.5.1. Location of the secondary sources

Table 2.1 separately shows the noise level reduction of the passive barrier and the extra attenuation with the active noise control at the receivers. The total noise level reduction of the active noise barrier is the summation of these two noise control strategies. This table

shows that the passive barrier operates more efficiently at high frequencies than low frequencies. However, the active noise control compensates for the weak performance of the passive control at low frequencies. Table 2.1 also shows that for a flat spectrum, the overall attenuation achieved by means of the active control is higher than that of the passive.

As a general trend, Table 2.1 shows that the active attenuation diminishes as the frequency increases, which is in complete agreement with all previous studies. Moreover, this table shows that the presence of ground reflection could negatively affect the performance of the active noise barrier, specifically at very low frequencies, as was found by Guo [92]. This is probably due to the more complex sound fields generated by the ground reflections on both sides of the barrier [79,92].

The positions for the control sources, presented in Table 2.1, are the locations where the active noise barrier maximally reduces the narrowband noise of the primary source. Although these positions are generally at the incident side of the barrier, their exact locations highly depend on the operating frequency of the noise source and the quality of the soil wave reflections. A more general trend can be found observing Fig. 2.4, which shows the average insertion loss at the receivers ($\overline{IL}_r$) when the control sources are located at other candidate positions in the barrier zone. This figure shows that besides the suitable positions presented in Table 2.1, there is a wide region of candidate positions where the control sources at these positions can obtain reductions comparable to the maximum one. Thus it is possible to change the position of the control sources without losing significant performance, which is a general result consistent with previous observations [76,77,79]. This observation is more obvious in the case of completely hard soil than absorbent soil.

From Fig. 2.4-ii, and generally speaking, it seems that most of the incident region is suitable for placing the secondary source, except a small domain just above the edge of the barrier which corresponds to those locations of the secondary sources that are seen only by part of the receivers. Taking this relation into account, it seems advisable to divide the position of control sources into three different domains (Fig. 2.6). Domain I includes those locations of control sources where all of the receivers are under the purely diffracted field of control sources. This domain is at the incident side and below the path that connects the furthest receiver to the edge of the barrier. The second domain (Domain II) is where some part of the receivers can see the control sources (they are under the direct and diffracted field) and the other part of the receivers is located only in the diffracted field of control sources. Domain III presents those locations of control sources where all of the receivers are under the direct and diffracted control field.

Locating the control sources in Domain II, the receivers are exposed to a mixture of direct and diffracted wavefronts from the control sources. This mixture of different acoustic fields in the shadow zone seems to significantly lower the efficiency of active noise control. In order to find out whether this is the case, the phase of the primary and secondary fields is measured at several points when the control sources are placed at each of those three domains. The measuring points are located 1 m far from the edge and on a plane orthogonal to the barrier and centered at the edge of the barrier [83]. These points are in the angle range between 274º and 293º, which covers the direction from the edge of the barrier to all receivers (Fig. 2.6). The control sources are located at SS1, SS2, and SS3 with coordinates of $(SS_x, SS_z) = (-0.5, 2.2)$, $(SS_x, SS_z) = (-0.5, 2.7)$, and $(SS_x, SS_z) = (+0.5, 2.0)$ respectively.

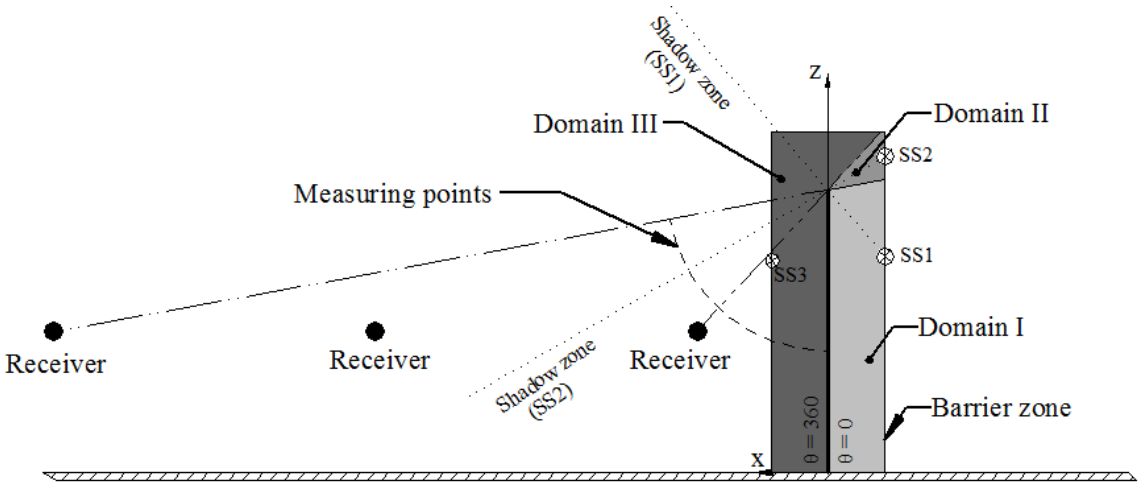


Fig. 2.6: Schematic diagram of measuring points and three different domains for the control sources close to the barrier.

Fig. 2.7 shows the active attenuation at the receivers for secondary sources at SS1, SS2, and SS3. This shows that the control system performs better when the secondary sources are placed in Domain I (Fig. 2.7a) than in the other two domains. The average insertion loss at receivers ($\overline{IL}_r$) when the secondary sources are located at SS1, SS2, and SS3 is 29.7 dB, 10.4 dB, and 14.7 dB, respectively.

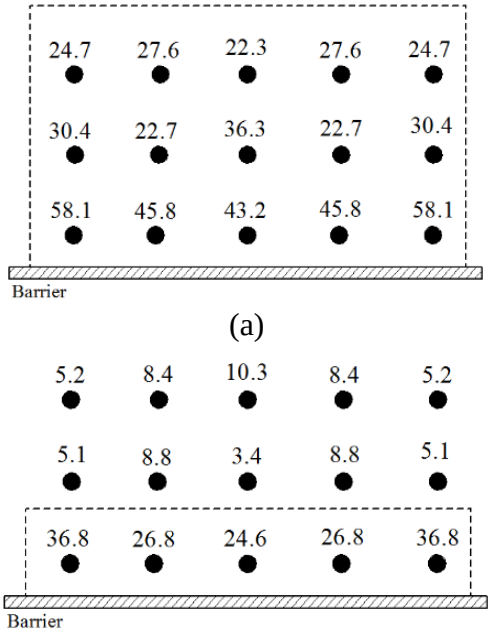

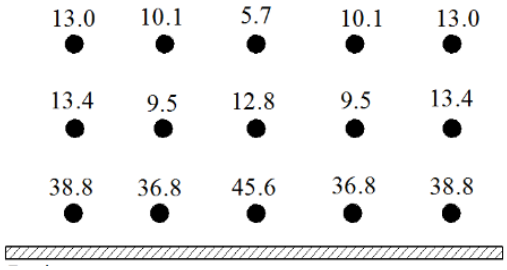


(c)

Fig. 2.7: Insertion loss [dB] at receivers, when secondary sources are at (a) SS1 ($SS_x = -0.5$, $SS_z = 2.2$) [m], (b) SS2 ($SS_x = -0.5$, $SS_z = 2.7$) [m], (c) SS3 ($SS_x = 0.5$, $SS_z = 2.0$) [m]. The dash-line shows the boundary of the secondary sources' shadow zone. $f$= 125 Hz and hard soil.

Fig. 2.8 denotes the phase of the primary field ($\emptyset_0$), secondary field ($\emptyset_{SS}$), and their difference ($\Delta\emptyset$) at the measuring points. This figure indicates that when the secondary sources are at SS1, the primary and secondary fields are almost out of phase, which causes a decrease in the sound level. However, for the other locations of secondary sources, $\emptyset_0$ and $\emptyset_{SS}$ are almost in-phase, which degrades the efficiency of the control system.

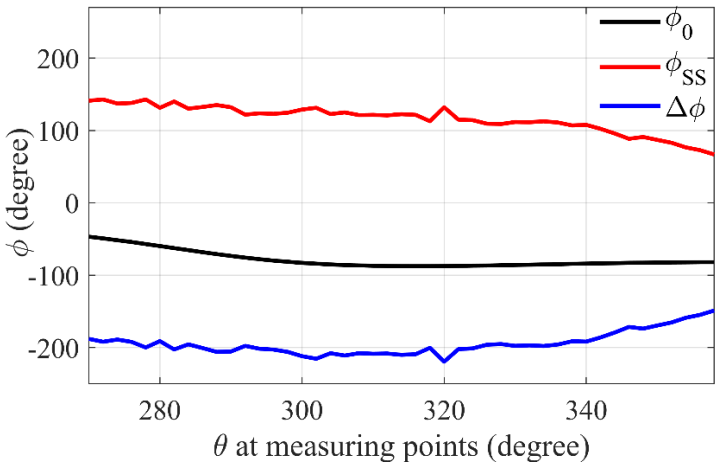


(a)

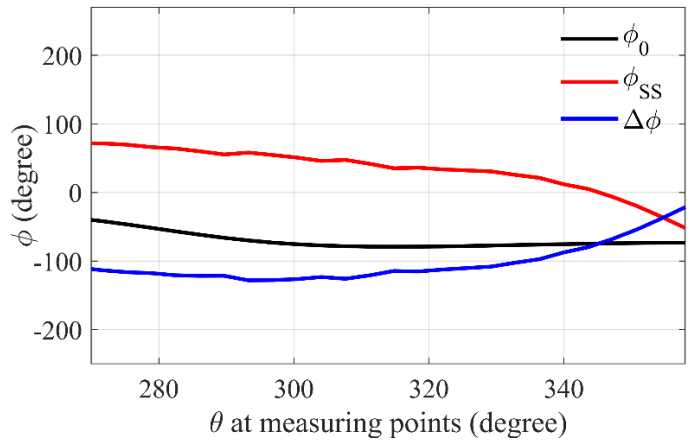


(b)

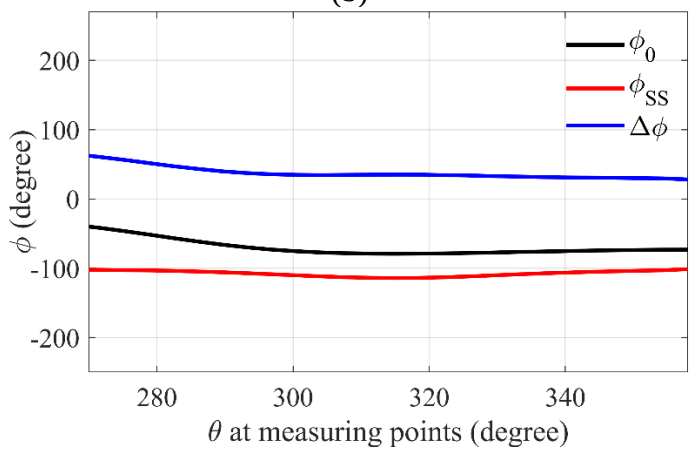


(c)

Fig. 2.8: Phase of the primary field ($\emptyset_0$) and secondary field ($\emptyset_{SS}$) and their difference $\Delta\emptyset$ at measuring points 1m from the top edge. Secondary sources are located at (a) SS1 ($SS_x = -0.5$, $SS_z = 2.2$), (b) SS2 ($SS_x = -0.5$, $SS_z = 2.7$), (c) SS3 ($SS_x = 0.5$, $SS_z = 2.0$). $f$ = 125 Hz and hard soil.

From the previous studies [83], and Fig. 2.8a, it is perceived that active noise control performs better when $|\Delta\emptyset|$ are close to 180°. Thus, for further investigation to achieve a more general conclusion, the difference in phase of the primary and secondary fields ($|\Delta\emptyset|$) is compared with the active attenuation ($\overline{IL}_r$) in Fig. 2.9. This comparison straightforwardly shows a high correlation between these two variables ($|\Delta\emptyset|$ and $\overline{IL}_r$). This figure also confirms that the active noise control performs more efficiently at those positions of secondary sources that $|\Delta\emptyset|$ are closer to the 180º, i.e. the primary and control fields are out of phase.

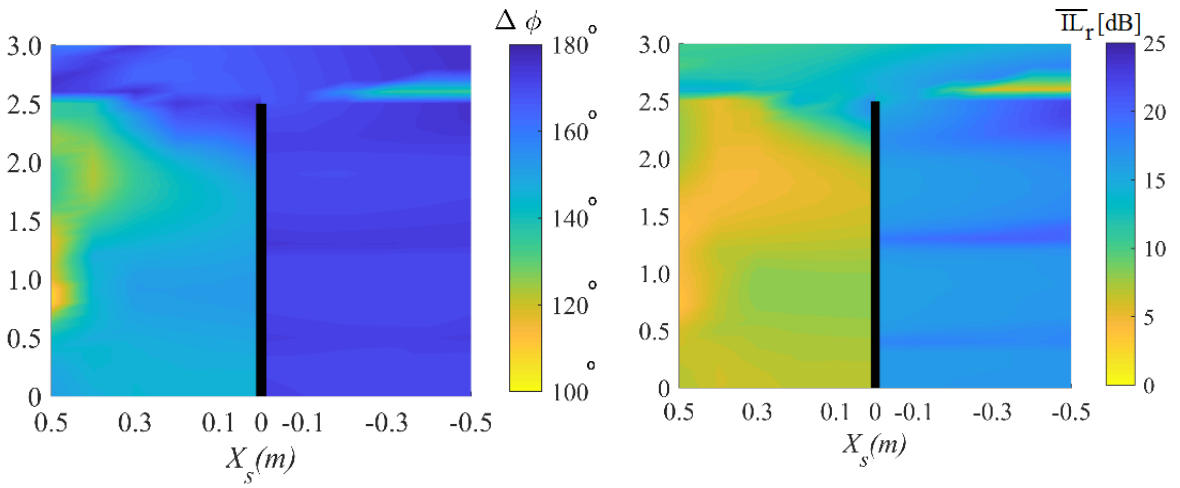


(a) (b)

Fig. 2.9: (a) Difference between the averaged phase of the primary and secondary field at receivers ($|\Delta\emptyset|$), (b) $\overline{IL}_r$, for different locations of secondary sources in the barrier zone. $f$ =200 Hz and hard soil.

As a conclusion of the analysis performed in Fig. 2.6 to Fig. 2.8, it can be stated that the active control at the shadow zone is maximally achieved when the diffracted waves of the noise source are canceled by the control sources diffracted wavefronts. This general result is also supported by previous observations [67,75–77]. These results, therefore, indicate that the proper locations of the control sources are in Domain I, where the primary diffracted field is controlled by a purely secondary diffracted field. For some frequencies, however, Table 2.1 shows that the best position for the secondary source is out of this domain, although it is worth noting that these positions are rather isolated and cannot be used as general criteria. Moreover, the use of the general criteria should lead to a more robust configuration of the active noise barrier, as small errors in locating the secondary sources and the use of real and relatively bulky secondary sources would bring almost the same attenuation results.

Previous findings are reinforced enforced even when considering broadband spectra. For the broadband spectra (formed by the single-center frequencies of the 1/3 octave band in the range of this investigation, forming flat spectra), an entirely different calculation is performed to define the new suitable positions of control sources. For this purpose, Equation 2.10 is

used to calculate the overall insertion loss of the whole frequency spectra. As shown in Fig. 2.4f, the overall insertion loss of the whole spectra is less depending on the position of the control sources, than the single frequencies. Moreover, attenuation is achieved at any suitable position of the secondary sources, although the best zone is again in Domain I, as far as possible from the barrier.

### 2.5.2. Location of the error microphones

The results shown in Table 2.2 define the maximum $\overline{IL}_r$ at the shadow zone when the control sources are located at their best positions of the single frequencies presented in Table 2.1 and the error microphones are at their best positions. In general terms, the efficiency of the active noise barrier diminishes when attempting to reduce the primary field at the receivers by canceling the pressure at error microphones out of the receiver zone, which is a rather expected result. Attenuation also decays with the increase of frequency, but with a trend that is not as smooth as for the secondary sources, since there is a dip in attenuation for those frequencies where the control sources are out of Domain I, i.e. where the general criteria for the location of secondary sources are violated. (More notable in Table 2.2 at $f$ = 63 Hz of absorbent soil, and $f$ = 80 Hz and $f$ = 315 Hz of hard soil).

Moreover, Table 2.2 shows that the proper locations of error microphones are mostly at the shadow side of the barrier and as close as possible to the receivers in the shadow zone, although these positions change by frequency. Similar to the previous step and in order to define a suitable region for the error microphones, Fig. 2.5 displays the $\overline{IL}_r$ for all candidate positions of the error microphones in the barrier zone. This figure shows that the best positions presented in Table 2.2 are not unique points, but there is a region of candidate points

with positions in which the error microphones could be located without any significant loss of attenuation at the shadow zone.

All the results definitively suggest that the control source positions located outside of Domain I are completely isolated results and lead to significantly poorer performance in a real-life system such as one including error microphones. By modifying the positions of the control sources and locating them in Domain I, for instance, at the best position of the broadband noise, and repeating the second step, greater attenuations at those frequencies are achieved. The results are presented in Table 2.3. These results are in a better correlation with those presented in Table 2.2 for other frequencies.

Table 2.3: $\overline{IL}_r$ [dB] with the modified positions of control sources and error microphones.

| Freq. [Hz] | Soil type | $(X_s, Z_s)$ [m] | $(X_e, Z_e)$ [m] | $\overline{IL}_r$ [dB] |
|---|---|---|---|---|
| 63 | absorbent | (-0.5, 0) | (0.5, 2.4) | 15.5 |
| 80 | hard | (-0.5, 1.8) | (0.5, 1.6) | 12.5 |
| 315 | hard | (-0.5,1.8) | (0.3, 0.2) | 8.0 |

Generally speaking, as long as the control sources are in Domain I, the suitable region for the location of error microphones is on the shadow side and below the barrier edge. This trend simply suggests that the error microphones must be placed at any position so that they are under the diffracted fields of primary and secondary sources. In order to prove that hypothesis, the averaged phase difference at the receivers ($\Delta\emptyset$) is calculated at all of the candidate positions for error microphones, and the results are compared to the $\overline{IL}_r$ for the same configuration. Fig. 2.10 compares $\Delta\emptyset$ with the $\overline{IL}_r$ at 200 Hz when the secondary sources are in the best position according to Table 2.1 ($SS_x = -0.5$, $SS_z = 2.4$). The comparison of Fig. 2.10a and Fig. 2.10b clearly shows that when the error microphones are located in the shadow zone of the barrier and the secondary sources are located in Domain I,

the pressures of the primary and control sources are out of phase, which improves the performance of the active control system.

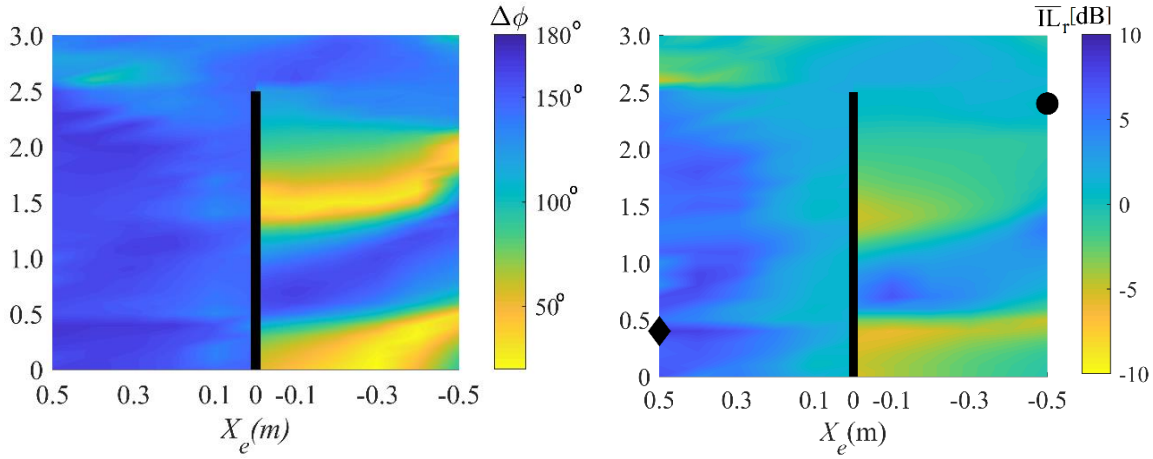


(a) (b)

Fig. 2.10: (a) Difference between the average phase of the primary and secondary field at receivers (Δ∅), and (b): $\overline{IL}$ [dB], for different locations of error microphones when the secondary sources are at $SS_x = -0.2$, $SS_z = 2.4$.

Consequently, the result shown in Fig. 2.10 proposes that the active noise barrier operates more efficiently when the error microphones are located in the same acoustic field of all sources as the receivers are placed.

## 2.6. Conclusions

In this chapter, it is shown that the best absolute location of the control sources and error microphones depends on the operating frequency of the noise source and type of soil, but it is possible to find a region for transducers close to the barrier where the active noise barrier could operate almost as efficiently as at its absolute best configuration. The control sources should be located on the incident side and below the path that connects the furthest receiver to the edge of the barrier. Moreover, the error microphones should be located at the receiver side in the shadow zone of both primary and control sources, i.e. the control system will perform more efficiently when the diffracted field of primary source controls with the

diffracted field of secondary sources and the error microphones are under the diffracted sound field of both the primary and secondary sources.

Furthermore, the results show the significant effect of the soil's reflection on the performance of the control system in the narrowband cancellation. This effect, however, is not reported for the broadband noise cancellation in terms of the location of transducers, and the general criteria hold for both completely reflective or completely absorptive soil.

It is also found that the two-step optimization approach (first find the best position for the secondary sources and then the best position for the error microphones) is suitable for the design of a compact active noise barrier whose cancelation zone is far away from the shadow zone, although it probably fails in finding the absolute best configuration if the determined general criteria are ignored.

# *Chapter 3* : *Suitability of active noise barriers for construction sites*

### 3.1. Introduction

Construction noise is a topic of recognized importance in terms of its impact on workers due to the high noise level generated [8,93]. The issue has gained added significance given the ever-increasing environmental sensitivity of the general public and the corporate sector alike in recent years as construction noise can cause annoyance [94,95] and have adverse behavioral effects [6] on the neighborhood. Among others, the ubiquity of noise sources, the variability of the noise itself, the existence of the flows of materials, people, and vehicles, the size of the whole plant, the limited efficiency of most solutions in the low-frequency range, and even the difficulty of assessing the effect of mitigating measures [96] all contribute to on-site noise control.

Noise control in this complex scenario generally calls for joint action on the transmitter, using low acoustic emission equipment [97] or managing the schedule and simultaneity of the performances [98], and on the transmission channel [38]. Alternatively, if all else fails, an action can be taken on the receiver [56].

A measure that is gradually being taken is the use of mobile noise barriers that adapt to the construction process [99–101], despite their limited efficiency in the low-frequency range, which predominates in construction noise. The recent study [2] defined the difficulties of the application of active noise barriers in open space. It is known, however, that active noise control is especially efficient in the low-frequency range, and that is why recent research has focused on applying this strategy to construction noise control, with promising results [55,98]. A natural outgrowth of these recent studies consists of the investigation of the applicability of active noise barriers (ANBs) in construction, which combines portability with maximum efficiency.

This study sets out to investigate the suitability of applying active noise control on barriers for construction sites and defining the configuration of the control devices, which gives the maximum attenuation. The suitable locations for the transducers are found among 341 potential positions around the barrier. The cancelation targets for noise control are the neighboring street area, defined by a horizontal plane of receivers at the shadow zone of the barrier, and buildings close to the construction site, defined by a vertical plane of receivers' places away from the barrier.

In this regard, two stages are involved in discovering the best location of the transducers close to the barrier [102–104]: First, the position of the control sources is found ensuring the maximum attenuation of acoustic pressure in the receiver zone. Second, a suitable position is selected for the error microphones that give the greatest attenuation in the shadow area for the location of the control sources found in the first stage.

## 3.2. Theory

### 3.2.1. Diffraction Model

The diffraction model developed by Macdonald is again used in this study as it was employed in the previous study.

### 3.2.2. Active Noise Barriers

The overall objective of adding active noise control sources to the barriers is to extend the efficiency of the acoustic barriers at low-frequency spectra, typical of construction noise [8]. An effective design of an active noise barrier defines the location of the error microphones and secondary sources properly. Installing the transducers close to the barrier can be advantageous in terms of supporting them on the barrier itself. The optimized position of

transducers highly depends on the position of the noise source and the target area where it is aimed to control the sound level.

In this study, the locations of transducers are optimized for different positions of the noise sources and two different target areas, namely, the street area and the façade of the neighboring building. The optimization procedure is followed by a two-step method. The first step is to determine the positions of the control sources, which ensures the maximum noise level reduction in the target area. Once the suitable location of the control source has been found, the position of the error microphones is defined. It bears noting that the objective in the second step is not to maximize the attenuation in the error sensors but to minimize the sound level in the target area.

### 3.3. Method

Acoustic barriers are commonly used in cities to control the construction noises in the street area and neighboring buildings. These kinds of barriers are generally composed of several short-length segments (Fig. 3.1) so that they can be installed, moved, and adapted to the boundary of the construction sites. In this study, three zones are considered to model the construction site and its nearby areas: (I) the construction site (Fig. 3.1a), where the activities are progressing and the noise sources are located; (II) the building area, representing close buildings; and (III) the street area, representing the sidewalk zone between neighborhood buildings and the construction site (Fig. 3.1b).

(a) (b)

Fig. 3.1: On-site noise control barriers. (a) Construction site area. (b) Sidewalk and neighboring buildings.

In the simulation, the barrier with rigid surfaces on both sides and a practical height of $H_b$=2.5 m is considered between the construction site and the sidewalk and buildings area (Fig. 3.2). The thickness of the barrier is considered negligible vis-a-vis the noise wavelength. In the calculations, the ground is also assumed to be hard and the reflected pressures at both sides of the barrier are computed based on the image method [84].

To address the movement of the noise source in the construction site, the simulation is conducted for different positions of the noise source. The distance of the noise source from the barrier, $d_{pr}$, ranges from 1 to 7 m, and for simplicity, it is always located at plane $Y$ = 0 and a height of 0.3 m. The frequency spectra throughout this work are formed by the center frequency of each third-octave band from 63 Hz to 1 kHz and the power output of the noise source is 1 W at each considered frequency.

Fig. 3.2 schematically shows the construction site and the nearby areas. In this figure, the control zone is the region close to the barrier, reserved to place the transducers. This zone is intentionally selected near the barrier so that the transducers can be installed in real applications and also the active barrier remains as a unique, portable device. For this study, the control zone surrounds the barrier with a size of 1 × 3 $m^2$.

The positions of the transducers are optimized through the control zone to minimize the sound level in the target areas (shaded areas in Fig. 3.2). The street area with a size of 10 × 8 $m^2$ is recognized as the first target area that is covered with 15 points for computing the pressure. These points are located at a height of 1.65 m.

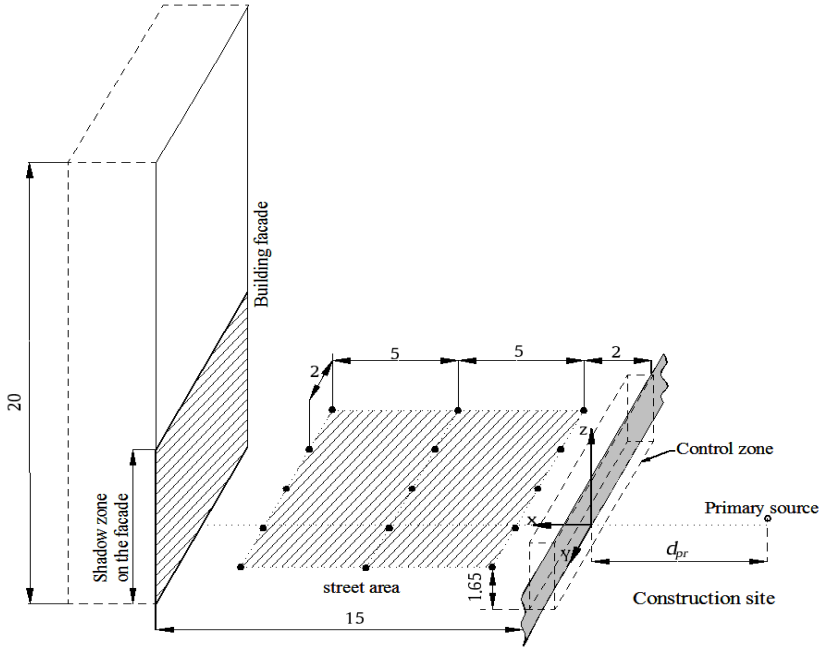


Fig. 3.2: Schematic diagram of an infinite barrier and different target zones (dimensions are in meter).

The second target area in this research is the shadow zone on the façade of the neighboring building. The whole building façade is 20 × 8 $m^2$, located on the plane $X$ = 15 m (Fig. 3.2) and placed symmetrically with respect to the Y-axis. The size of the shadow zone on the façade depends on the relative location of the noise source from the barrier. In the current work, the same density of points as the street area is always considered to compute the pressure on the façade.

The set of control sources is defined by an array of Ns = 10 control sources arranged linearly along the Y-direction and distributed symmetrically with respect to the $X$-axis. The space between the adjacent control sources in the Y-direction is $d_s = 0.2$ m, which is close to half

the shortest wavelength at 1 kHz, a distance that gives a better performance for an array of control sources [71,90]. The suitable location for the control sources is found among 341 candidate positions in the control zone (Fig. 3.2), defined by a grid of 0.1 m steps in both *X*- and *Z*-direction. For each candidate position, the strength of the control sources is calculated so that the acoustic pressure is minimized at the observational points in the target areas, calculated using Equation 2.10. The position that gives the maximum attenuation is considered the best location for the control sources.

Once the best location of the secondary sources has been defined, minimizing the acoustic pressure level in the target areas is attempted using a set of error sensors within the control zone. To this end, an array of $N_e$ = 41 error microphones is arranged linearly along the *Y*-direction, with distances $d_e = 0.2$ m between them, and distributed symmetrically with respect to the *X*-axis. The distance between error sensors is close to half the shortest wavelength which, based on ref. [71,90], is the optimum value for the separation space of error sensors, and $N_e$ = 41 is chosen to cover the width of the target areas in *Y*-direction. With the secondary sources fixed at the best position of each frequency, the strength of the control sources is calculated to minimize the squared pressure at the error microphones in all candidate positions in the control zone. The position that, after the previous calculation, gives the maximum attenuation in the target area, calculated by Equation 2.10, should provide the best setup of the control sources and error microphones within the control zone.

### 3.4. Results

This section introduces the best locations of the transducers in the control zone when different regions are considered as the target zones.

### 3.4.1. Target Area: Street Area

Table 3.1 shows the position of transducers, which gives maximum attenuation in the street area for the various distances of the noise source from the barrier ($d_{pr}$). This table also illustrates the different values of attenuations reached in the street area ($\overline{IL}_s$), the shadow zone on the façade ($\overline{IL}_{F.s}$), and at the whole building façade ($\overline{IL}_F$), considering passive and active noise control mechanisms.

Table 3.1: Best positions for the transducers and the insertion loss achieved when the street area is the target zone. $d_{pr}$ is the distance of the noise source from the barrier and $\overline{IL}_s$, $\overline{IL}_{F.s}$, and $\overline{IL}_F$ are the average insertion loss in the street area, in the shadow zone of the façade, and in the whole building, respectively. The insertion loss with the passive noise barrier, PNB, is the difference of the average sound pressure level in the observational points with and without barrier, and the insertion loss of the active noise barrier (ANB) is computed by Equation 2.10. $(X_s, Z_s)$, $(X_e, Z_e)$ are the coordinates of the control sources and error sensors, respectively.

| $d_{pr}$ | $(X_s, Z_s)$ | $(X_e, Z_e)$ | $\overline{IL}_s$[dB] | | $\overline{IL}_{F.s}$[dB] | | $\overline{IL}_F$[dB] | |
|---|---|---|---|---|---|---|---|---|
| [m] | [m] | [m] | ANB | PNB | ANB | PNB | ANB | PNB |
| 1 | (−0.5, 0) | (0.5,2.4) | 16.4 | 14.9 | 17.9 | 10.8 | 17.9 | 10.8 |
| 2.5 | (−0.5,1.8) | (0.5,1.1) | 11.9 | 13.2 | 10.8 | 9.6 | 0.9 | 8.7 |
| 4 | (−0.5, 1.8) | (0.5,0.9) | 10.9 | 12.3 | 8.4 | 9.5 | −0.3 | 8.3 |
| 5.5 | (−0.5, 1.8) | (0.4,0.4) | 9.9 | 11.8 | 8.1 | 9.2 | −0.4 | 8.3 |
| 7 | (−0.5, 1.8) | (0.4,0.2) | 9.3 | 11.4 | 7.9 | 9.1 | −0.1 | 8.3 |

This table shows that the best position of the transducers varies depending on the location of the noise source. As changing the position of the transducers according to the distance between the noise source and the barrier is not a practical solution, it is worth seeking whether there are regions in the control zone for the control devices where the active noise control can achieve comparable attenuations for different locations of the noise source. Fig. 3.3-i shows the reduction in the street area ($\overline{IL}_s$) achieved from the first step for different positions of the control sources in the control zone. The location of the noise source changes from $d_{pr}$ = 1 m (Fig. 3.3a-i) to $d_{pr}$ = 7 m (Fig. 3.3e-i). In this figure, the barrier is shown by a black bar and * represents the best position of the control sources. Form the second step, Fig.

3.3-ii illustrates the reduction in the street area ($\overline{IL}_s$) when the control sources are located in the best position (the star position) and the total square pressure is minimized in different positions of the error sensors in the control zone. In Fig. 3.3-ii, ■ is the most suitable position for the error microphones.

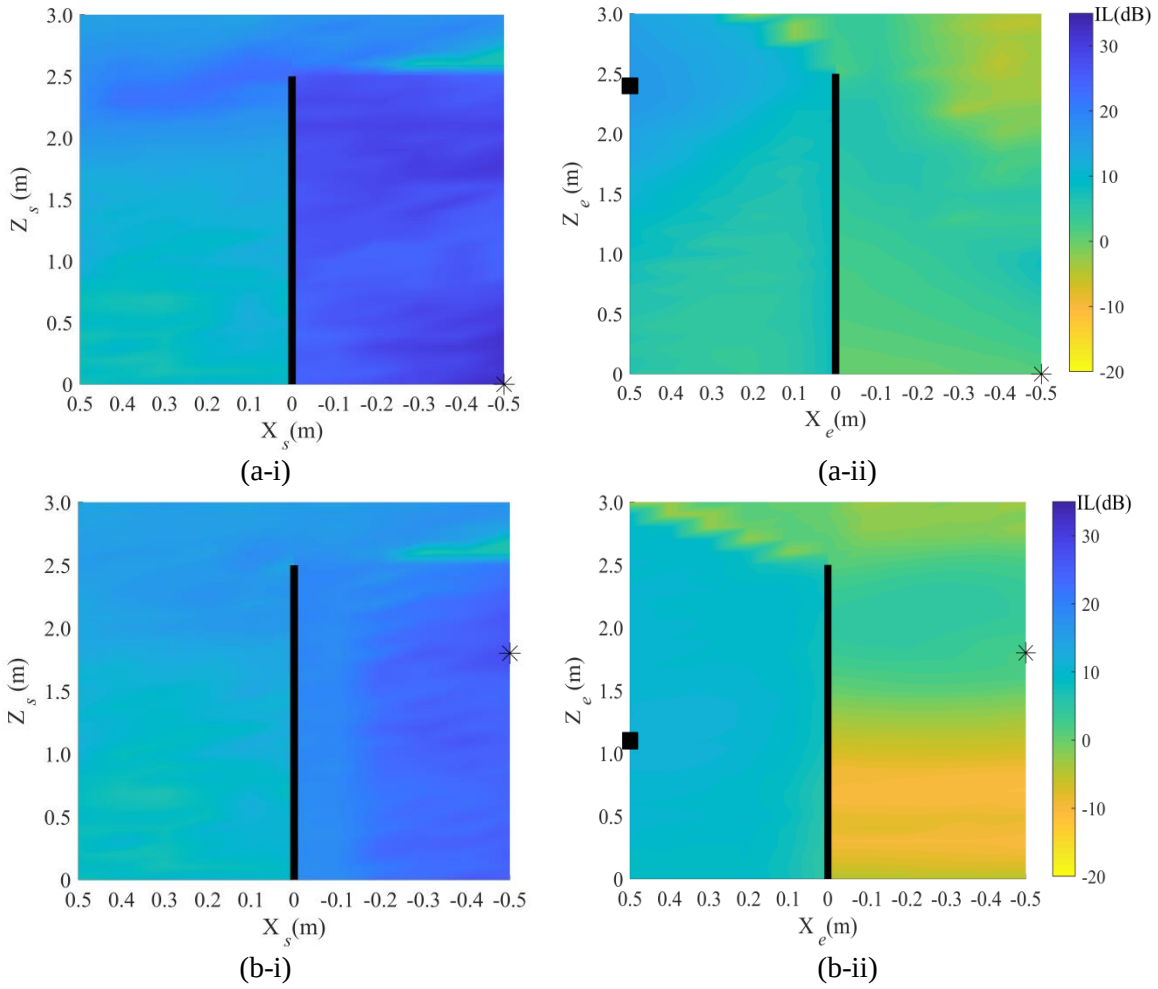


(a-i) (a-ii)

(b-i) (b-ii)

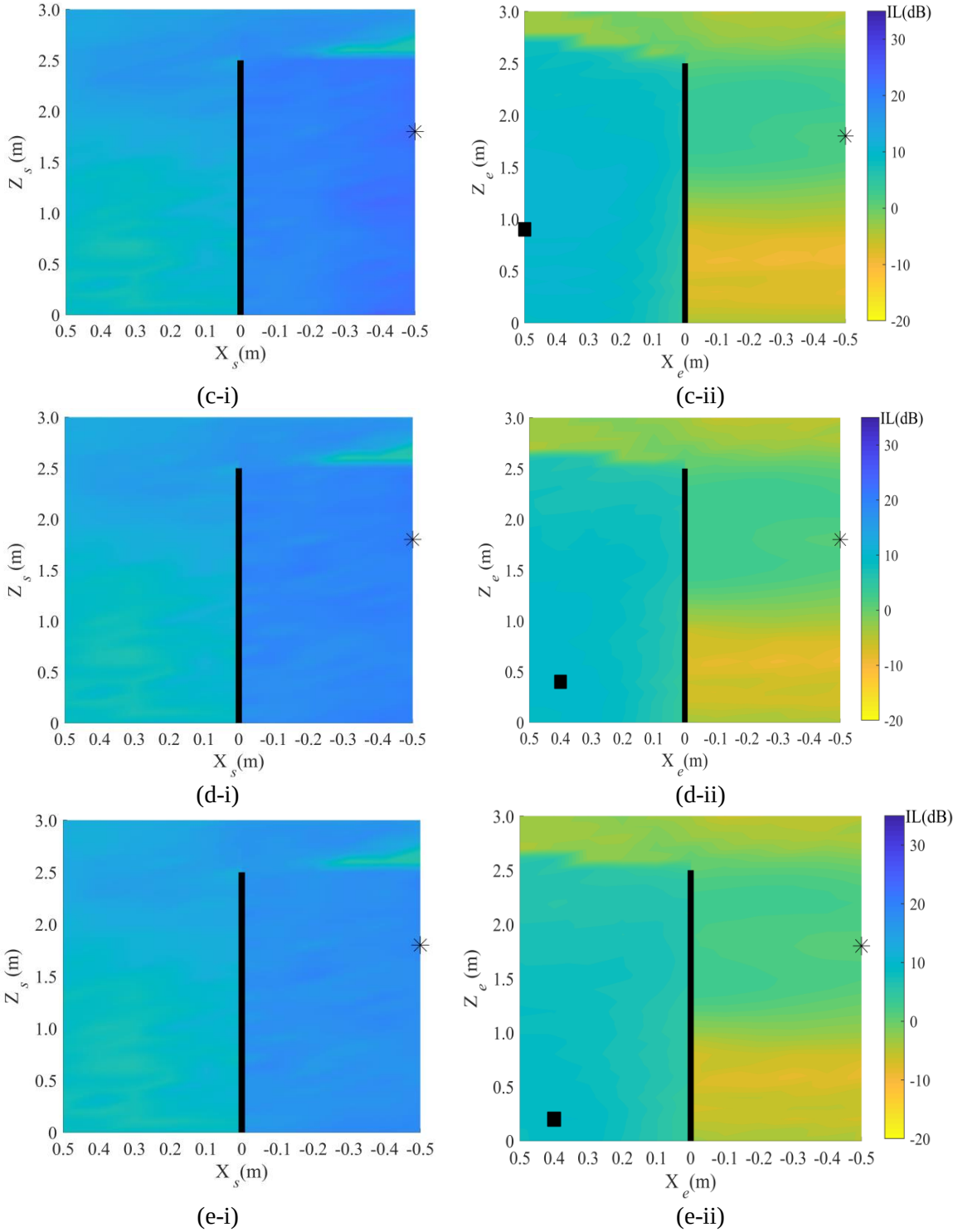


Fig. 3.3: $\overline{IL}_s$ (dB) for different positions of (i) secondary sources and (ii) error microphones, in the control zone. The distance of the noise source from the barrier ($d_{pr}$) is (a): 1 m, (b) 2.5 m, (c) 4 m, (d) 5.5 m, and (e) 7 m. The barrier is presented by the black bar, and * and ■ represent the best positions of the control sources and error microphones, respectively.

### 3.4.2. Target Area: Shadow Zone of the Façade

More studies have simulated the effect of noise cancelation by the barrier on the façade of a tall building nearby a construction site. In this subsection, the shadow zone on the façade is considered as the target area to control the noise of construction activities. The height of the shadow zone on the façade depends on the distance of the barrier to the building and the distance of the noise source from the barrier ($d_{pr}$). In this study, the height of the shadow zone on the façade changes from 7 m for the noise source at $d_{pr}$= 7 m to the whole façade for $d_{pr}$= 1 m. Table 3.2 demonstrates the most suitable configurations of the transducers when the shadow zone of the façade is considered as the control target area.

Table 3.2: The best positions of the secondary sources and error microphones in the control zone, when the target zone is the shadow zone of the façade. Variables are similar to Table 3.1.

| $d_{pr}$ | $(X_s, Z_s)$ | $(X_e, Z_e)$ | $\bar{I}\bar{L}_s$[dB] | | $\bar{I}\bar{L}_{F.s}$[dB] | | $\bar{I}\bar{L}_F$[dB] | |
|---|---|---|---|---|---|---|---|---|
| [m] | [m] | [m] | ANB | PNB | ANB | PNB | ANB | PNB |
| 1 | (−0.5, 0) | (0.2, 2.3) | 11.8 | 14.9 | 22.0 | 10.8 | 22.0 | 10.8 |
| 2.5 | (−0.5,1.9) | (0.5, 0.5) | 11.4 | 13.2 | 12.1 | 9.6 | 0.6 | 8.7 |
| 4 | (−0.5,1.8) | (0.3, 0.3) | 10.3 | 12.3 | 9.7 | 9.5 | −0.5 | 8.3 |
| 5.5 | (−0.5,2.3) | (0.5, 0.2) | 10.7 | 11.8 | 9.4 | 9.2 | 1.1 | 8.3 |
| 7 | (−0.5,2.3) | (0.3,0.4) | 8.3 | 11.4 | 8.9 | 9.1 | 0.1 | 8.3 |

Fig. 3.4 illustrates the average reduction in the shadow zone on the façade ($\bar{I}\bar{L}_{F.s}$) for different positions of the secondary sources and error sensors described in Fig. 3.3. In this figure, the target area is the shadow zone on the façade.

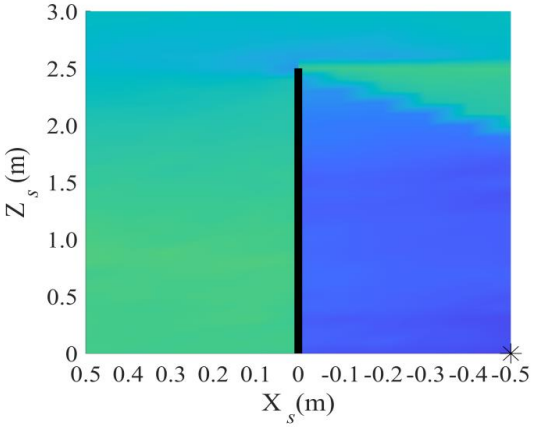


(a-i)

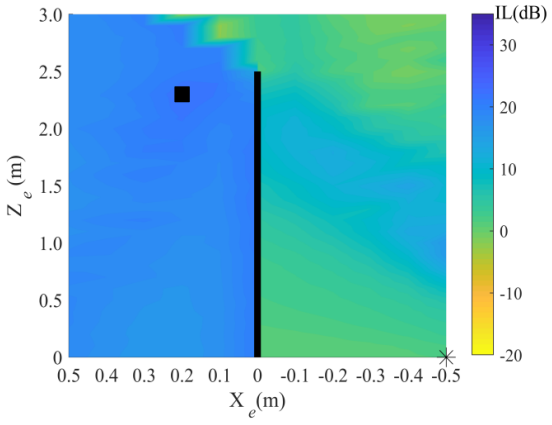


(a-ii)

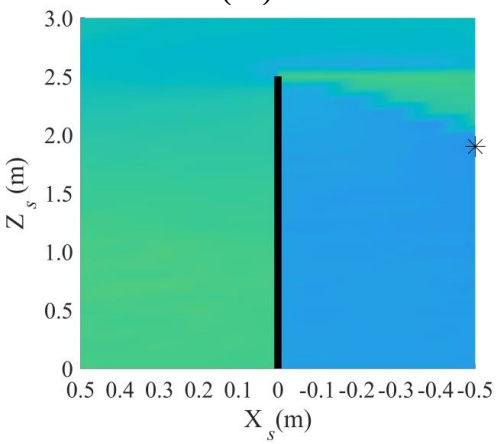


(b-i)

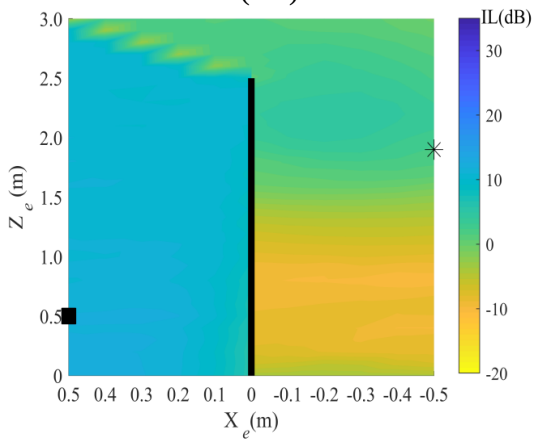


(b-ii)

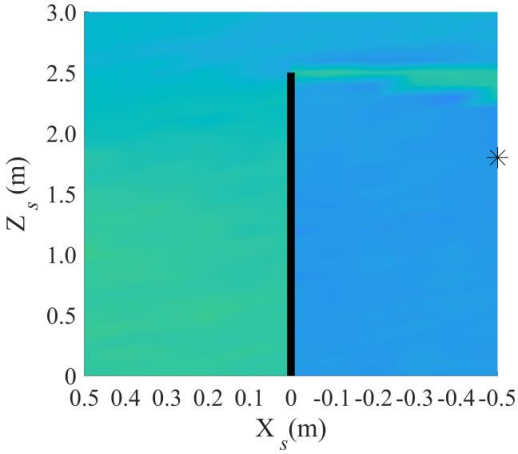


(c-i)

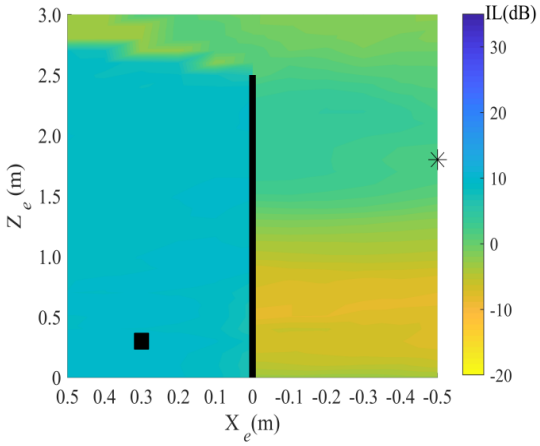


(c-ii)

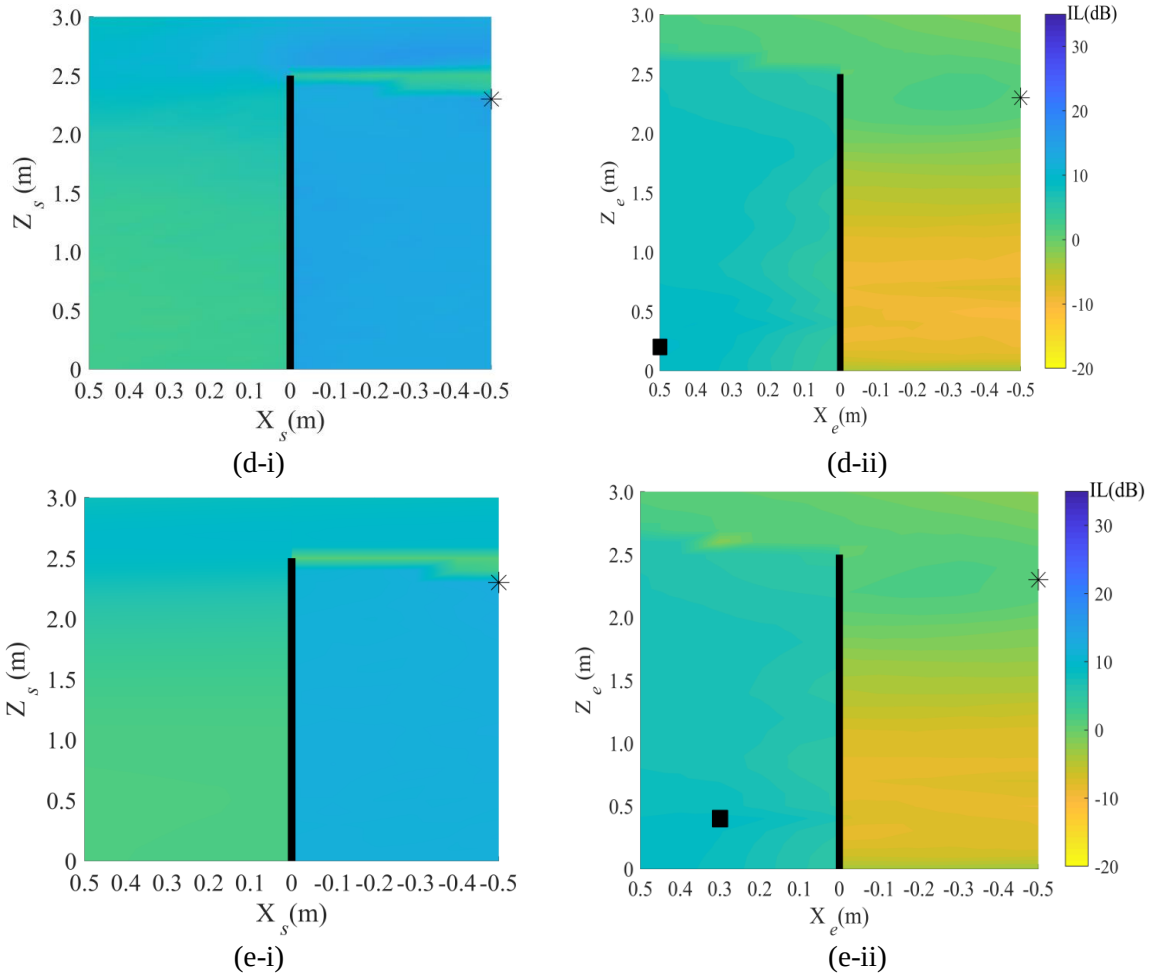


Fig. 3.4: $\overline{IL}_{FS}$ [dB] for different positions of (i) secondary sources and (ii) error microphones in the control zone. The distance of the noise source ($d_{pr}$) is (a) 1 m, (b) 2.5 m, (c) 4 m, (d) 5.5 m, and (e) 7 m. * and ■ represent the best positions of the control sources and error microphones, respectively.

## 3.5. Discussion

### 3.5.1. Target Area: Street Area

Table 3.1 shows that the performances of both active and passive noise control mechanisms in the shadow zone of the barrier are of the same order for the range of distance of the noise source from the barrier ($d_{pr}$) studied in this investigation. It shows the farther the noise source from the barrier, the lower the attenuation achieved by both passive and active noise control mechanisms. The attenuation of active noise cancellation in the street area is in the

range of 9.3 to 16.4 dB when the $d_{pr}$ changes from 7 to 1 m, respectively. Passive attenuation, however, is more stable and varies from 11.4 to 14.9 dB for the same distances of the noise source. The loss of attenuation with the active mechanism is not very noticeable for $d_{pr}$ more than 2.5 m. The same results were observed for the attenuation attained in the shadow zone of the façade. These observations imply that the active cancellation is more sensitive than passive noise control to the changes in the distance of the noise from the barrier.

Table 3.1 also shows when the target zone is the street area, the active noise barrier can reduce the noise level at the shadow zone of the façade, but it fails to achieve reductions in the whole façade for $d_{pr}$ from 4 to 7 m. The possible explanation for this result is the noise source farther from 4 m, the number of observational points on the top parts of the façade, which receive direct wavefronts of the noise source, and diffracted wavefronts from the control sources increase, and the control source diffracted field cannot reduce the direct field of the noise source. This suggests that the noise control mechanism is to cancel the diffracted wavefronts rather than the primary noise radiation.

Moreover, the positions for the control sources and error sensors show that they are always located on the incident side and shadow side of the barrier, respectively. However, the locations are different for each position of the noise source, and for a practical active noise barrier in a changing environment such as a construction site, it is mandatory to seek a unique configuration for the whole range of the noise source's position.

Fig. 3.3 reveals that the position of the control sources and the error microphones significantly contributes to the performance of the control system. Fig. 3.3-i shows that when the squared pressures are minimized directly at the observational points in the street area, there is a rather wide suitable region on the incident side of the control zone for the control

sources to be located. However, there is a narrow region in the incident side of the barrier where the control sources achieve lower attenuation in the street area (Fig. 3.3-i). When the control sources are placed in this narrow region, some observational points receive both direct and diffracted wavefronts, while other observational points just receive diffracted wavefronts. This mixture of control sources' field in the target area likely explains the weak performance of the control system for noise control, as it is shown for example in the work of Chen et al. [83] where the active cancellation of the barrier is basically achieved in the region of the diffracted primary sound field. Thus, taking into account the position of the street area, the suitable region for the secondary sources is a relatively broad region below the edge of the barrier at the incident side.

Fig. 3.3-ii displays that the active noise barrier is more efficient for those positions of the error sensors in the control zone where they receive the same wave-fronts from the noise source and secondary sources as the target area. Considering the best positions of the control sources presented in Table 3.1, the suitable region for the error sensors is the shadow side of the barrier and below the noise source-edge line.

There is no prior study that considered a whole range of positions for transducers around the barrier, but some previous studies confirm the results of the current investigation. Omoto et al. [71] and Fan et al. [67] showed that for both straight and T-shaped active noise barriers, better performance achieves when the control sources are placed in the incident side of the barrier, along the line that connects the noise source to the edge of the barrier.

### 3.5.2. Target Area: Shadow Zone of the Façade

The same method is used to define the suitable regions of the transducers when the target area is the shadow zone on the façade. As shown in Table 3.2, the optimal positions for the

secondary sources are at the noise source incident side and the error sensors are at the shadow side. This table also illustrates that when the shadow zone on the façade of the building is considered as the target area, the active noise control is as effective as the passive noise barrier to reduce the noise level. The trend of insertion loss is rather similar to the results obtained when the street area was considered as the target area.

Generally speaking, Fig. 3.4 demonstrates that the suitable regions for the control sources and error sensors are below the line that connects the noise source to the barrier edge at the incident and at the shadow side, respectively. These regions closely match the locations previously proposed for the street area. Locating the transducers above this line adversely affects the performance of the active noise barrier. Results of Ref. [105] also, confirm that the error microphones placed in the shadow zone of the barrier could create a large quiet zone in the shadow area. The comparison of noise reductions at the street area and the shadow zone of the façade (presented in Table 3.1 and Table 3.2) proposes a unique configuration for the positions of the control means that are close to the barrier.

Fig. 3.5a,b illustrates the distribution of insertion loss in the street area when the noise source is at $d_{pr} = 7$ m and the transducers are located in the positions presented in Table 3.1 and Table 3.2, respectively. This figure shows approximately the same noise level reduction in the street area regardless of the location of the control zones. On the other hand, Fig. 3.6 shows the insertion loss (dB) in the shadow zone of the façade for the same condition. This figure reveals that the active noise barrier achieves more reduction on the building façade when this area is considered as the control zone. Comparing these two figures reveals that the active noise barrier achieves better noise reduction in both areas when the shadow zone on the façade is considered as the target area.

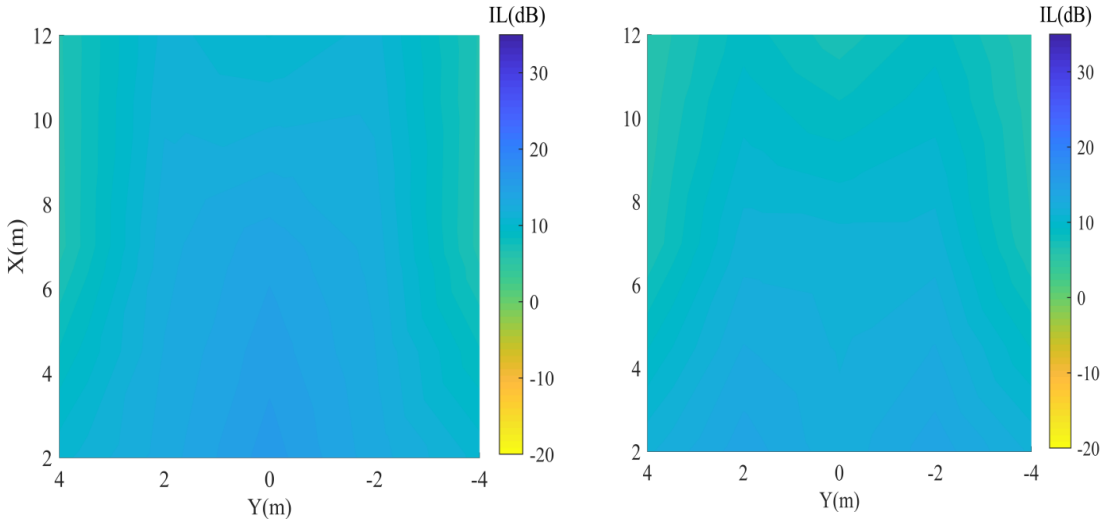


(a) (b)

Fig. 3.5: Distribution of insertion loss [dB] in the street area when the noise source is at $d_{pr} = 7$ [m] and the control zone is (a) the street area $(X_s, Z_s) = (-0.5, 1.8)$, $(X_e, Z_e) = (0.4,0.2)$ and (b) the shadow zone on the façade $(X_s, Z_s) = (-0.5, 2.3)$, $(X_e, Z_e) = (0.3,0.4)$.

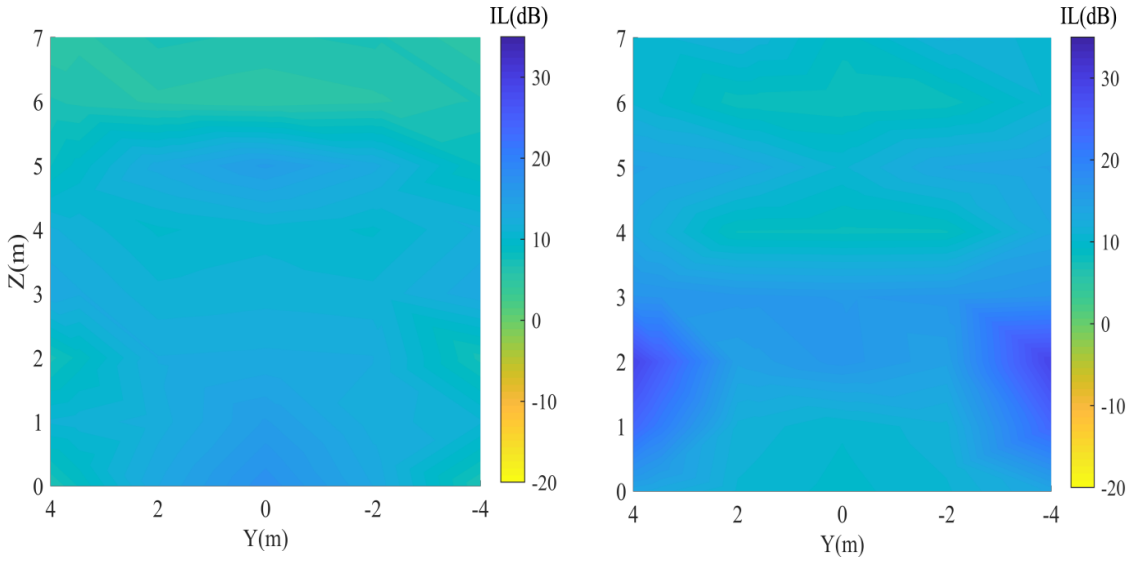


(a) (b)

Fig. 3.6: Insertion loss at the observational points in the shadow zone of façade, $\overline{IL}_{FS}$ [dB], when (a) street area $(X_s, Z_s) = (-0.5, 1.8)$, $(X_e, Z_e)$= (0.4,0.2) and (b) shadow zone on the façade $(X_s, Z_s) = (-0.5, 2.3)$, $(X_e, Z_e) = (0.3,0.4)$ are the target areas.

### 3.6. Conclusions

Successful implementation of an active noise barrier close to a construction site requires an effective configuration for the control devices and a good understanding of different scenarios for a moving noise source. The main contribution of this chapter is studying the suitability of an active noise barrier to control the construction noise activities in the neighboring street area and the nearby building façade for a noise source in the construction site. The noise source is represented by a point source placed at different positions regarding the barrier (as a mobile source would do) and operates with the typical sound spectra of construction noises.

The results confirm that for a moving source with the broadband frequency, there are suitable regions for locating the transducers where the active noise barrier performs as efficiently as optimal configuration. Similar to the conclusion of the previous chapter, the suitable region for the control sources is whatever position below the line that connects the noise source to the edge of the barrier and as far as possible from the barrier (0.5 m in this study). Besides, the appropriate region for the error sensors is whatever position in the diffracted field of the shadow zone and as possible from the barrier (0.5 m in this study), which is below the line between the edge of the barrier and the farthest receiver.

Those configurations that follow these rules and for the number of sources and error sensors considered in this study, good attenuation results are yielded in the whole shadow zone behind the array of the error sensors, as cancellation at any of the two target areas has always been achieved good attenuation in the other zones. It is shown that when the noise source is 7 m far away from the barrier, the passive barrier reduces the noise level up to 11.4 and 9.1 dB in the street area, and the shadow zone of the façade, respectively. Moreover, the active cancellation system with the optimized configuration for the control transducers can increase

the noise mitigation level to up 20.3 and 17.4 dB in the street area and the shadow zone of the façade, respectively (when the shadow zone of the façade is the target area). From these results, it can be deduced that the active noise barrier can successfully reduce more construction noise levels when the transducers are placed properly.

Also, the findings of this study proposed that in order to reduce the risk of raising the noise level in the top part of the building, the barrier should be placed as close as possible to the noise source. However, the overall performance of the proposed configuration is also relatively independent of the position of the noise source, as the attenuation in the shadow zone of the barrier remains almost unchanged for distances between the noise source and the barrier between 2.5 and 7 m.

# *Chapter 4 : Exploring the optimal parameters of an active noise barrier by Genetic Algorithm*

## 4.1. Introduction

In the previous chapters, the performance of an active noise barrier is optimized by searching the best locations of control sources and error sensors with repetitive calculations. With this method, only the coordinates of transducers could be optimized. However, more parameters may affect the efficiency of the active noise barrier. Furthermore, with the two-step method, it is not possible to optimize all parameters (those related to the control sources and error microphones) simultaneously. In this chapter, the optimization is performed by defining the optimal values for more parameters.

There are a variety of optimization methods that may optimize several parameters simultaneously. Bracketing, Local descent, First-order, Annealing algorithms, and Genetic algorithms are only a few examples of these algorithms. Some of these methods use the derivative of the objective functions to define the optimal values of the parameters. However, the others are derivative-free methods and optimize the objective functions regardless of their nature and constraints. Genetic algorithms are in the latter category. These are global optimization methods, which have a greater chance of obtaining a global solution rather than a local one [106].

In the field of the noise barrier, the studies [107–111] focused on optimizing the parameters with genetic algorithms for the passive barrier. For instance, Duhamel [107] optimized the shapes of the passive noise barriers to minimize the sound pressure level in a domain behind the barrier with genetic algorithms. Baulac et al. [108] optimized the efficiency of a T-shaped noise barrier that was covered by a series of wells on its top by the genetic algorithm optimization method. In their study, they considered the shape of protection (the depths of the wells on the crowning) and the flow resistivity of absorbing materials as the optimization

variables. Gounod et al. [109] performed an optimization to find the position of sources in the equivalent source method (ESM). Based on their findings this technique gives good reconstitution of the pressure field by using very few mono-poles. Also, Tao et al. [110] used the Genetic Algorithm to optimize the position of the control sources where the maximum reduction could be achieved and also investigated the frequency range that the active control system would benefit from the reflection of the surface.

Also, genetic algorithms are utilized to optimize specific parameters in some applications of active noise control [112–115]. For example, Montazeri et al. [112] found the optimal placement of two control sources and four error microphones in an enclosure for the active noise control system with the GA. Their model achieved 52.7 dB reductions in the potential energy of the enclosure after searching more than 700 locations for the transducers. Also, Manolas et al. [113] achieved 6.4 dB reductions inside an aircraft after using the genetic algorithms to define the actuator positions for an active noise control system. However, no studies have been published to use these optimization algorithms for active noise barriers.

The significance of appropriate placements for error microphones and control sources as well as their numbers in an active noise barrier to achieve the highest possible decrease in acoustic pressure necessitates a global optimization technique that can determine these parameters properly. In particular, this chapter focuses on optimizing the performance of an active noise barrier with genetic algorithms. The objective is to find more optimal parameters than previous chapters and propose a configuration for the transducers which obtain a higher reduction in the shadow zone of the barrier. The optimized parameters throughout this chapter are the positions, interval, and the number of control sources and error microphones.

The optimizations are performed by two different approaches: “Two-step” and “Multi-parameter”. The objective function for both approaches is the averaged extra insertion loss achieved by the control system at a target zone located in the shadow zone of the barrier.

### 4.2. Genetic algorithms model and workflow

The division of optimization algorithms depends on how they optimize the objective functions, and if the objective functions are differentiable or non-differentiable. Those algorithms that use the derivative of objective functions are fast, but they are ineffective for the optimization of non-differential objective functions or those whose derivatives can only be computed for a single or specific domain [116]. On the other hand, certain optimization algorithms, including Direct, Evolutionary, and Stochastic algorithms, operate directly on the objective functions. These algorithms are so-called black-box optimization algorithms because of the minor information they require about the function.

Genetic Algorithms (GAs) are differential-free optimization methods that classify in a larger category of algorithms, calls Evolutionary Algorithm (EA) [117–119]. The principal concept of these algorithms is to mimic the natural process of biological evolution [120], inspired by Darwin’s theory. The theory states that individual specimens of a population compete with one another for resources, shelter, and partners. Those individuals that are the best suited in the competition, have a higher survival rate and can produce a greater number of children. At the same time, the genetic characteristics of each individual are rearranged and transferred to the next generation. The next generations will be more adapted to the environment, because of the larger rate of mating and modified characteristics by the best fit individuals of the previous generation [121]. The first attempt to import the GA features into computer

algorithms was performed by John Holland [122] by developing methodologies that simulate natural adaptation mechanisms.

The first step in developing the optimization with GA is to define the parameters together with their lower and upper boundaries. Then, the algorithm starts by generating the first population, randomly. Each population is made up of individuals who are formed by a set of parameters. The parameters are selected inside the boundaries that are defined previously. Then the algorithm creates a sequence of new populations. At each step, the algorithm uses the individuals in the current generation to create the next population.

The new population is created by passing the following step:

1- The algorithm scores each member of the current population by computing its fitness value. These values are called the raw fitness scores.

2- The raw fitness scores are scaled to create a more useable range of values, which are called expectation values.

3- The members of the new population are selected based on their expectations value. These members are called parents.

4- Those individuals of the current population with lower fitness are selected as elite. These elite individuals are passed to the next population.

5- The new children are born from parents. These children are created either by making random changes to a single parent (mutation) or by combining the vector entries of a pair of parents (crossover).

6- The children are replaced with the current population to produce the next generation.

The optimization procedure continues till the stopping criteria are accomplished. These criteria are the maximum generations and the defined tolerance for convergence. When the maximum change in the fitness values of all generations is less than the defined tolerance the

optimization finishes. Also, if all of the fitness values of the generations are calculated without fulfilling the ending condition, the algorithm considers that convergence is not achieved and terminates the optimization procedure.

### 4.3. Methodology

#### 4.3.1. Model

In this chapter, the optimizations are performed based on the genetic optimizer using the MATLAB Optimization Toolbox. The objective function used in this chapter is the average insertion loss at the target zone which has been presented by Equation 2.9.

The target zone where the insertion losses (objective function) are minimized is an area of size 10×8 $m^2$ with a height of 1.65 m behind a thin and infinite barrier with $H_b = 2.5$ m tall. The efficiency of the active noise barrier is measured by calculating the average noise reduction at 15 discrete observation points placed at the target zone. The observation points are distributed evenly in the target zone. The noise source is located at a stationary point, 7 m away from the barrier, and operates at 200 Hz with a strength of $q_p$= 0.0477 ($m^3\ s^{-1}$). Fig. 4.1 schematically shows the target zone, the barrier, the primary noise source, and the zones around the barrier where the candidate positions for the transducers can be placed.

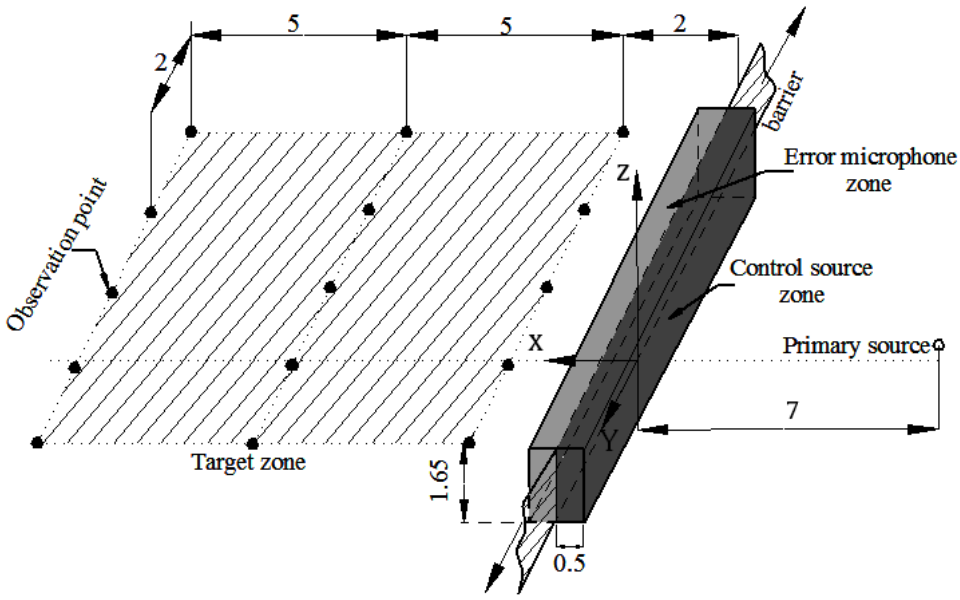


Fig. 4.1: Schematic model of the target zone and observation points behind the barrier.

In the previous chapters, it is shown that the performance of an active noise barrier increases when the control sources located on the incident side of the barrier and all the receivers in the target zone were out of their direct fields. Also, the error microphones are placed at the shadow side and below the height of the barrier.

Therefore, in this chapter, the "Error microphone zone" and "Control source zone" (Fig. 4.1) are established in a way that the candidate positions for error microphones and control sources correspond to the previous results. The "Error microphone zone" and "Control source zone" respectively illustrate the boundaries for the locations of error microphones and control sources during the optimization process with the GA. These zones are intentionally selected close to the barrier's surface to avoid interference with the activities in the shadow region, as well as to ensure that the control units can be installed in a practical application. The candidate positions for the transducers in these zones are defined by a grid of positions with the size of 0.1 m in both X- and Z-directions.

The optimization parameters throughout this chapter are the *X*- and *Z*- coordinates of secondary sources ($SS_x$ and $SS_z$), the *X*- and *Z*- coordinates of error sensors ($ES_x$ and $ES_z$), and the space between adjacent control sources ($d_s$) and error microphones ($d_e$). Fig. 4.2 shows the optimization parameters schematically. The maximum generations and the tolerances of convergence that are defined as the stop points of the optimization procedure are 100 and $10^{-6}$, respectively.

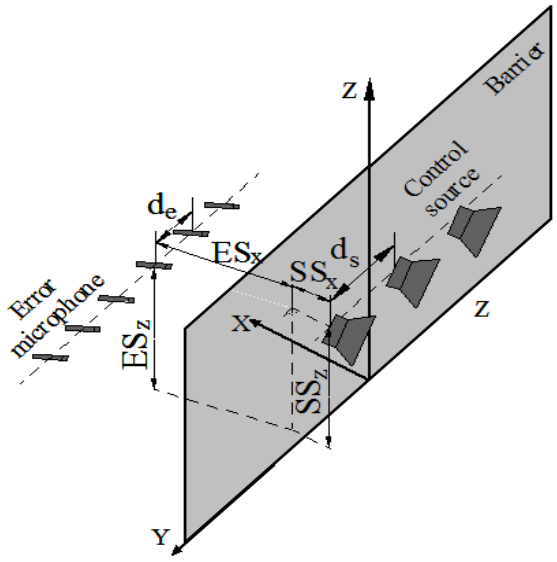


Fig. 4.2: Optimization parameters of the active noise barrier.

The limits of $d_s$ and $d_e$ are selected to be less than half of the wavelength [49,71] in the frequency range of 100 to 500 Hz which is the most efficient range for the active noise barrier [74,123]. Table 4.1 represents the parameters and the corresponding lower and upper boundaries in the optimization procedure.

Table 4.1: Boundaries of the parameters for the GA optimization procedure

| | Parameters of Control sources | | | Parameters of error microphones | | |
|---|---|---|---|---|---|---|
| | $SS_z$ [m] | $SS_x$ [m] | $d_s$ [m] | $ES_z$ [m] | $ES_x$ [m] | $d_e$ [m] |
| Lower boundary | 0 | -0.5 | 0.3 | 0 | 0 | 0.3 |
| Upper boundary | 2.5 | 0 | 1.7 | 2.5 | 0.5 | 1.7 |

### 4.3.2. Calculation procedure

In this chapter, two approaches are followed in order to optimize the performance of the active noise barrier at a tonal noise of 200 Hz. In this work, these approaches are called the "Two-step" and "Multi-parameters" approaches.

In the "Two-step" approach the parameters are optimized by the genetic algorithms after two steps [51,63,87]. This approach is the same method described in the previous chapters, but here in each step, more parameters are optimized by the genetic algorithms.

In Step 1, the parameters corresponding to control sources ($SS_x$, $SS_z$, and $d_s$) are optimized. In this step, the strengths of control sources are calculated by Equation 2.8 to minimize the squared pressure at the position of observation points in the target zone. This configuration of error microphones assures the maximum achievable noise level reduction in the target zone [69]. In Step 2, the parameters of the error microphones are defined while the control sources are placed at the positions found in the previous step, and the total squared pressure is minimized at the error microphones that are located at the positions close to the barrier (in the Error microphone zone shown in Fig. 4.1). The strength of control sources in this step is calculated with Equation 2.12. The objective function during both steps is the average insertion loss at the target area which is described by Equation 2.10.

The second approach that is followed in this chapter to define the optimal values for the parameters is the "Multi-parameters". In this approach, all the variables that have been presented in Table 4.1 are optimized simultaneously in a single step.

## 4.4. Results and discussion

In this section, first, the correct implementation of the GA is validated by comparing the outputs with the results provided for the model provided in Chapter 3. Afterward, the

optimizations with both approaches explained in the previous section are followed for different numbers of control sources and different target zones. Lastly, the results of these approaches are compared and discussed.

All the optimization procedures of this chapter are performed with a high-performance cluster with 2 GHz Intel® Xeon® Gold 6138 CPU (with 40 cores), however, the calculations are performed with 10 cores.

### 4.4.1. Model validation

To ensure that the optimization procedure is carried out properly, the outputs of the genetic algorithm are compared with the results provided in Table 3.1. This model contains 10 control sources and 41 error microphones linearly arranged within a zone close to the barrier. The spaces between adjacent transducers are fixed at $d_s = d_e = 0.2$ m.

Table 4.2 represents the optimum positions of transducers together with the achieved insertion loss obtained from the repetitive method and the genetic optimizer.

Table 4.2: Validation of genetic algorithms with Ref. [63].

| $d_{pr}$[m] | $(SS_x, SS_z)$ [m] | $(ES_x, ES_z)$ [m] | $IL_{repetitive}$ [dB] | $IL_{GA}$ [dB] |
|---|---|---|---|---|
| 1 | (-0.5, 0) | (0.5,2.4) | 16.4 | 16.4 |
| 2.5 | (-0.5,1.8) | (0.5,1.1) | 11.9 | 11.9 |
| 4 | (-0.5, 1.8) | (0.5,0.9) | 10.9 | 10.9 |
| 5.5 | (-0.5, 1.8) | (0.4,0.4) | 9.9 | 9.9 |
| 7 | (-0.5, 1.8) | (0.4,0.2) | 9.3 | 9.3 |

Table 4.2 confirms that the GA optimizer performs appropriately and it can find the same transducer positions as presented in Table 3.1. In subsequent computations, the spaces between the transducers ($d_s$ and $d_e$) are considered as the variables during the optimization process.

### 4.4.2. Optimization with the Two-step approach

#### 4.4.2.1. Step 1: Minimization at the observation points

The number of control sources is not a variable in this study since the algorithm always selects the configurations with the most control sources that result in the greatest reduction in the target zone [75,80]. However, in order to investigate the impact of the number of control sources on their optimal locations and the effectiveness of the active noise barrier, optimizations are carried out over a range of control sources ($N_s$) progressively increasing from 2 to 10.

The optimized values for parameters corresponding to control sources ($SS_z$, $SS_x$, and $d_s$) together with average insertion loss at the target zone are shown in Table 4.3. These values are found by GA after the first step of the two-step approach.

Table 4.3: Optimized parameters related to control sources obtained by the Two-step approach at 200 Hz.

| $N_s$ | 2 | 3 | 4 | 5 | 6 | 7 | 8 | 9 | 10 |
|---|---|---|---|---|---|---|---|---|---|
| $SS_z$[m] | 0.5 | 0 | 2.5 | 0.4 | 0.4 | 0.9 | 1.7 | 2.5 | 2.5 |
| $SS_x$[m] | -0.5 | -0.5 | -0.5 | -0.5 | -0.5 | -0.5 | -0.5 | -0.5 | -0.5 |
| $d_s$[m] | 1.5 | 1.0 | 1.3 | 0.5 | 0.5 | 0.5 | 0.5 | 0.5 | 0.5 |
| $IL_{Step\ 1}$[dB] | 3.1 | 4.3 | 8.4 | 12.4 | 12.1 | 17.3 | 15.1 | 21.1 | 20.7 |
| $\text{Time}_{\text{step 1}}$ [h] | 0.8 | 1.0 | 2.2 | 3.4 | 4.1 | 5.2 | 7.4 | 8.6 | 9.6 |

Generally speaking, the higher insertion losses are obtained when the number of the control sources increases, as is reported in the previous studies [75,90]. However, the results presented in Table 4.3 show this general rule may fail if the locations of control sources during the optimization process are limited to specific regions. For instance, the outcome of optimizations at $N_s = 6$, $N_s = 8$, and $N_s = 10$ in Table 4.3 are less than $N_s = 5$, $N_s = 7$, and $N_s = 9$, respectively. Probably, the results for $N_s = 6$, $N_s = 8$, and $N_s = 10$ improve if a wider "Control source" zone or more candidate positions inside this zone are considered.

Additionally, Table 4.3 illustrates that for different numbers of control sources, there is no general trend for the $Z$- coordinate of the secondary sources $SS_z$. On the other hand, the optimal positions of $SS_x$ are always the furthest from the barrier and closer to the noise source.

Previous empirical research [49,71] found that when the distance between the control sources is less than half wavelength, better results are produced, however, Elliot et al. [91] recently demonstrated that this distance should be less than a complete wavelength. In this study, the optimal spaces between the control sources are less than a wavelength ($\lambda = 1.70$ m), which agrees with the previous studies. However, when a few control sources are included in the active control system, the GA outputs reveal that this space can expand more than half a wavelength for better results, but they are always less than a wavelength [91].

#### 4.4.2.2. Step 2: Minimization at the error microphones

In Step 2, the error microphones are used to calculate the strength of the control. Thus, in addition to the location of error microphones, it is important to define the lowest number of error microphones to prevent additional project expenses while ensuring the optimal performance of the active control system. To this end, the optimizations are carried out with different numbers of error microphones $N_e$ for each number of control sources $N_s$. Fig. 4.3 illustrates the average insertion loss at the target zone with $N_s = 3$ and $N_s = 4$ and different numbers of error microphones up to $N_e = 10$. This figure indicates that in the Two-step approach when the position of control sources are fixed, increasing the number of error microphones more than $N_s$+2 has no meaningful effect on the performance of the active noise barrier, because for large values of $N_e$ the error sensors cover the target zone while the

distance between the error sensors $d_e$ is less than the wavelength. Therefore, adding more error sensors will not improve the performance of the active control system.

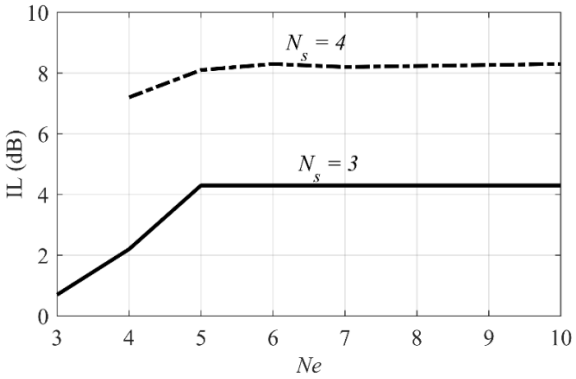


Fig. 4.3: Average insertion loss with different numbers of error microphones.

Therefore, the optimizations are attempted with different numbers of error microphones from $N_e = N_s$ to $N_e = N_s + 2$. The results reported in Table 4.4 show the best outcome of these calculations.

Table 4.4: Optimized parameters related to error microphones obtained by the Two-step approach at 200 Hz.

| $N_s$ | 2 | 3 | 4 | 5 | 6 | 7 | 8 | 9 | 10 |
|---|---|---|---|---|---|---|---|---|---|
| $N_e$ [m] | 2 | 5 | 5 | 5 | 7 | 8 | 10 | 10 | 10 |
| $ES_z$[m] | 2.3 | 2.4 | 0.8 | 2.5 | 2.5 | 2.3 | 2.4 | 1.1 | 1.1 |
| $ES_x$[m] | 0.3 | 0.5 | 0.5 | 0.5 | 0.5 | 0.5 | 0.5 | 0.5 | 0.5 |
| $d_e$[m] | 1.2 | 1.5 | 1.5 | 1.6 | 1.1 | 1.0 | 0.7 | 0.8 | 0.8 |
| $IL_{Step\ 2}$[dB] | 3.1 | 4.3 | 8.1 | 8.4 | 8.1 | 12.5 | 10.0 | 15.7 | 16.0 |
| $\text{Time}_{\text{step 2}}$ [h] | 1.9 | 3.0 | 3.7 | 5.4 | 9.1 | 10.4 | 12.0 | 13.3 | 14.5 |

As it can be observed in

Table 4.4, there is not any defined trend for the location of the error microphones, although the error sensors should be placed as far as possible from the barrier surface like the result obtained for secondary sources. In addition, by comparing the positions of secondary sources and error microphones shown in Table 4.3 and

Table 4.4, it is clear that the optimum positions of error microphones are close to the top edge when the control sources are placed close to the ground surface. In contrast, when the control sources are located near the top edge, the GA found the optimum positions of error microphones at a height close to 1.0 m. Furthermore, the comparison of Table 4.3 and Table 4.4 clearly shows that the average insertion loss obtained by the active control system with error microphones at the actual points of interest (observation points) is higher than a setup with error microphones far from the target zone, which is an expected result. This reduction of performance is more evident for a system that includes more control sources.

To demonstrate how the active control system reduces the noise levels behind the barrier it is interesting to see the noise reduction at all shadow zone [63,92,105].

Fig. 4.4 illustrates the distributions of insertion loss at different heights when 10 control sources are placed in the position presented in Table 4.3 and the error microphones are located at the positions of Table 4.4. This figure shows that although the target zone (rectangular dash) is a restricted area of size 8×10 $m^2$, the active control system reduces the noise level at the other areas.

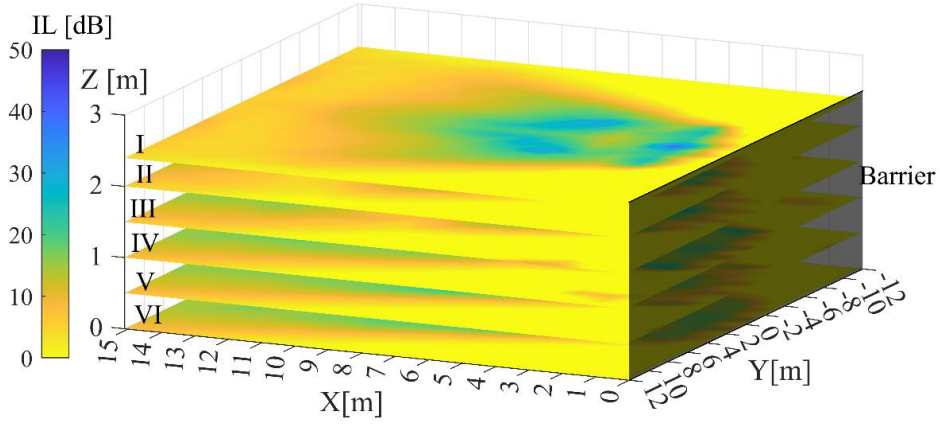

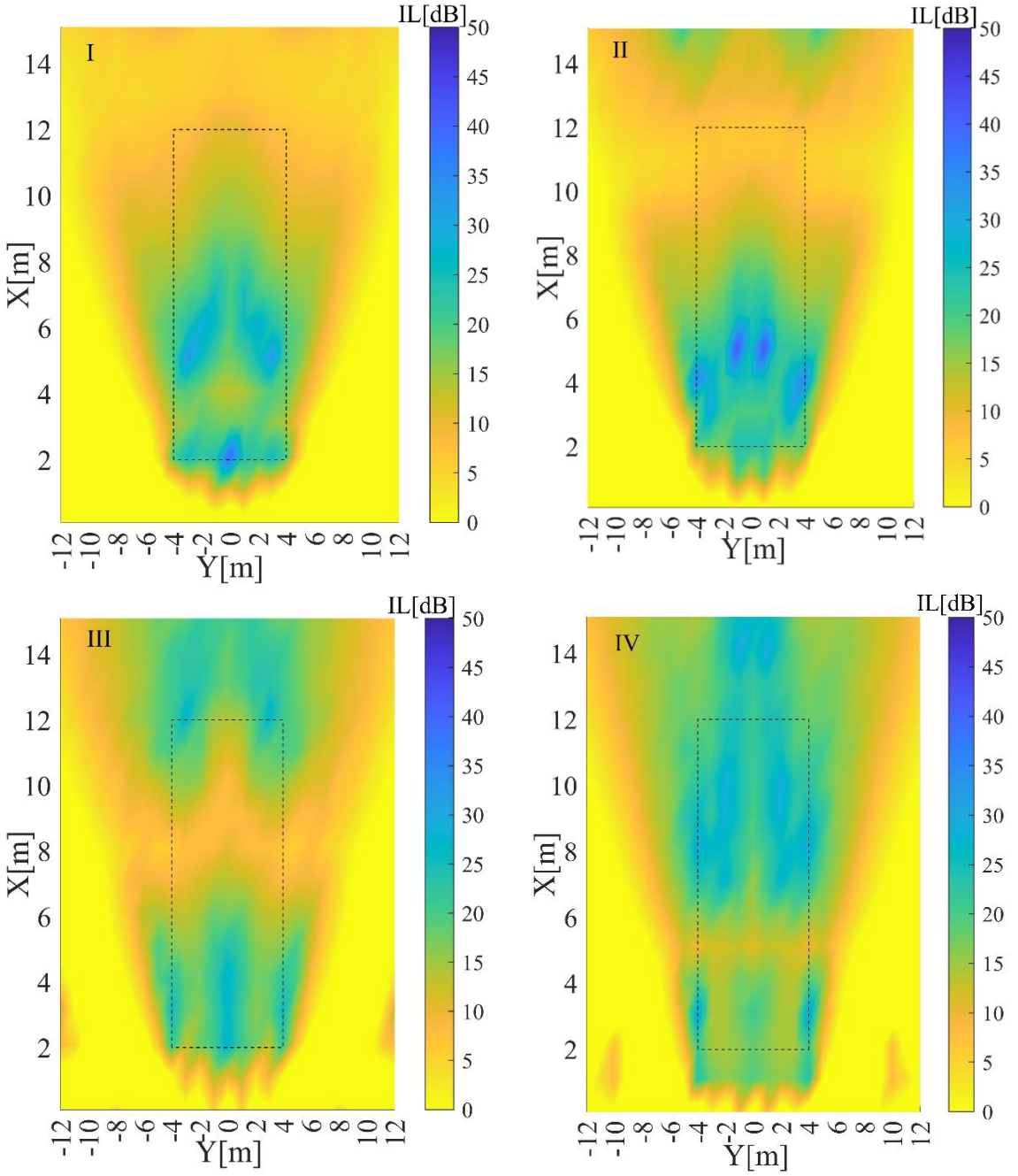
I
II
III
IV
IL[dB]
X[m]
Y[m]

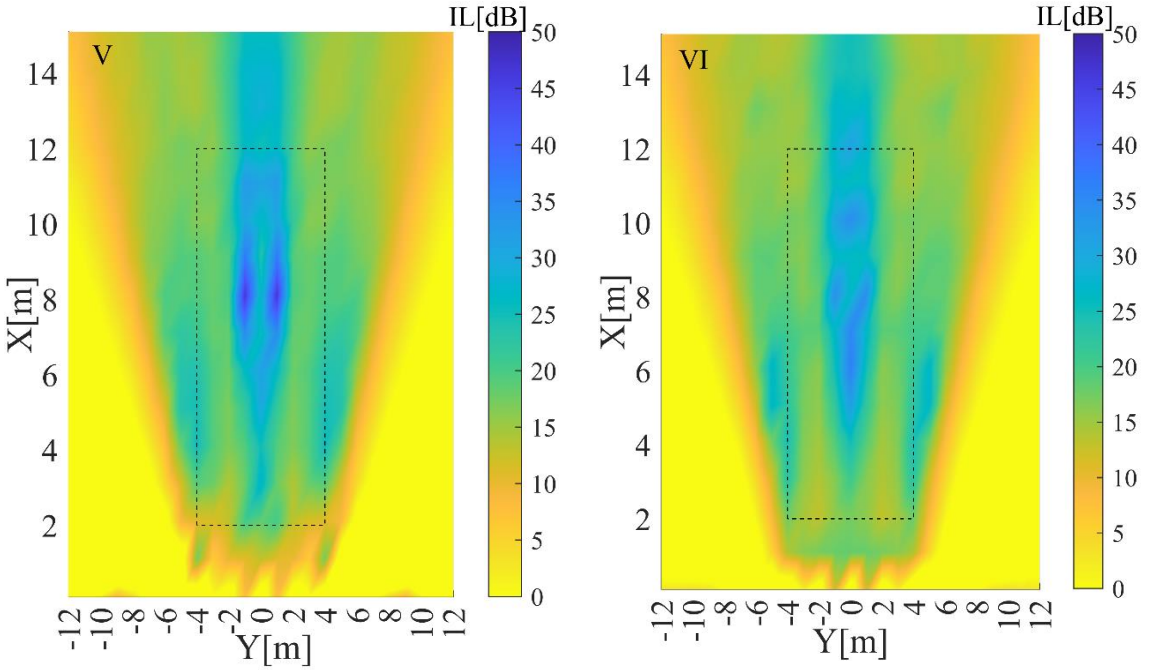


Fig. 4.4: Distribution of *IL* [dB] in the shadow zone of the barrier at different heights, with the optimized configuration of the Two-Step approach for $N_s = 10$. (I): 2.5 m, (II): 2.0 m, (III): 1.5 m, (IV): 1.0 m, (V): 0.5 m, (VI): on the ground. The rectangular dash illustrates the target zone.

### 4.4.3. Optimization with the Multi-parameters approach

The optimizations with this approach are done by considering all the parameters corresponding to control sources and error sensors positions ($SS_x$, $SS_z$, and $d_s, N_e, ES_x$, $ES_z$, and $d_e$) except for the number of control sources, that have been fixed at each calculation. The boundary limits for the positions follow the ones described in Table 4.1. The lower boundary limit for the number of error sensors ($N_e$) is the same as the number of control sources ($N_s$), and the upper boundary limit is 20, corresponding to twice the maximum number of control sources. The GA outputs for the optimization of all these parameters are presented in Table 4.5.

Table 4.5: Optimal values for parameters with the Multi-parameters approach at 200 Hz.

| $N_s$ | 2 | 3 | 4 | 5 | 6 | 7 | 8 | 9 | 10 |
|---|---|---|---|---|---|---|---|---|---|
| $SS_z$[m] | 0.5 | 0 | 2.5 | 0.1 | 0.2 | 0.1 | 2.4 | 2.5 | 2.4 |
| $SS_x$[m] | -0.5 | -0.5 | -0.5 | -0.5 | -0.5 | -0.5 | -0.5 | -0.5 | -0.5 |
| $d_s$[m] | 1.5 | 1.0 | 1.3 | 0.9 | 1.1 | 0.5 | 1.1 | 0.8 | 0.7 |
| $N_e$ [m] | 8 | 8 | 10 | 8 | 13 | 16 | 19 | 16 | 10 |
| $ES_z$[m] | 2.5 | 2.3 | 0.9 | 2.3 | 2.2 | 2.3 | 1.0 | 1.1 | 1.1 |
| $ES_x$[m] | 0.5 | 0.4 | 0.5 | 0.5 | 0.4 | 0.5 | 0.5 | 0.5 | 0.5 |
| $d_e$[m] | 0.4 | 0.9 | 0.7 | 0.9 | 1.1 | 0.5 | 0.4 | 0.5 | 0.9 |
| $IL$[dB] | 3.1 | 4.3 | 8.3 | 9.7 | 10.7 | 14.6 | 13.3 | 16.7 | 16.9 |
| Time [h] | 6.7 | 9.5 | 10.6 | 12.5 | 13.0 | 14.4 | 15.4 | 18.5 | 21 |

The results show that the optimum $X$-coordinates of control sources ($SS_x$) and error microphones ($ES_x$) are mostly at the farthest position from the barrier's surface, and that the system with few control sources may perform better to suppress the noise when the spaces between them are less than the wavelength $d_s < \lambda$, the same result as obtained in the two-step calculations and are supported by previous studies [90,91].

On the other hand, the positions obtained by the Multi-parameters approach (Table 4.5) are different from those achieved by the Two-step approach (

Table 4.4). In the Multi-parameters approach, the span of control sources' and error microphones' distribution are greater than the Two-step approach and also more error microphones are used.

Another set of optimizations is performed with fewer error microphones. In this case, the optimizations are performed by a specific value for error microphones starting from $N_e = N_s$ and then progressively increasing the number of error microphones. The procedures are finished when the increase of attenuation due to the addition of one error sensor is less than 0.5 dB. The outputs of these calculations are presented in Table 4.6.

Table 4.6: Optimal values of variables with the Multi-parameters approach at 200 Hz.

| $N_s$ | 2 | 3 | 4 | 5 | 6 | 7 | 8 | 9 | 10 |
|---|---|---|---|---|---|---|---|---|---|
| $SS_z$[m] | 0.5 | 0 | 2.5 | 0.1 | 0.8 | 2.2 | 1.3 | 2.4 | 2.4 |
| $SS_x$[m] | -0.5 | -0.5 | -0.5 | -0.5 | -0.5 | -0.5 | -0.4 | -0.4 | -0.5 |
| $d_s$[m] | 1.5 | 1.0 | 1.3 | 0.9 | 1.1 | 0.5 | 1.1 | 0.8 | 0.7 |
| $N_e$ [m] | 2 | 5 | 5 | 8 | 6 | 9 | 10 | 11 | 10 |
| $ES_z$[m] | 1.4 | 2.4 | 0.7 | 2.3 | 2.3 | 0.4 | 0.2 | 1.0 | 1.1 |
| $ES_x$[m] | 0.1 | 0.5 | 0.5 | 0.5 | 0.4 | 0.5 | 0.2 | 0.4 | 0.5 |
| $d_e$[m] | 0.9 | 1.5 | 1.4 | 0.9 | 1.0 | 0.9 | 1.1 | 0.8 | 0.9 |
| $IL$ [dB] | 2.8 | 4.2 | 8.1 | 9.7 | 10.3 | 12.9 | 13.0 | 16.7 | 16.9 |
| Time [h] | 1.8 | 2.4 | 2.8 | 3.6 | 5.3 | 6.8 | 8.0 | 9.4 | 11.3 |

Table 4.6 demonstrates that with fewer error microphones but larger distances of $d_e$, the active control systems can work as efficiently as the benchmark case presented in Table 4.5. Also, the distance between control sources $d_s$ is the same for both sets of optimizations, showing that the optimum distance for $d_s$ is independent of the number and positions of error microphones, as shown in Tables 4.5 and 4.6.

Comparing the average insertion losses of

Table 4.4 and Table 4.6 shows that with the same number of error microphones the configuration of the Multi-parameters approach is more efficient than the Two-step approach, especially when the number of secondary sources increases. Also, because the Multi-parameters technique has fewer generations than the Two-step approach, less computational effort is required with this method.

The distributions of insertion loss are provided in Fig. 4.5 while the transducers are located at the optimal positions presented in Table 4.6 for $N_s = 10$. The rectangle dash in this figure displays the boundaries of the target zone. This figure clearly shows that an active control system with the optimized configuration of the Multi-parameters approach may reduce the

noise level on a wider area (at the same plane) than the configuration found by the Two-step method.

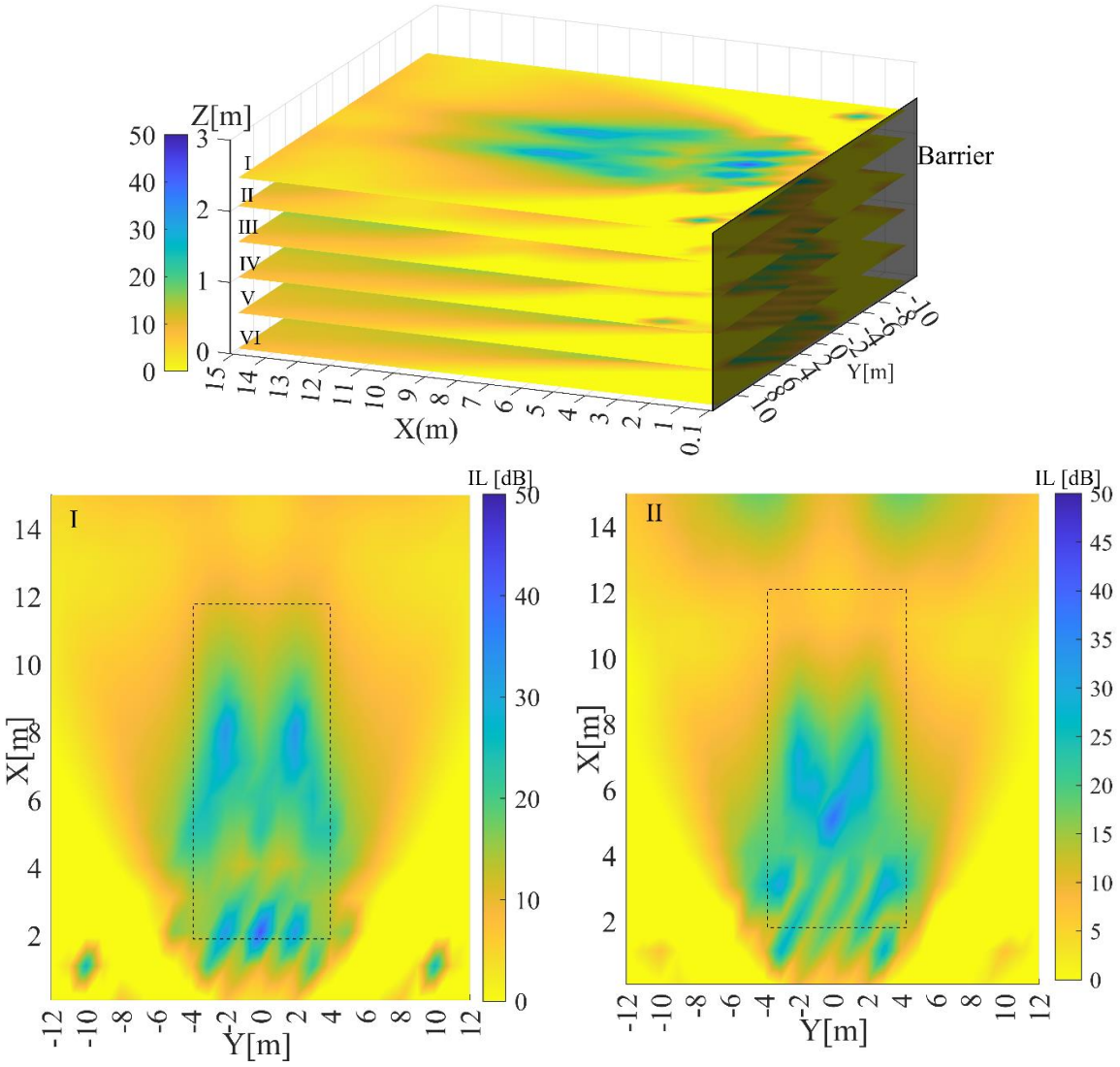

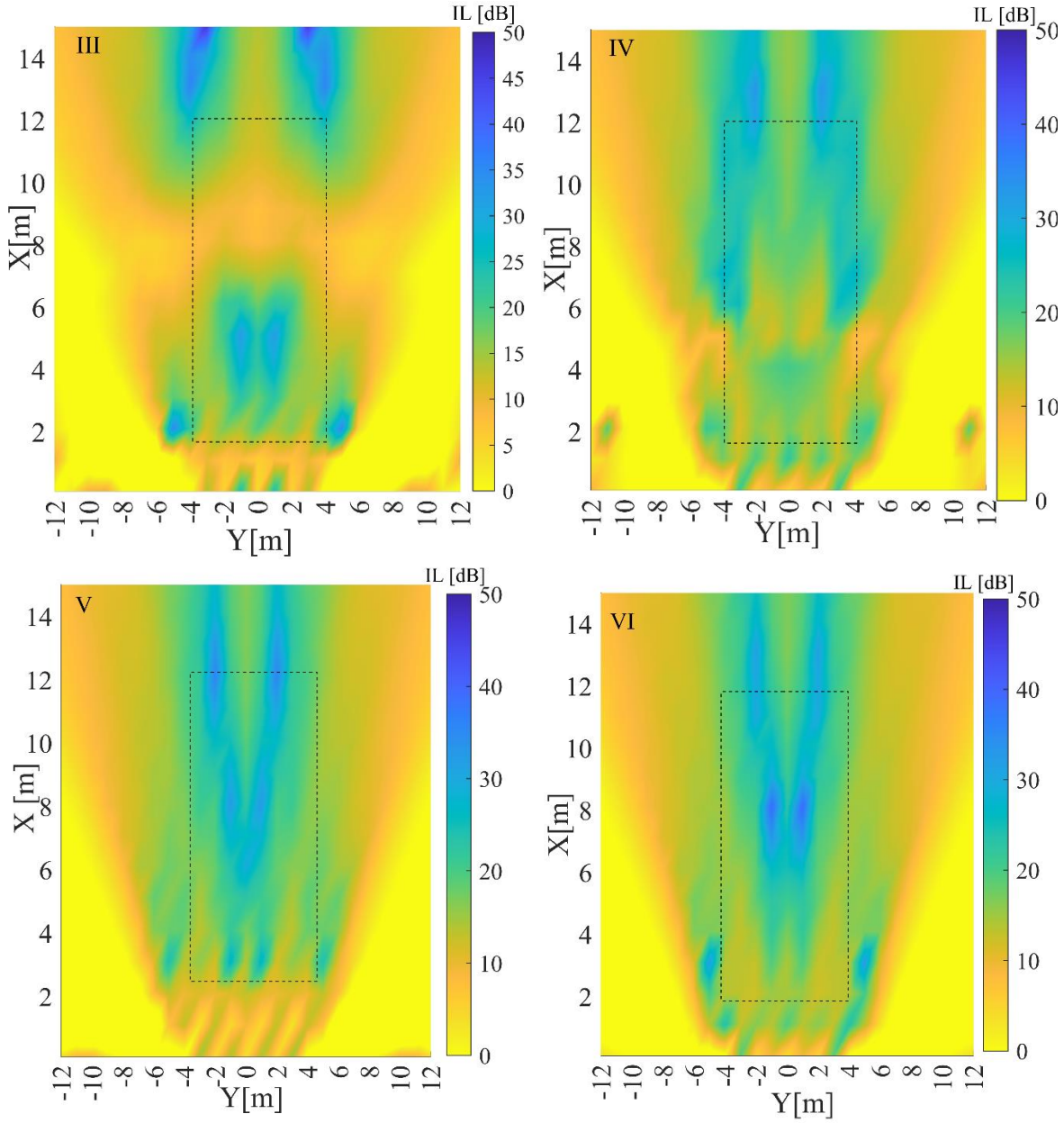


Fig. 4.5: Distribution of *IL* [dB] in the shadow zone of the barrier at different heights, with the optimized configuration of the Multi-parameters approach for $N_s = 10$. (I): 2.5 m, (II): 2.0 m, (III): 1.5 m, (IV): 1.0 m, (V): 0.5 m, (VI): on the ground. The rectangular dash illustrates the target area.

### 4.4.4. Size of the target area

An optimization study considering a wider target zone can be interesting to address the effect of the size of the target area on the optimized parameters, especially the distance between transducers. To this end, the optimizations with the same boundaries for the parameters as

mentioned in Table 4.1 are conducted with the Multi-parameters method for a wider target zone. The size of the new target area in the shadow zone is 10×16 $m^2$ as illustrated in Fig. 4.6. This target zone is covered with 27 observation points which is the same density as the previous one.

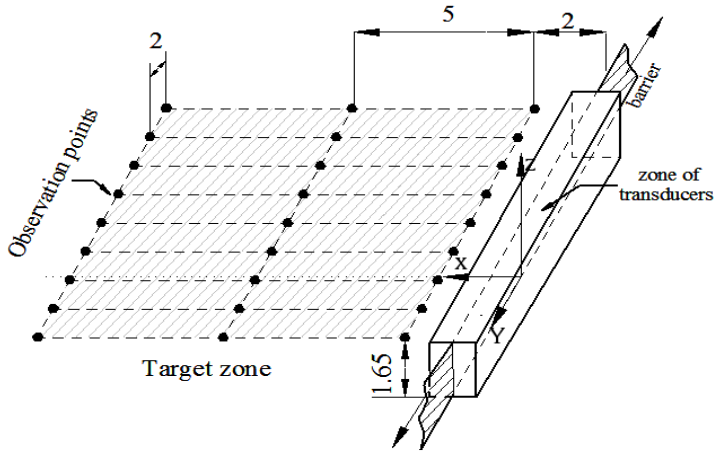


Fig. 4.6: Target area size of 10×16 $m^2$. Units are in meters.

The results of the GA for this target area are presented in Table 4.7.

Table 4.7: Optimal values of variables with 10 control sources, found by the two-step at 200 Hz
(area of target zone 10×16 $m^2$).

| $N_s$ = 10 | | | |
|---|---|---|---|
| $N_e$ | 10 | 11 | 12 |
| $SS_z$[m] | 0.2 | 1.0 | 0.3 |
| $SS_x$[m] | -0.5 | -0.5 | -0.5 |
| $d_s$[m] | 0.7 | 0.6 | 0.6 |
| $ES_z$[m] | 2.3 | 2.3 | 2.3 |
| $ES_x$[m] | 0.5 | 0.5 | 0.5 |
| $d_e$[m] | 1.1 | 1.1 | 1.0 |
| *IL* [dB] | 11.3 | 10.9 | 11.5 |

Although changing the target zone may impact the optimal locations of the transducers, the distances between the control sources $d_s$ and error microphones $d_e$ do not change significantly, as shown in Tables 4.6 and 4.7. Probably optimal values of these distances are more dependent on the position of the noise source than the size of the target zone. Fig. 4.7

demonstrates the distribution of insertion loss behind the barrier when the target zone is the size of 10×16 $m^2$ and the coordinate components of control sources are $SS_z$= 0.3 m, $SS_x$= -0.5 m, and $d_s$= 0.6 m and for the error sensors are $ES_z$= 2.3 m, $ES_x$=0.5 m, and $d_e$= 1.0 m.

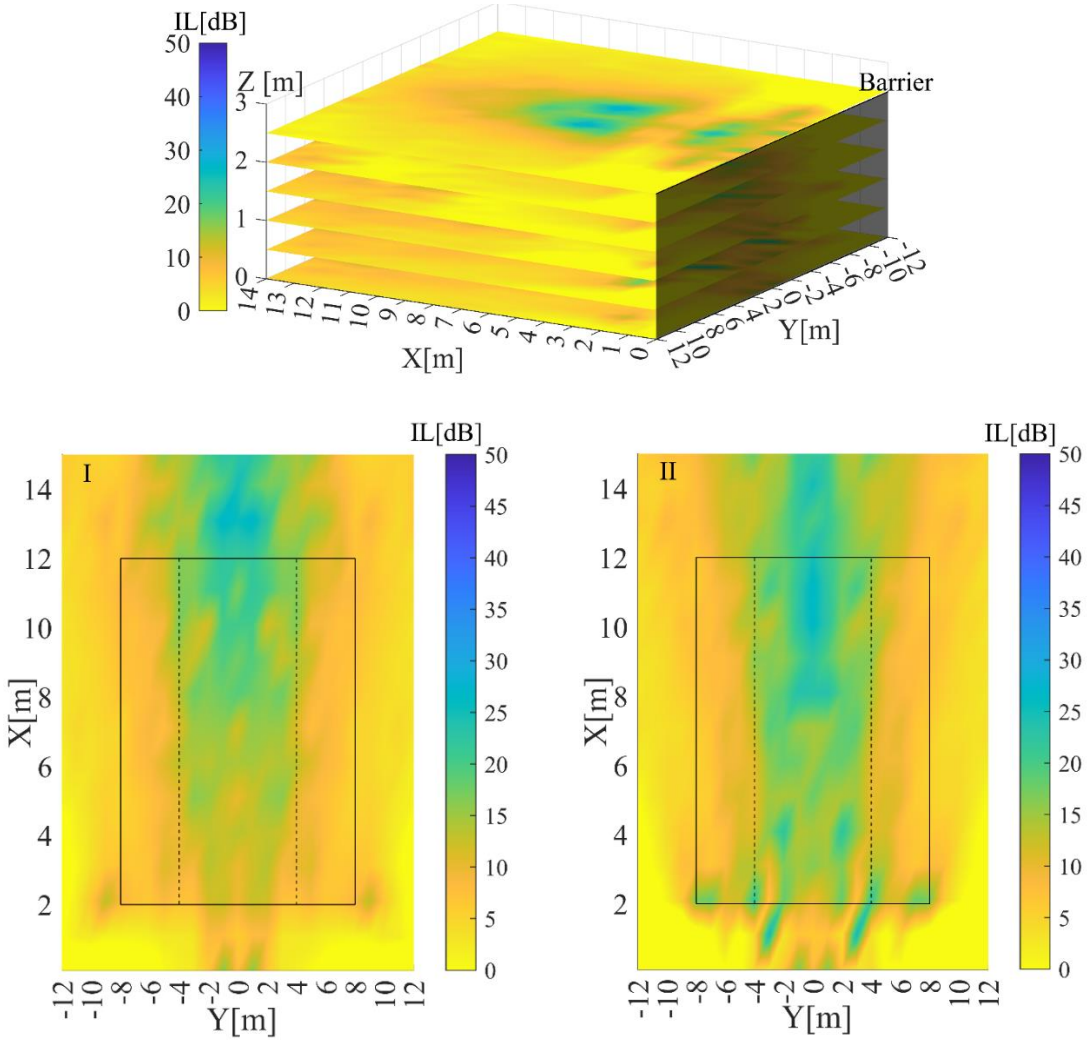

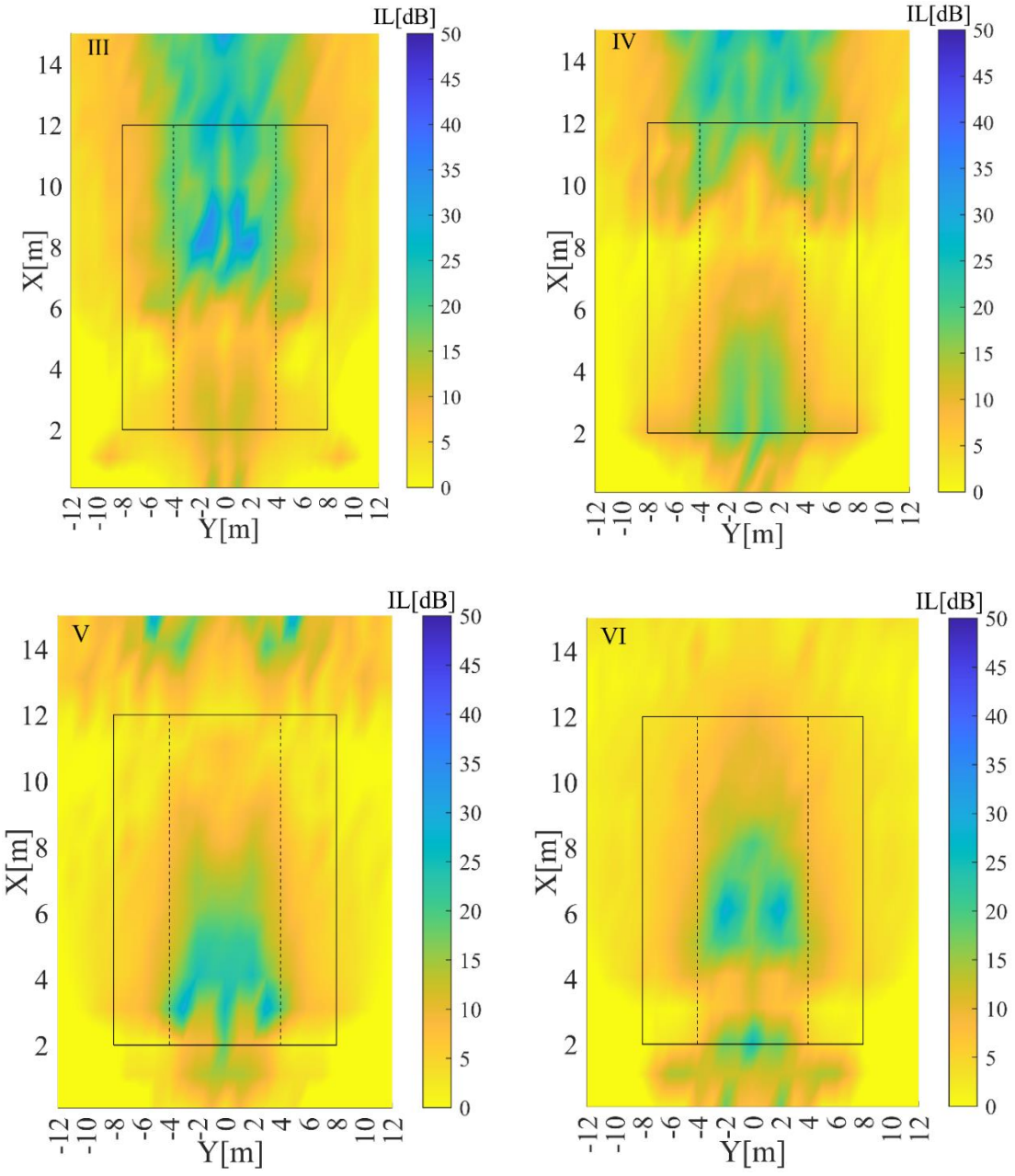


Fig. 4.7: Distribution of insertion loss at planes with different heights behind the barrier when the target zone is the size of 16×10. (I): 2.5 m, (II): 2.0 m, (III): 1.5 m, (IV): 1.0 m, (V): 0.5 m, and (VI): 0 m. dash and solid rectangles show the boundaries of the target area of size 8×10 and 16×10 respectively.

The comparison of Fig. 4.7 and Fig. 4.4 illustrates that when the target zone is broader, the insertion losses at different heights of the shadow zone are more homogeneous, but the values of $\bar{IL}$ decrease, which is an expected result.

Table 4.8 compares the average insertion at different areas when the target zone changes. This table confirms that the noise cancellation at a wider target region can result in reductions in other narrow areas as well.

Table 4.8: Average insertion loss in different areas.

| Target zone | $\overline{IL}$ [dB] at 8×10 [$m^2$] | $\overline{IL}$ [dB] at 16×10 [$m^2$] |
|---|---|---|
| 8×10 [$m^2$] | 16.9 | -1.8 |
| 16×10 [$m^2$] | 12.0 | 11.5 |

## 4.5. Conclusion

In this chapter, the optimizations are performed with the genetic algorithm to improve the efficiency of the active noise barrier, and it is shown that the GA optimizer can find similar configurations as the repetitive method when the parameters are the same.

Two approaches followed to define the optimal values for the parameters that affect the performance of the control system: Two-step and Multi-parameters approaches. The Multi-parameters approach is preferable because (1) it requires less computation effort, (2) higher reduction obtained at the target zone with the same number of control sources, and (3) the noise level reduces in a wider area in the shadow zone when the parameters are defined by the Multi-parameters approach.

Also, whatever the optimization approach, using the error microphone far from the target zone reduces the performance of the active control system. This decrease in performance is more noticeable when the active control system contains more than 4 control sources. For example, the average insertion losses reduce by 5.4 dB and 4.7 dB when $N_s = 9$ and $N_s = 10$, respectively. Furthermore, the results show that the spacing between adjacent control sources should increase by more than half of the noise wavelength to achieve higher performance when a few control sources are used in the active control system.

Moreover, in the Two-step approach, the optimum positions of error microphones are close to the top edge when the control sources are placed close to the ground surface. In contrast, when the control sources are located near the top edge, the GA found the optimum positions of error microphones at a height close to 1.0 m. This trend may change when the optimization performs with the Multi-parameter approach.

The optimization of parameters for different sizes of target zones illustrates that the optimal value for the distance between error microphones $d_e$ depends on the width of the target zone, however, the space between control sources $d_s$ did not change significantly when the size of the target zone changed.

# *Chapter 5 : Active noise control of open windows*

## 5.1. Introduction

Several methods have been proposed to control the noise passing through the windows in urban areas, including employing an active noise control system in double glazed windows [124,125], plenum windows [126–128], and perforated panels [129–131]. However, these solutions block or reduce ventilation, and thus in hot or humid regions, they are less appealing. Active noise control for open windows is another method that could provide acoustic shielding and ventilation simultaneously.

In prior researches, two arrangements have been widely used for the location of control sources and error microphones for the active noise control of open windows. These arrangements include the boundary control, which places the control sources on the frame of the windows [132–136], and the planar arrangements [137–139] with the control sources located on the surface of the apertures.

Huang et al. [132] showed that for a staggered window, the best position for the control sources is in the center at the bottom. In their study, they employed the mode expansion technique and the coupled cavities theory to solve the sound field inside the natural ventilation window and the room. Their setup achieved 10 dB reductions at the observational points inside the room.

Kwon et al. [133] proposed an active control system with a feedforward method to reduce the exterior traffic noise entering a room. In their system, the control sources were located on the frame of the window, inside the room, and the error microphones were placed outside the room. The cut-off frequency for their proposed single-channel system was 390 Hz, but it could be increased to 420 Hz using a double-channel ANC system. A study on active noise control for sliding windows and a so-called “Active labyrinth” with control sources on the

frame of the window was conducted by Carme et al. [140,141]. Their results showed that a combination of passive and active control systems gave a broadband reduction of around 15 dB for both types of windows.

More recently, Wang et al. [134] investigated single and double layer arrangements for the control system on the boundary of the windows, and the cancellation mechanisms were explained using the modal decomposition method [135]. Their findings showed that the double-layer arrangement had a better performance than a single layer because secondary sources at the edge of the single layer cannot excite some modes effectively while those at the other height in the double layer compensate for it. Furthermore, it was demonstrated that a planar virtual sound barrier (PVSB) had better performance than the edge arrangement, as with this setup, the secondary sources were closer to the nodal lines of some modes. Further, in another study, different positions of control sources in the boundary of the windows and incident angles of the primary source were analytically modeled to evaluate the performance of the active noise windows [70,136]. The cut-off frequency depended on the shortest side of the opening. It was also shown that when the number of secondary sources is small or the opening is narrow, the output of the boundary control system may be superior to that of the surface control system. Further, the performance of the boundary control system did not differ significantly for oblique incidence with high incident angles.

On the other hand, different attempts have been made to control the noise passing through apertures by locating the control units on the surface of openings. The application of a single-input single-output (SISO) active noise control for open bottom hinged windows was measured by Pamies et al. [50]. Their setup achieved a 3 dB reduction inside the room. Shi et al. [137] used centralized and decentralized open-loop [142] for the implementation of the ANC system to cope with the computational complexity. Their results demonstrated that the

centralized control does not guarantee to outperform the decentralized inverter whilst the decentralized inverter has obvious advantages in computational complexity and scalability. Murao et al. [143] proposed to use the mixed-error approach to reduce the computational complexity of a multi-channel active noise control (MCANC) system. This approach simplifies an MCANC system to a single-channel ANC system that takes the summed output of an error microphone array as the error signal [144]. Their method led to a similar global noise reduction performance as the MCANC for open windows but with the lowest computational complexity.

Another study showed that for a normal incident plane wave the control system performed well when the separation distance between uniformly-spaced sources was less than the wavelength [138,145], i.e. active windows with uniformly distributed control sources have good performance for the frequencies up to $f = c_0 / d$, where $d$ is the distance between control sources and $c_0$ is the speed of sound.

Lam et al. [54,139] defined the physical limits of an effective noise control system for the open windows by considering various configurations for the control sources. Their study suggested that positioning the control sources away from the edges of the window results in maximum attenuation, and for practical implementations, the least degradation in the efficiency of the control system is achieved when the control sources are located centrally in the depth of the walls. They also showed that the number of control sources depends on the dominant angle of the incident and the sound wavelength. Considering the previous studies, the objective of this chapter is to compare two planar and boundary arrangements and find suitable positions for control sources and error microphones.

The objective of this chapter is to propose a proper configuration for the control units of an active noise control window. To this end, the diffraction model of Svensson [26] is used to

study different scenarios for the location of transducers in an active noise window. Finally, the arrangement which achieves the highest reduction is proposed as the best configuration.

### 5.2. Diffraction of finite edges

There are several methods that estimate the diffraction of finite edges. In 1978, Thomasson [146] proposed a method for calculating the insertion loss (IL) of a finite barrier on the ground, focusing on the interference phenomenon. This model was based on the Kirchhoff-Helmholtz integral formulation and physical-optic assumptions. The calculation of this model was considerable time demanding when the source and/or receiver are close to the barrier, which is a frequent case in practical situations. Medwin [22] suggested calculating the insertion loss of a finite length barrier using a separate Huyghens-Fresnel interpretation of the diffraction results. He computed the impulse response using the Biot-Tolstoy theory [21] and by positioning a series of small secondary sources along the edge and changing their strengths so that together they provide the known exact solution. This approach also needs significant computation effort.

In 1999 Svensson et al. [23] developed the method proposed by Medwin [22] based on the concept of secondary edge sources. Their model accurately estimates the first- and second-order diffraction. In 2013, Asheim and Svensson [26] presented a formulation for the scattering of obstacles with edges. In the following, a brief explanation of this formulation is described.

The diffraction wave from an infinite wedge can be written as a line integral along the edge with an integrand which includes spherical divergence factors as well as analytical directivity factors and with the position along with the physical wedge as integration variable [23]. The diffraction of a finite wedge is computed by adjusting the integration range to the physical

finite edge. Assuming the source strength, the diffracted field from a point source $S$ at a receiver location $R$ (Fig. 5.1) is represented by the integral below.

$$P_{\text{diffracted}} = -\frac{\nu}{4\pi}\int_{z_1}^{z_2}\frac{\mathrm{e}^{-jkr_{R,z}}}{r_{R,z}}\frac{\mathrm{e}^{-jkr_{Z,S}}}{r_{Z,S}}\beta(R,z,S)dz \tag{5.1}$$

where $r_{a,b}$ denotes the Euclidean distance between points $a$ and $b$, and $\nu$ is wedge index and equals to $\nu = \frac{\pi}{\theta_W}$ which $\theta_W$ is the wedge angle formed by the two wedge planes (Fig. 5.1). The function $\beta(R,z,S)$ is the directivity function and expressed by

$$\beta(R,z,S) = \sum_{i=1}^{4}\frac{\sin(\nu\emptyset_i)}{\cosh(\nu\eta)-\cos(\nu\emptyset_i)} \tag{5.2}$$

where the angles $\emptyset_i$ are

$$\begin{aligned}\emptyset_1 &= \pi+\theta_S+\theta_R, \qquad \emptyset_2 = \pi-\theta_S+\theta_R\\ \emptyset_3 &= \pi-\theta_S-\theta_R, \qquad \emptyset_4 = \pi-\theta_S-\theta_R\end{aligned} \tag{5.3}$$

The angles $\theta_S$ and $\theta_R$ refer to the angle between the planes containing the edge and $S$, and $R$ and a reference wedge plane, respectively, as illustrated in Fig. 5.1.

The function $\eta$ is an auxiliary function [26]

$$\eta = \cosh^{-1}\frac{\cos\emptyset_S\cos\emptyset_R+1}{\sin\emptyset_S\sin\emptyset_R} \tag{5.3}$$

where the angles $\emptyset_S$and $\emptyset_R$ refer to the angle between the edge and $S$ and $R$, respectively, which is also illustrated in Fig. 5.1.

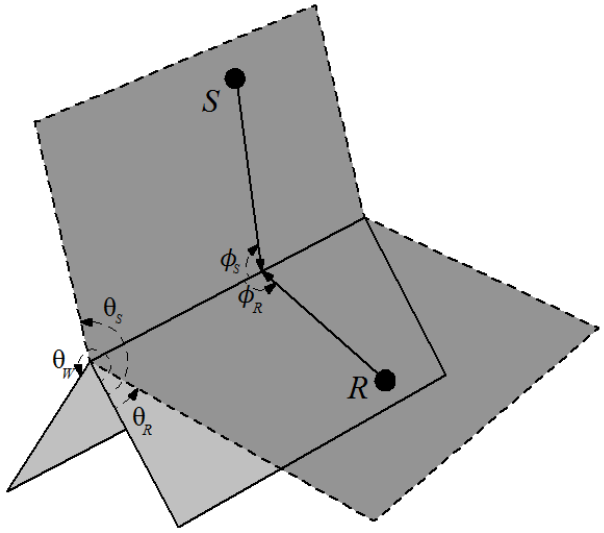


Fig. 5.1: A Single wedge [26].

In the following sections, a MATLAB toolbox called "ED-toolbox" [147] is used to compute the diffracted pressure based on Svensson's model. This model is used in various studies [23,26,148] for computing the diffraction of finite length edges.

### 5.3. Method

For an active noise control window, the sound pressure at a receiver is the superposition of a primary field and a secondary field, which is the contribution of secondary sources. In this study, we decompose the propagation through the aperture into a direct wave and diffracted waves, caused by the aperture's edges. Fig. 5.2 shows a 2D view with an aperture in a wall, a single sound source, and snapshots of the direct sound, reflection, and first-order diffraction wavefronts. A receiver that is on the opposite side of the wall (than the sound source) will be reached by four first-order diffraction waves, from the four edges of an aperture. If the receiver locates inside the visibility zone of the direct sound, indicated by thin dashed lines in Fig. 5.2, then also a direct sound is added to the received sound field. For a receiver on the

source side of the wall, there might be a reflection wave as well, if the receiver is in a visibility zone of the reflection. The direct sound, reflection, and diffraction waves are computed by the Matlab ED-toolbox [147] which is based on Svensson's model for finite edges [26].

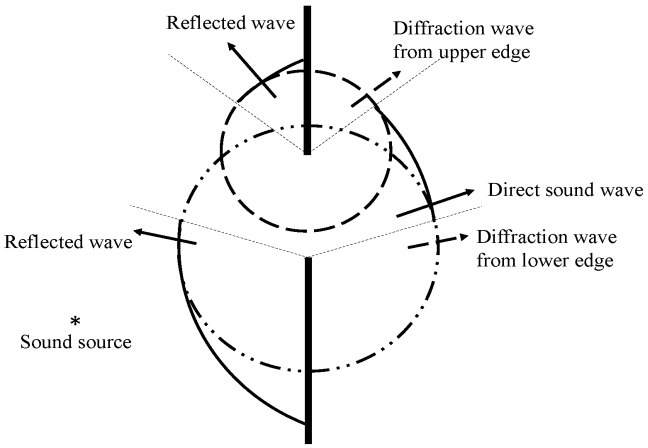


Fig. 5.2: 2D view of an opening in a thin wall and a single sound source. Snapshots are shown for the direct sound wave, which reaches only a limited visibility zone on the opposite side of the wall; the reflected sound wave which also reaches a limited visibility zone on the source side of the wall; and two diffraction waves that reach everywhere. The diffraction wavefronts undergo polarity switches at the visibility zone boundaries, indicated by thin dashed lines.

In this study, a square opening of size $1 \times 1$ m$^2$ in a thin and infinite rigid baffle is simulated and the objective is to reduce the average sound pressure level at several observation points behind this opening by active noise control means. Fig. 5.3 shows a schematic diagram of the opening and the half-sphere where the observation points are placed. The baffle is positioned at $z = 0$, and a plane wave with the incident angle of $\theta_i$ (in Y-Z plane) is considered as a primary noise field.

A spiral pattern on a half-sphere was chosen for the observation points to allow straightforwardly change the number of observation points [149,150], and to measure the radiated sound from the aperture in all directions, as well. In the further calculations, 100

observation points with the distance of $R$ = 5 m from the center of the apertures are considered (Fig. 5.3 (b)) to compute the average insertion loss at each frequency by using Equation 2.9.

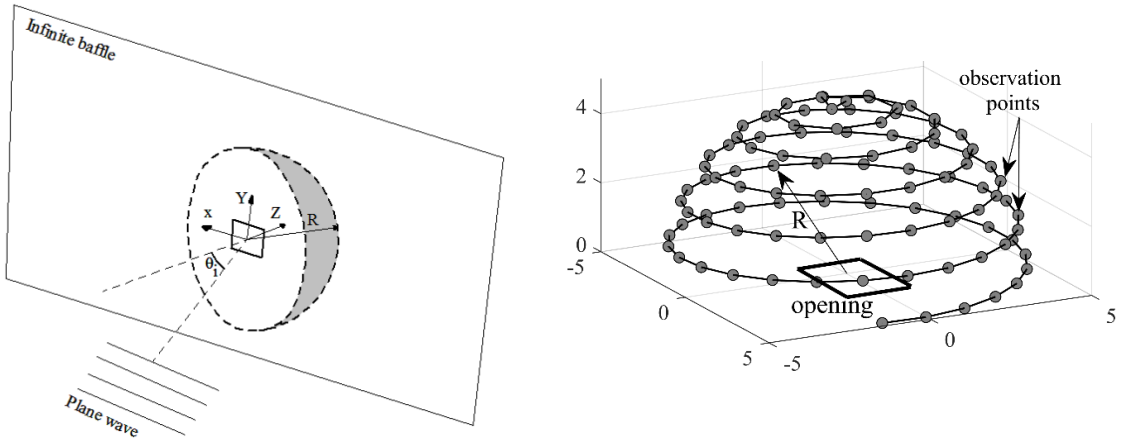


(a) (b)

Fig. 5.3: Geometry of (a) the opening in an infinite baffle and (b) the observation points on the half-sphere.

Following the previous chapters, the two-step approach is employed to define the best locations for the control sources and the error microphones of an active noise control window. In the first step, the objective is to compare different configurations for the control sources and specify the suitable one which more efficiently minimizes the potential energy directly at the observation points. To follow this step, five candidate arrangements are proposed for the placement of control sources. In order to evaluate the frequency impact on the performance of each arrangement, the calculations are performed for the frequencies of 100 Hz, 200 Hz, 300 Hz, and 500 Hz.

The proposed candidate arrangements for control sources are:

(1) The first arrangement (Set 1) is defined based on the findings of previous chapters for the active noise barrier that suggests the suitable locations for the control sources are on the incident side, and below the edge of the barrier [63]. According to this conclusion, the control sources are linearly arranged at the distance $r_{ss}$ from the center of the opening and

with the angle of $\theta_{ss}$ (see Fig. 5.4), and its performance is assessed for different $r_{ss}$ and $\theta_{ss}$. This setup is proposed to cancel the diffracted field.

(2) Set 2 is the second candidate arrangement for the control sources. This arrangement includes control sources that are linearly placed perpendicular to the opening face and on the incident side with a distance of $d_{ss}$ from the center of the opening. This setup is proposed to cancel the direct field and support the active control system to have better performance at the plane waves with the incident angles close to perpendicular to the opening's surface. The efficiency of this setup is measured for different incident angles and different $d_{ss}$.

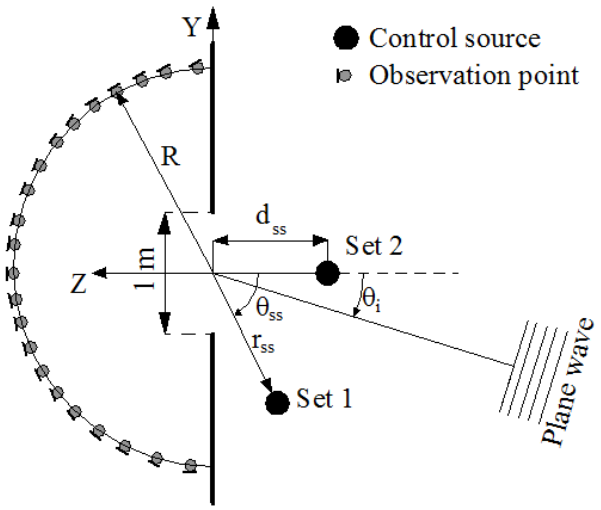


Fig. 5.4: Candidate arrangements for the control sources.

(3) The third candidate arrangement for the position of control sources is the combination of Set 1 and Set 2. This arrangement is proposed to have both the direct and diffracted cancellation at the same time. With this arrangement, the number of control sources at Set 1 and Set 2 is half of the case when the single set is used. So the total number of control sources with this arrangement is the same as the others.

(4) The fourth candidate arrangement for the control sources is boundary arrangement, which is selected based on the previous studies [134–136,151], see Fig. 5.5 (a). In this arrangement, the control sources are installed along the edge of the opening.

(5) The last candidate configuration for the control sources is the planar arrangement, shown in Fig. 5.5(b). This arrangement is widely used in previous studies [54,91,138,139,145,152,153].The control sources with this arrangement are distributed on the surface of the opening.

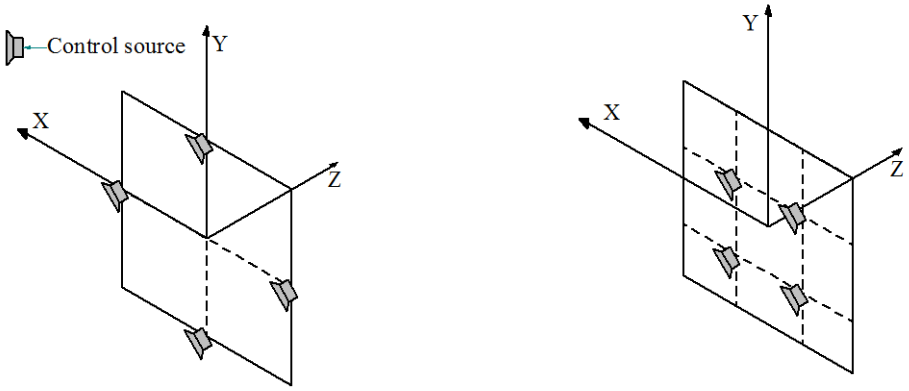


(a) (b)

Fig. 5.5: (a) boundary and (b) Planar arrangements of control sources.

The impacts of different parameters on the performance of active control systems with these proposed arrangements are studied. Then, their performances are compared and the one that obtains the maximum reduction is selected for the control sources.

In the second step, the suitable position for the error microphones will be defined while the control sources are placed at the selected position of the previous step. Throughout this study, three arrangements are proposed for the placement of the error microphone, and the one that achieves the highest noise reduction at the observation points is selected. The proposed candidate arrangements for error microphones are:

(1) The first arrangement suggested for the location of error microphones is the combination of Set 1 and Set 2. With this arrangement, the error microphones in Set 1 are linearly arranged at the distance $r_{es}$ from the center of the opening and with the angle of $\theta_{es}$ and the error microphones in Set 2 are linearly placed perpendicular to the opening face with a distance of $d_{es}$ from the aperture, shown in Fig. 5.6. In this study, the performance of the active control system with this arrangement is measured for three configurations, including the error microphones in Set 2 (a) on the receivers' side, (b) on the aperture's surface, and (c) on the incident side. In all of these three configurations, the error microphones in Set 1 are placed on the receivers' side to reduce the diffracted field.

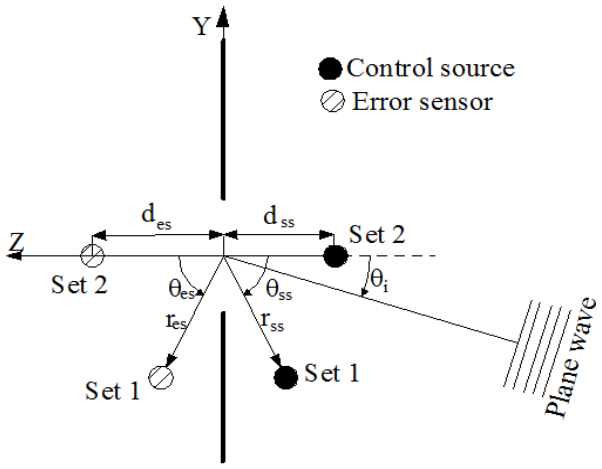


Fig. 5.6: Error microphones are placed in the position of Set 1 and Set 2.

(2) The second arrangement for the error microphones is the boundary control. In this arrangement, the control sources are placed on the edge of the opening and the error microphones are always placed aligned with the control sources at a certain distance from them. The error microphones can be located on the receivers' side or the incident side, which are represented in Fig. 5.7 (a) and Fig. 5.7 (b), respectively,

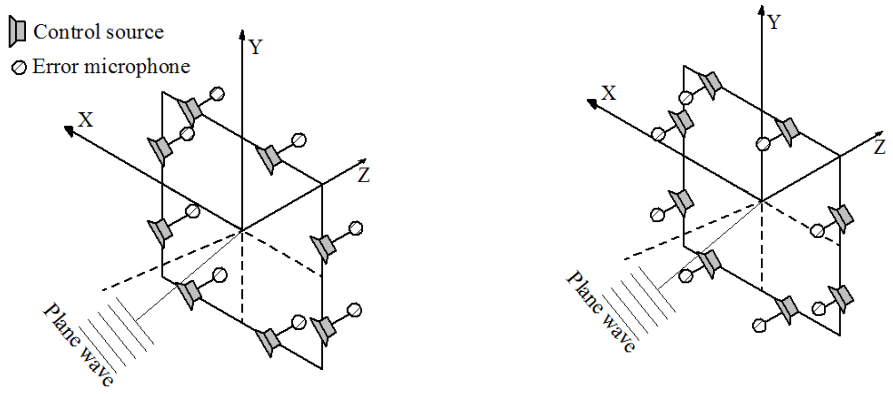


(a) (b)

Fig. 5.7: Error microphones with boundary arrangement. (a) Error microphones on the receivers' side (b) Error microphones on the incident side.

(3) The last arrangement of the error microphones is the planar control. In this arrangement, the control sources are distributed on the surface of the window and the error microphones are always are placed aligned with the control sources on the receivers' side or incident side of the aperture. Fig. 5.8 shows these setups schematically for the error microphones on the receivers' side and on the incident side.

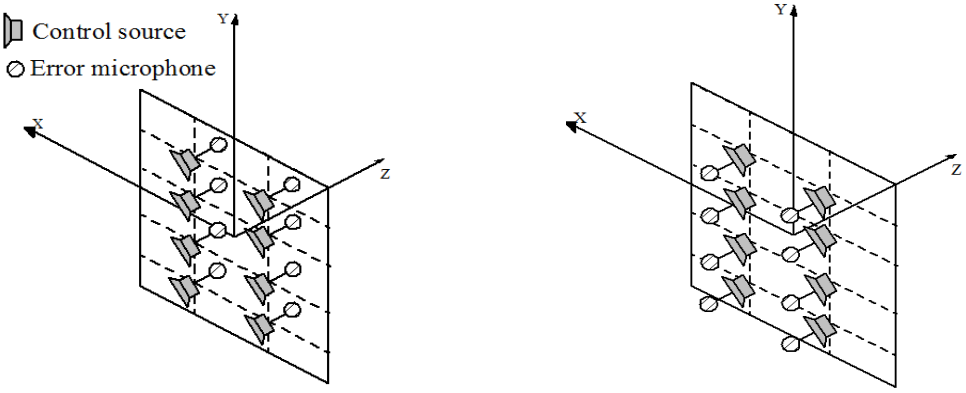


(a) (b)

Fig. 5.8: Error microphones with the planar arrangement. (a) Error microphones on the receivers' side (b) Error microphones on the incident side.

## 5.4. Results and Conclusions

### 5.4.1. Step 1: Minimizing the square pressure at the observation points

**Control sources with the arrangement of Set 1**

Fig. 5.9 shows the average insertion loss achieved at the observation points with a linear array of 4 control sources that are placed at the position of Set 1 (Fig. 5.4). The control sources are placed at the distance of $r_{ss}$ and the angle of $\theta_{ss}$. The distance between adjacent control sources is 0.3 m which is less than the half of shortest wavelength at 500 Hz [49,71]. The incident angle of the plane wave is $\theta_i = 60°$ and calculations are repeated for different frequencies.

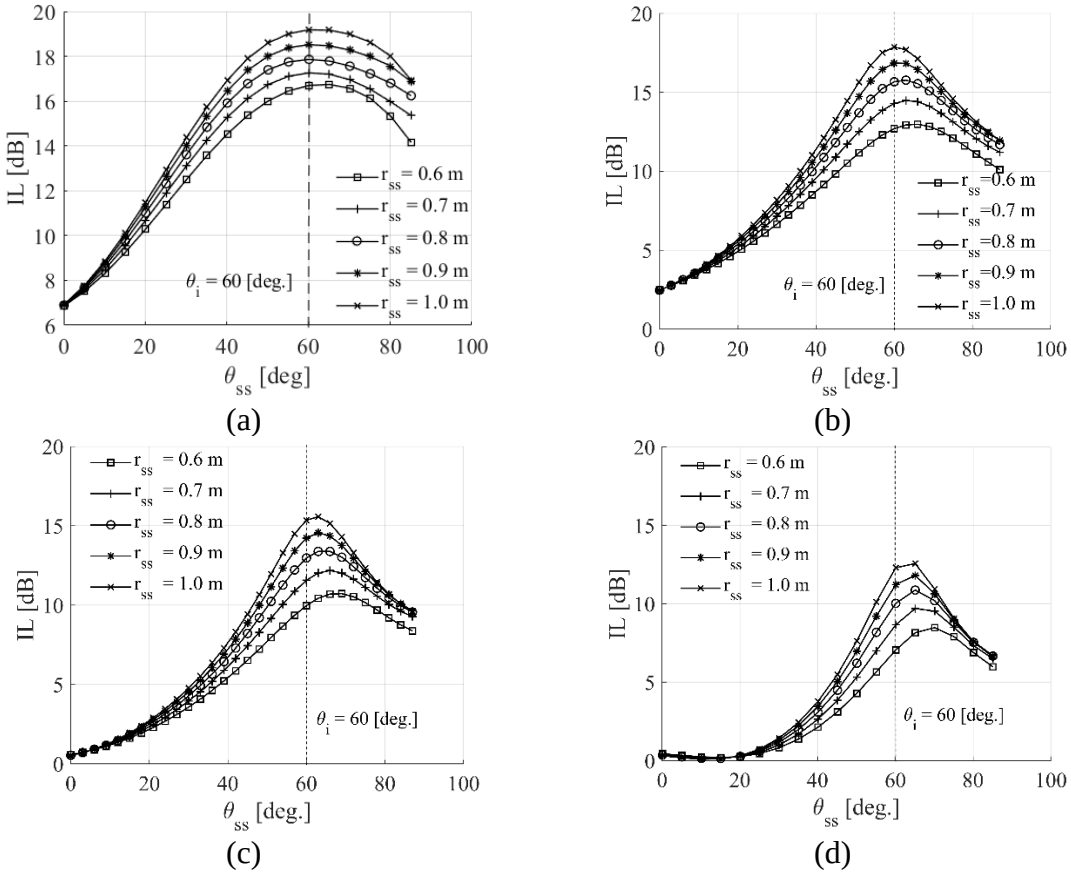


Fig. 5.9: Average insertion loss at the observation points for the control sources at the position of Set 1 and the plane wave of $\theta_i = 60°$. (a) 100 Hz, (b) 200 Hz, (c) 300 Hz, and (d) 500 Hz.

Fig. 5.9 shows that when the control sources are placed with the arrangement of Set 1, the performance of the active control system not only depends on the frequency but also it depends on the distance of control sources from the aperture. The control sources farther from the opening, higher attenuation achieves at the observation points, because when the control sources are farther from the opening, more observation points are in the pure diffracted field of control sources, and consequently the performance of Set 1 improves.

Furthermore, Fig. 5.9 shows that at low frequencies, the maximum attenuation is obtained at $\theta_{ss} = \theta_i$, but at the high frequencies, the noise cancels more efficiently at $\theta_{ss}$ a few degrees greater than $\theta_i$. This latter result is the same as obtained for the barriers that the control sources should be located below the line that connects the noise sources to the edge.

Generally speaking, for the configuration of Set 1, the best position for the control sources is at $\theta_{ss} = \theta_i$ and at the furthest possible distance from the opening. Thus, for further calculations, when using Set 1 control sources will be placed at $\theta_{ss} = \theta_i$.

**Control sources with the arrangement of Set 2**

The calculations for the same plane wave of $\theta_i = 60°$ are repeated with four control sources that are placed in the arrangement of Set 2. Similar to Set 1, the distance between adjacent control sources is assumed to be 0.3 m.

Fig. 5.7 illustrates the average insertion losses at the observation points for different distances of control sources from the window, $d_{ss}$. Considering the facts that the average insertion loss does not change significantly for the $d_{ss}$ greater than 0.5 [m] and also the control sources should be close to the window to be feasible for installation in real applications, further calculations are performed with $d_{ss} = 0.5$ [m].

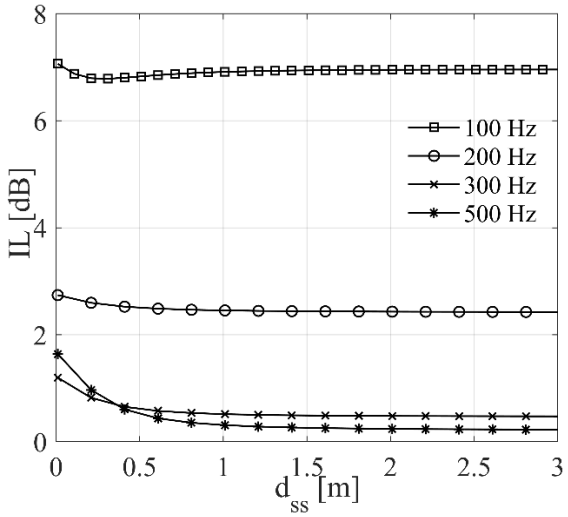


Fig. 5.10: Average insertion loss at the observation points for the control sources at the position of Set 2 with different $d_{ss}$.

When the control sources are perpendicular to the opening and the plane wave is oblique, the distance of the control source from the opening does not highly affect the performance. To address the effect of the incident angle on the performance of Set 2, the average insertion loss at the observation points are measured when the control sources are at $d_{ss} = 0.5$ m. The results are presented in Fig. 5.11.

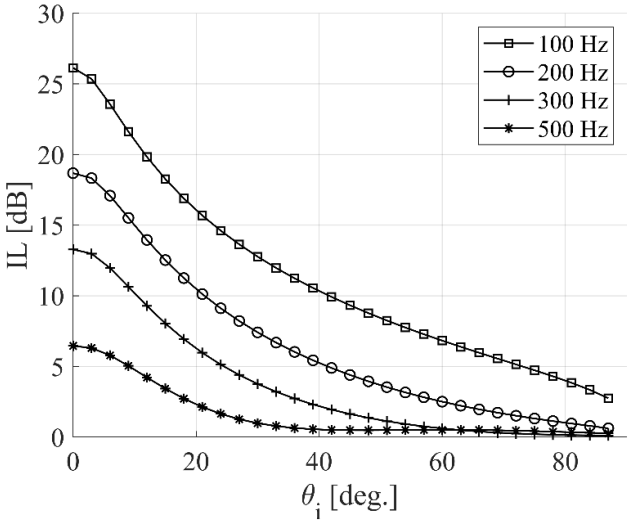


Fig. 5.11: Average insertion loss at different incident angles with the configuration of Set 2 for control sources.

The effectiveness of this configuration is significantly dependent on the incident angle and frequency, as shown in Fig. 5.11. The maximum performance of this arrangement is at $\theta_i = 0$.

**Control sources with the boundary arrangement**

A well-known arrangement of an active noise control system for aperture is to install the control sources on the boundaries of the opening. For active noise control windows with four control sources installed on the boundary, the suitable position is to place one control source at the middle of each edge [151]. Fig. 5.12 shows the average insertion loss at the observation points with four control sources.

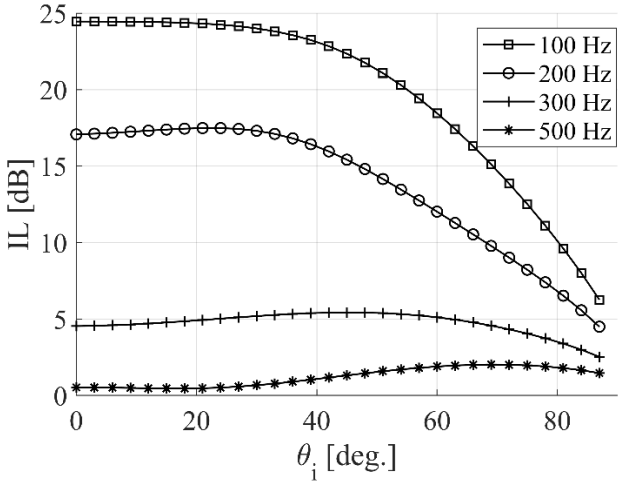


Fig. 5.12: Average insertion loss at different incident angles with the boundary control arrangement.

At high frequencies (more than 300 Hz), the active control system with boundary arrangement has fairly a constant efficiency at different incident angles (Fig. 5.12), while still at low frequencies, the efficiency of the active control system does not change significantly at $\theta_i < 40°$. As a consequence, compared to Set 1 or Set 2, this arrangement is less dependent on the incident angles.

**Control sources with the planar arrangement**

In the previous studies, the control sources with planar arrangement were mostly distributed evenly over the entire opening. The distances between adjacent control sources should be less than the $\lambda/(1+\sin\theta_i)$ where $\lambda$ is the wavelength of the noise and $\theta_i$ is the incident angle [139,156]. Therefore, when four control sources are employed for the active cancellation with the planar arrangement, each control source has a distance of 0.33 m from the closest edge to it. With this setup, the interval of control sources is 0.33 m which is less than half the wavelength at $\theta_i = 90°$ (the maximum incident angle). Fig. 5.13 shows the average noise reduction at the observation points with four control sources that are distributed evenly on the surface of the aperture.

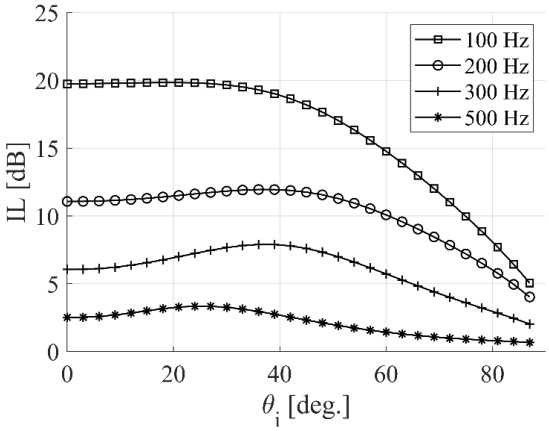


Fig. 5.13: Average insertion loss at different incident angles with the planar control arrangement.

The comparison of Fig. 5.12 and Fig. 5.13 shows that the boundary control is more efficient at low frequencies, however, better performance is achieved with the planar arrangement at higher frequencies. Furthermore, the achieved reduction does not change significantly for $\theta_i < 40°$.

**Comparison of candidate arrangements for the control sources**

In order to compare the performance of these arrangements, the average insertion losses at the observation points are calculated for the configurations with 4 and 8 control sources, and are shown respectively in Fig. 5.14 and Fig. 5.15. The control sources in the arrangement of Set 1 always are placed at $r_{ss} =$ 0.7 m and $\theta_{ss} = \theta_i$, and for Set 2 are placed at $d_{ss}$ =0.5 m.

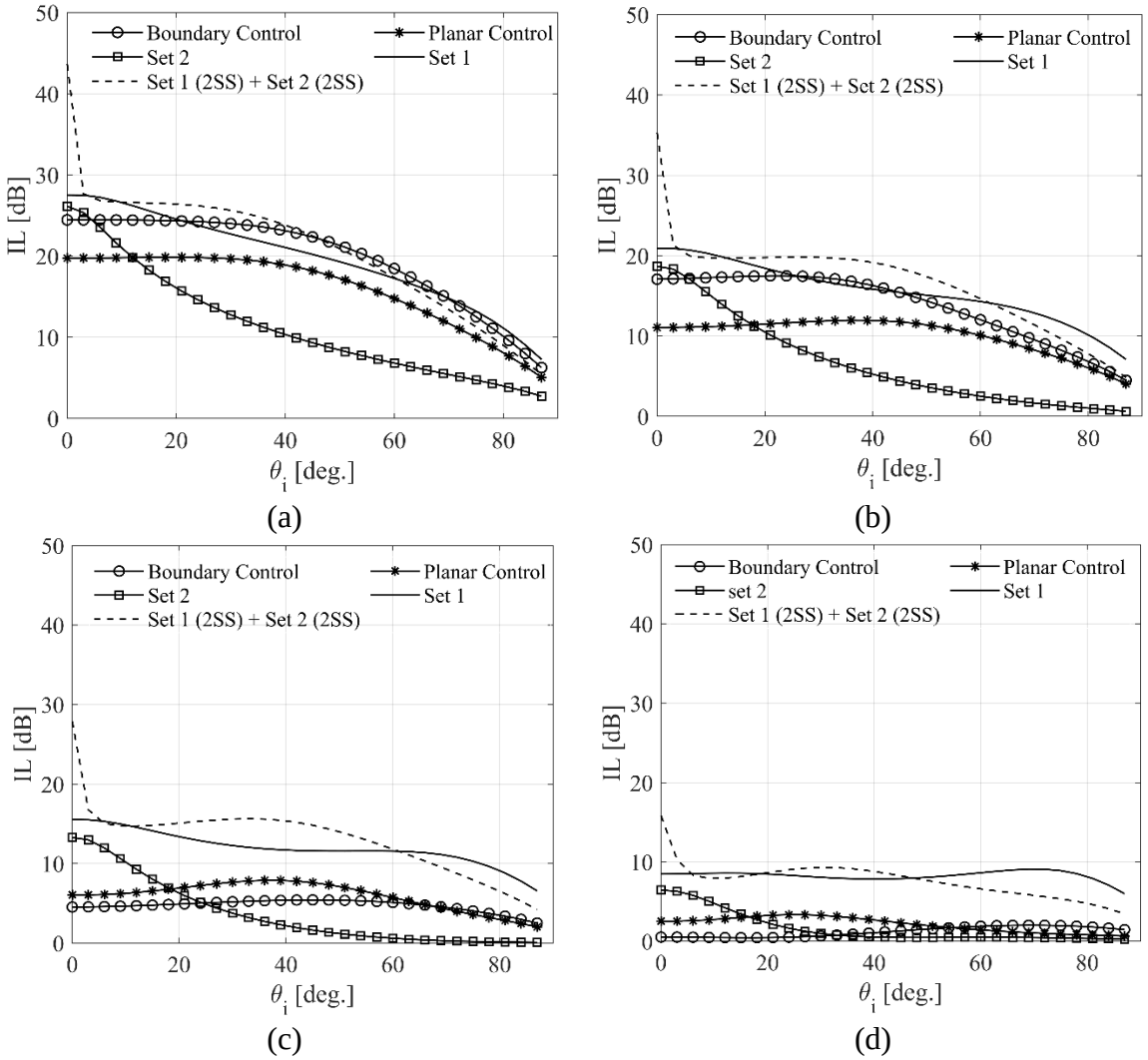


Fig. 5.14: Comparison of different arrangements with 4 control sources. (a) 100 Hz, (b) 200 Hz, (c) 300 Hz, and (d) 500 Hz

Fig. 5.14 shows that at low frequencies the control sources with arrangements of Set 1, the combination of Set 1 and Set 2, and boundary control perform more efficiently than the other configurations, but by increasing the frequency the performance of the boundary arrangement

decreases. At the high frequencies, however, planar arrangement achieves more reduction than the boundary control but still Set 1 or the combination of Set 1 and Set 2 are more efficient than the other arrangements. Also, Set 1 less depends on the incident angles and it achieves more noise reductions than the combination of Set 1 and Set 2 at high frequencies and high incident angles.

Fig. 5.15 represents the same results but with 8 control sources. For these simulations, the distance between adjacent control sources is 0.16 m.

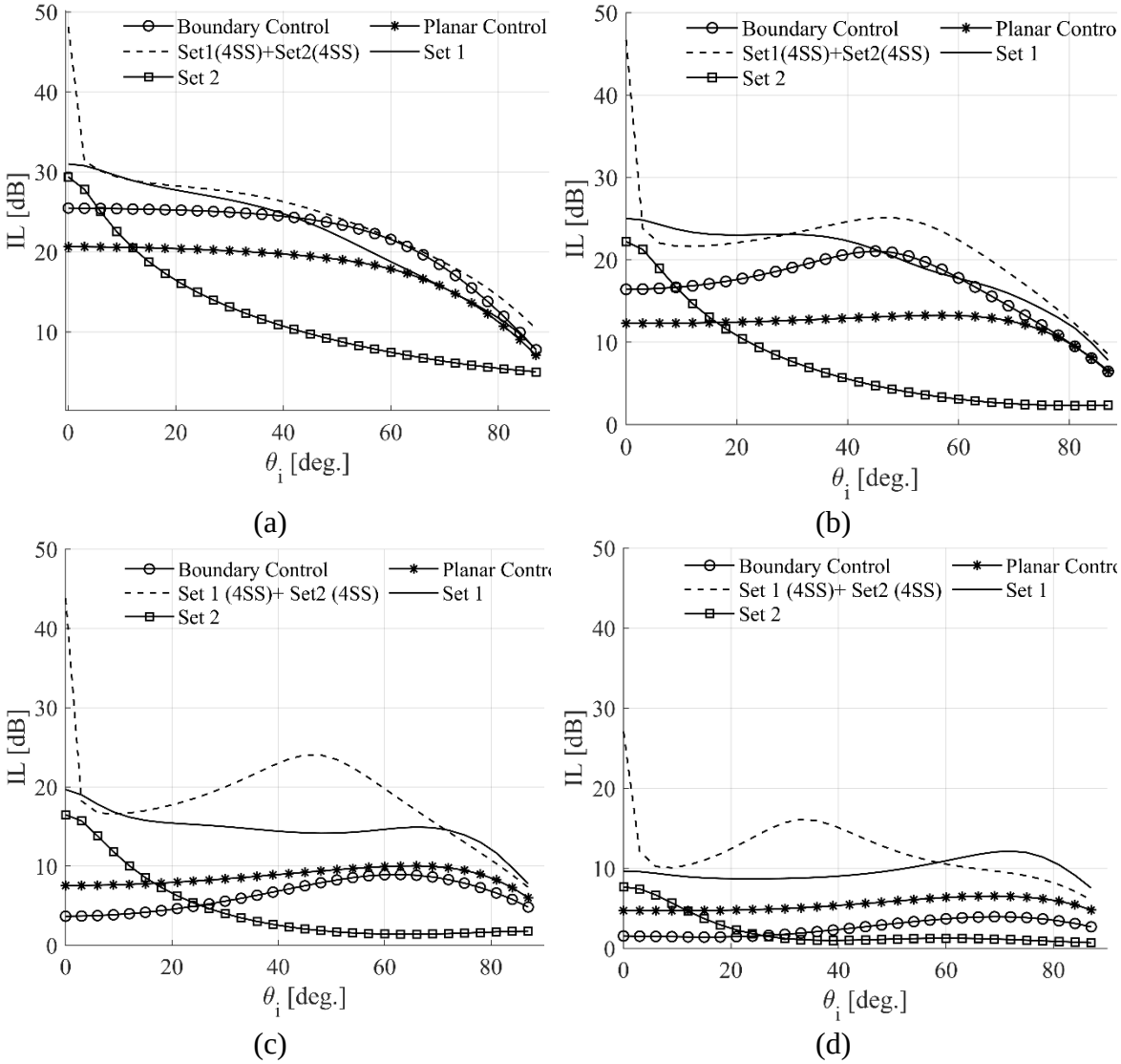


Fig. 5.15: Comparison of different arrangements with 8 control sources. (a) 100 Hz, (b) 200 Hz, (c) 300 Hz, and (d) 500 Hz

From Fig. 5.15 it can be concluded that the combination of Set 1 and Set 2 works better than the other arrangements. With this configuration, Set 1 can reduce the diffracted field while Set 2 controls the direct field. Furthermore, the comparison of Fig. 5.15 and Fig. 5.14 illustrates that increasing the number of control sources from 4 to 8 does not change the performance of boundary and planar arrangements noticeably, but it leads to achieving a constant performance for a wider range of $\theta_i$.

Also, it should be noted that the results obtained by the combination of Set 1 and set 2 are not the superposition of the performance of these two sets when they work separately. At high frequencies, Set 2 has poor performance but it constructively affects the performance of the combination arrangement at certain incident angles in the range of $20° < \theta_i < 50°$.

### 5.4.2. Step 2: Minimizing the square pressures at the error microphones

In the second step of the two-step approach, the error microphones are used to block the sound radiated from the noise source and transmitted through the aperture. Similar to the previous chapters, in this step, the square pressures are minimized at the error sensors, but the reductions presented in the figures are the average insertion losses at the observation points which are calculated by Equation 2.9.

In simulating the active noise window, the array of error microphones are mostly placed close to the plane of opening to be feasible for installation in real applications [54,70,154]. In this study, different configurations including the combination of Set 1 and Set 2, the boundary, and the planar installations are proposed for the placement of error microphones, but, they always are placed near the surface of the opening.

In order to specify the suitable positions of error microphones, the control sources are placed with the arrangement of the combination of Set 1 and Set 2, that from the previous step it is

found as the best arrangement among the suggested candidate setups. Then, the performance of this arrangement is compared with the boundary and the planar arrangements.

**Error sensors with the arrangement of Set 1 + Set 2**

In this arrangement, the combination of Set 1 and Set 2 (Fig. 5.6) is used as the placement of control sources and error microphones. The result of Fig. 5.16 is achieved for the control system with 8 secondary sources and 8 error microphones (4 units at each set). In both sets, the distances between the adjacent error sensors and control sources are 0.3 m.

From the findings of previous chapters, it is concluded that when the control sources are on the incident side, the error microphones should be placed on the receivers' side and in the shadow zone of both control and primary sources to better control the diffracted field. For this reason, in the combination arrangement, the control sources of Set 1 are located on the incident side at $r_{ss} = 0.7$ m and $\theta_{ss} = \theta_i$ and the corresponding error microphones are placed on the receivers' side with $r_{es} = 0.7$ m, and $\theta_{es} = \theta_i$.

However, the suitable positions should be searched for the corresponding error microphones of those control sources that are fixed at the position of Set 2. For this purpose, three configurations are tested for the placement of the error microphones of Set 2, including the error microphones on (1) the receivers' side with $d_{es} = 0.1$ m, (2) on the surface of the aperture with $d_{es} = 0$ and (3) on the incident side with $d_{es} = 0.1$ m, while for all these configurations the control sources of Set 2 are placed on the incident side at $d_{ss} = 0.5$ m.

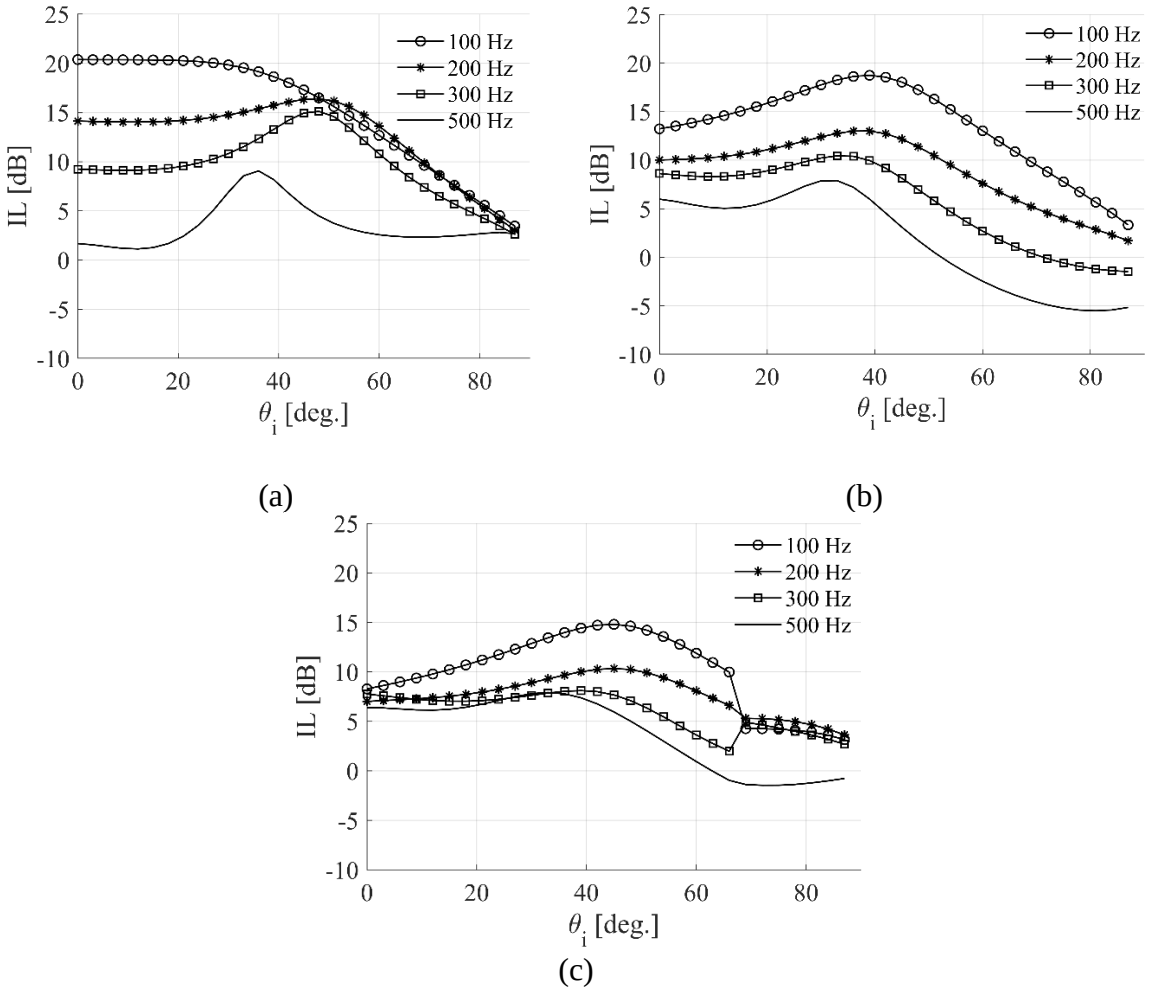


Fig. 5.16: Average insertion loss at observation points with different incident angles while error sensors of Set 1 are on the receivers' side and the error sensors of Set 2 are (a) on receivers' side, (b) on the surface of the aperture, and (c) on the incident side.

Comparing the achieved reductions at the observation points which are presented in Fig. 5.16 shows that the control system with all error microphones on the receivers' side (Fig. 5.16 a) has higher efficiency than other configurations. This result is in agreement with the previous findings for the barriers that the error microphones should be always at the receivers' side to obtain higher reductions.

**Error sensors with the boundary arrangement**

The boundary installation of control units is widely studied in previous studies [70,155]. Here, the boundary arrangement is simulated to report the suitable position of error microphones and to find the proper distance of each error microphone from the control sources. To this end, the performance of the active control system with boundary arrangement is assessed for various distances changed from 0.3 m to 0.1 m, on both sides of the aperture. Fig. 5.17 shows the average insertion loss achieved at the observation points with 8 control sources and 8 error microphones installed on the boundary of the opening and $ES_z$ referes to the Z-coordinates of error microphones, where the positive value of $ES_z$ is for error microphones on the receivers' side and vice versa.

There exist two control sources on each edge of the window. The distance between adjacent control sources on the edge is 0.33 m and also the distances from the control source to the corner of the edges are 0.33 m as well. This distance is less than half of the shortest noise wavelength that is studied in this work [49,71]. The error microphones are placed aligned with the control sources.

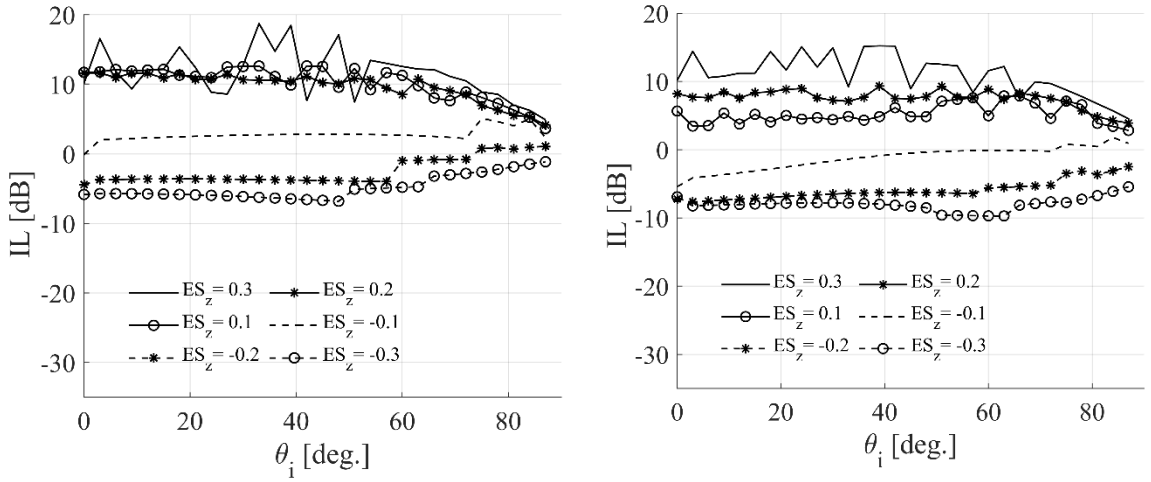


(a) (b)

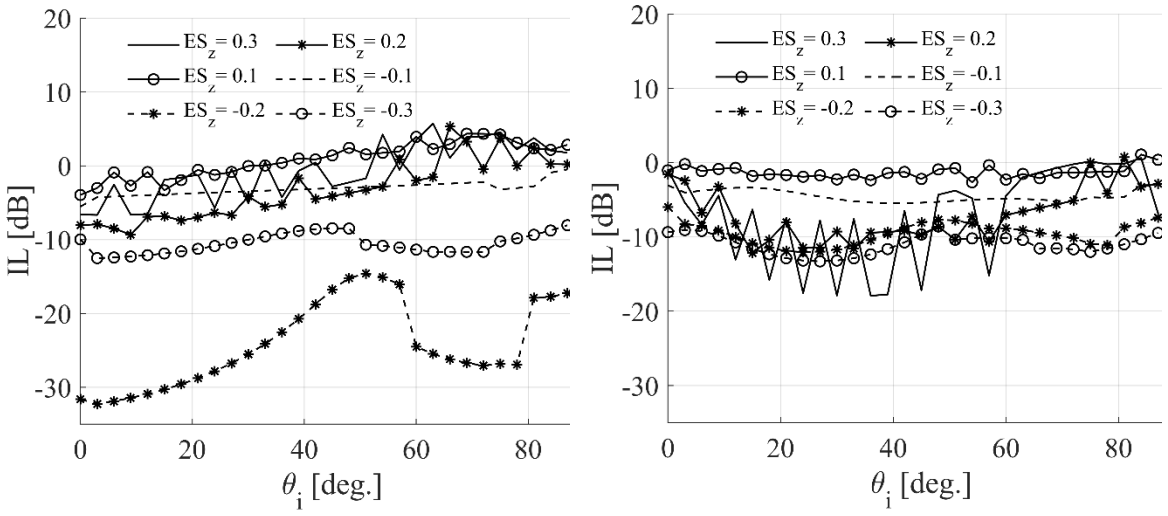


Fig. 5.17: Average insertion loss at observation points with boundary arrangement of transducers when error microphones are placed at various distances from the opening. $ES_z$ is the Z-coordinate of error sensors. The solid and dash curves are for the error microphones on the receivers' side and the incident side, respectively. (a) 100 Hz, (b) 200 Hz, (c) 300 Hz, and (d) 500 Hz.

Fig. 5.17 clearly shows that with the boundary arrangements for the transducers, the active control system obtains higher reduction when the error microphones are placed on the receiver side. This result is in agreement with the findings of previous studies [151,155]. Moreover, the active control system with error microphones in $ES_z = +0.3$ m is efficient at low frequency, although the results are unstable, and beyond that this distance not only decreases the transmitted noise at high frequency but also it leads to increasing the noise level at the observation points.

Generally speaking, the active control system performs successfully at most frequencies (except 500 Hz) when the error microphones are placed on the receivers' side and at a distance of 0.1 from the control sources ($ES_z = +0.1$).

**Error sensors with the Planar arrangement**

As indicated before, another well-known arrangement for controlling the transmitted noise through an opening is the planar installment of transducers [54,91,138,139,145,152,153]. The results of the active noise cancellation with 8 control sources distributed evenly on the plane of aperture with 8 error microphones aligned with control sources are shown in Fig. 5.18. The spaces between control sources are 0.3 m and 0.16 m in the X- and Y-directions, respectively, which are less than half the wavelength at $\theta_i = 90°$ (the maximum incident angle).

Similar to the boundary arrangement, two configurations of error microphones are studied for the planar arrangement: (1) the error microphones on the receivers' side and (2) the error microphones on the incident side. For both configurations, different distances of error microphones from the control sources are simulated. Fig. 5.18 illustrates the average insertion loss at the observation points for different positions of error microphones $ES_z$.

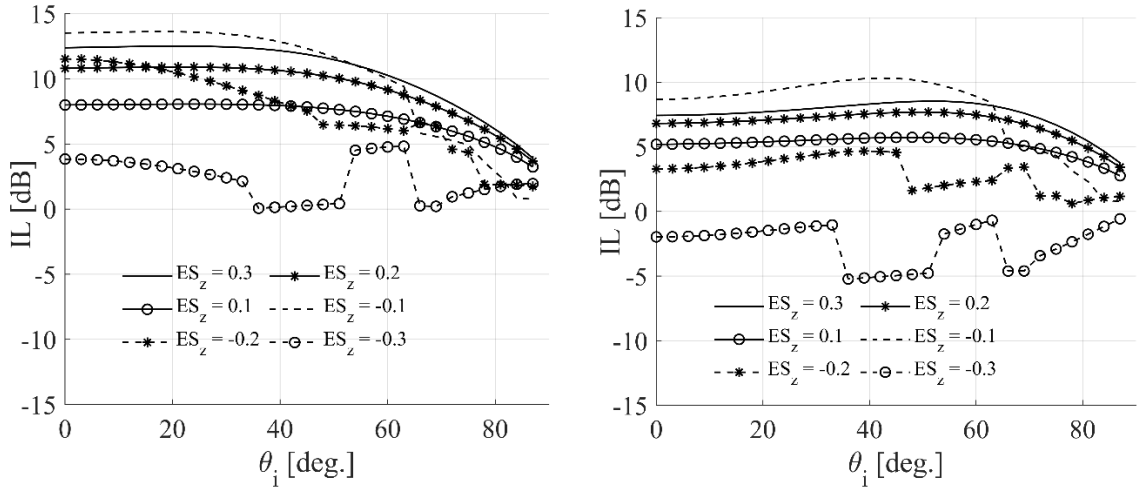


(a) (b)

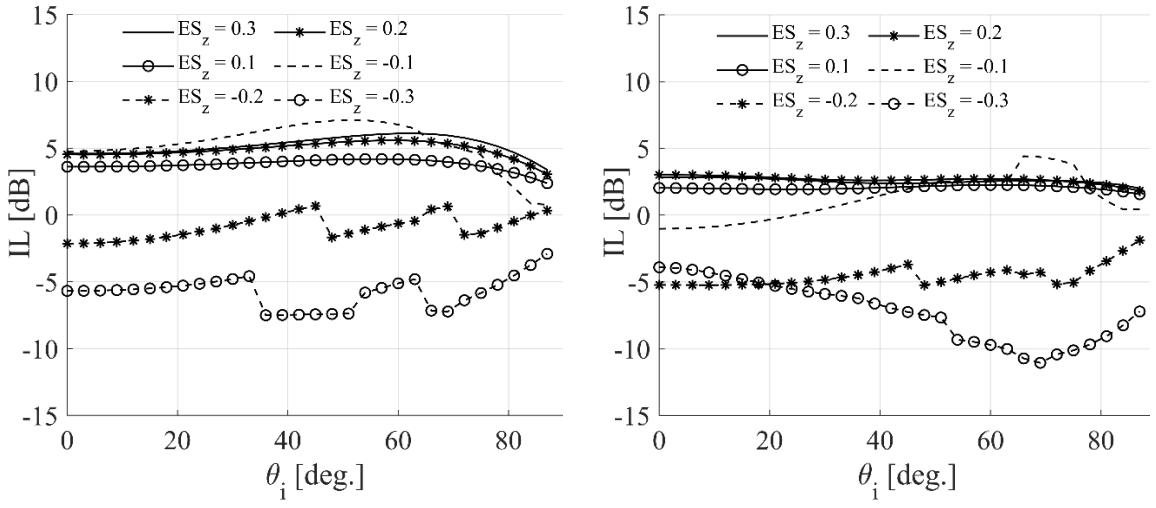


Fig. 5.18: Average insertion loss at observation points with the planar arrangement of transducers when error microphones are placed at various distances from the opening. $ES_z$ is the Z-coordinate of error sensors. The solid and dash curves are for the error microphones on the receivers' side and the incident side, respectively. (a) 100 Hz, (b) 200 Hz, (c) 300 Hz, and (d) 500 Hz. .

At low frequencies, the active noise control with the planar arrangement and with error microphones are on the incident side at $ES_z = -0.1$ m performs more efficiently at low incident angles ($\theta_i < 60°$), shown in Fig. 5.19. However, by increasing the frequency and the incident angle the efficiency of the control system reduces. On the other hand, the error microphones at $ES_z = +0.3$ m performs more stable at all frequencies and all incident angles.

**Comparison of candidate arrangements for the error microphones**

Fig. 5.19 illustrates the comparison of achieved reduction at the observation points with the boundary arrangement, planar arrangement, and the combination of Set 1 and Set 2.

For the boundary and the planar arrangements, the error microphones are at $ES_z = +0.1$ m and $ES_z = +0.3$ m, respectively, and the control sources are located on the plane Z= 0.

Also, the error microphones of the combination arrangement are on the receivers' side and at $r_{es} =$ 0.7 m, and $\theta_{es} = \theta_i$ for Set 1 and at $d_{es} = 0.1$ for Set 2.

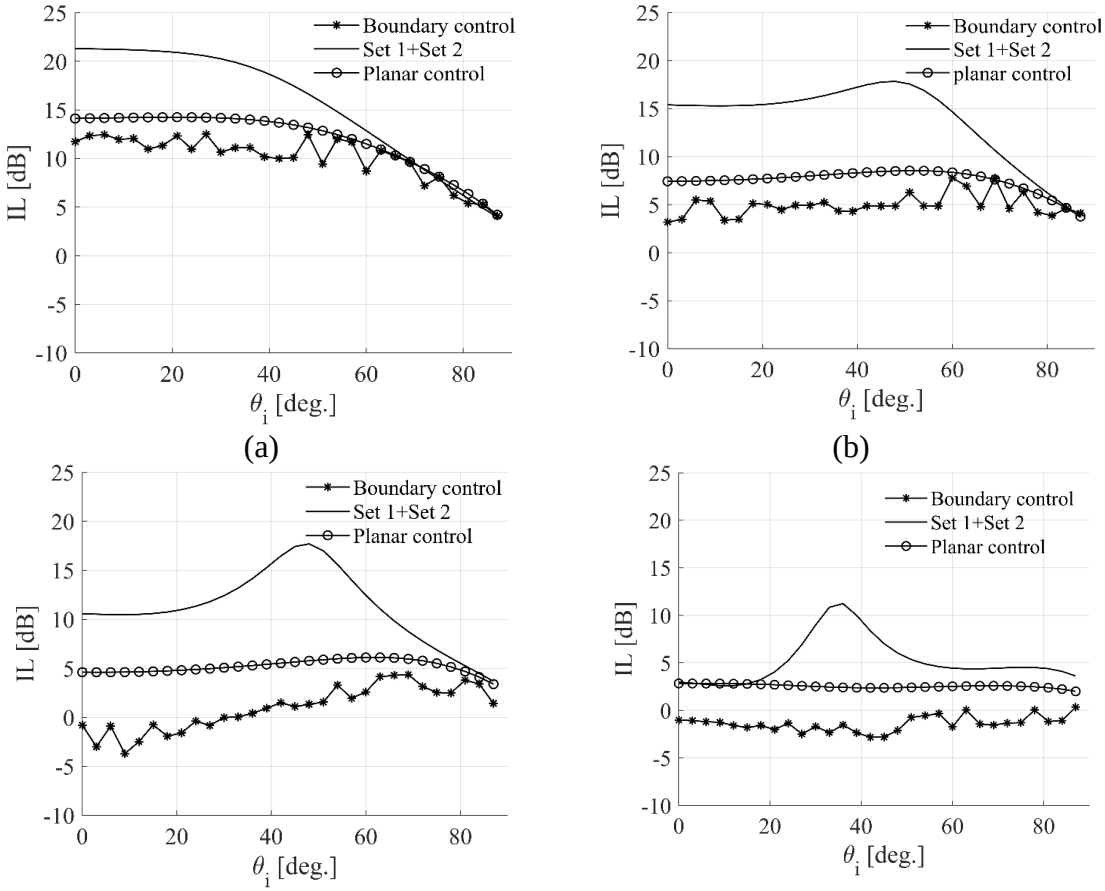


Fig. 5.19: Average insertion loss at observation points with different arrangements of control sources and error sensors. (a) 100 Hz, (b) 200 Hz, (c) 300 Hz, and (d)500 Hz.

Fig. 5.19 illustrates that the active control system with transducers distributed on the surface of the opening is more efficient than the boundary arrangement which is in agreement with previous studies [136]. Moreover, the results of Fig. 5.19 show that the combination of Set 1 and Set 2 can obtain even higher attenuation at the observation points than the planar arrangement. It is probably due to better cancellation of the diffracted field by Set 1 in this combination.

## 5.5. Conclusions

The application of active noise cancellation is studied for a square window of size $1\times1$ $m^2$. Different configurations are proposed for the location of control sources and the error microphones, and the configuration that obtains the highest noise reduction at the observation points is selected with the Two-step approach.

For the control sources, the best arrangement among the proposed ones is the combination of a set of sources that are placed at the same angle of the incident plane wave (Set 1) and another set that is perpendicular to the surface of the aperture (Set 2). This arrangement achieves a higher reduction in comparison with boundary and also planar arrangements, probably because the control sources of Set 1 can decrease the diffracted field at the observation points more effectively, while Set 2 controls the direct field.

In the second step, the suitable position for the error microphones is searched, when the control sources were fixed at the positions found in the previous step. Different placements are proposed for the error microphones including the error microphones on the receivers' side, on the face of the aperture, and on the incident side. The results illustrate that the active control system performs more efficiently when all of the error microphones are placed on the receivers' side which is in agreement with the findings of previous chapters.

Furthermore, the results show that for a noise wave impinging the opening with a known direction such as traffic noise, or the pass-by airplane noise that always comes from the same trajectory, the combination of Set 1 and Set 2 is a promising approach that can be tuned according to each case. For such noise waves, the performance of this setup is higher than the planar or boundary arrangements, however, more studies are required to address the efficiency of these arrangments for noise with random incidence.

On the other hand, the planar and boundary control seems to be more suitable for general-purpose control situations, although the limitation of placing the transducers on the plane of the window should be considered, because it may restrict access through the opening and reduce the ventilation ratio. This is also showed that for the boundary and planar control increasing the control sources from 4 to 8 units, does not significantly improve the noise cancellation at receivers, but it increases the range of incident angles which the control system achieves constant performance.

# Chapter 6: Conclusion and further work

## 6.1. Conclusions

### 6.1.1. Active noise barrier

The present research has established the basis of a complete framework to optimize the performance of the active noise barriers and active noise windows, which result in more reduction of the noise level transmitted through these two obstacles at the narrowband and broadband noises.

For the active noise barrier, the initial stage involved the development of a two-step approach that allows defining the locations of control sources in the first step and the location of the error microphones in the second step. Then, a repetitive calculation method is performed to define the suitable positions of transducers among 341 candidate positions close to the barrier.

In these calculations, the intervals between the transducers were lower than the shortest wavelength, and Macdonald's solution is employed to calculate diffracted field. The outcome of the repetitive calculation found regions for the control sources and error microphones instead of the unique positions. Considering this finding, general criteria are proposed for the location of transducers during the design of an active noise barrier.

Based on these criteria, to minimize the noise level in the barrier's shadow zone, control sources should be placed on the incident side and below the edge of the barrier, while error microphones should be placed in the shadow zone. If the installation of transducers meets these criteria then the attenuation is independent of the position of the target zone and the active noise control system can suppress the noise in the entire shadow zone.

Also, it is shown that probably there are other positions for transducers that violate the general criteria and yet the active noise control system has higher performance, however, it is

mentioned that these places are unique for single frequencies and may reduce the efficiency of the noise control at other frequencies or broadband spectra.

Moreover, it is shown that the overall performance of this configuration is relatively independent of the position of the noise source since the attenuation in the shadow zone of the barrier remains almost unchanged for different distances between the noise source and the barrier.

Furthermore, during the simulation process, the influence of the ground reflection on the performance of noise control is studied. For tonal noise, a totally reflecting ground reduces the effectiveness of the active noise barrier; nevertheless, it does not affect the control system's performance in the broadband spectrum.

Further investigations are carried out to address the mechanism of noise cancellation with the transducers surrounding the barrier. When the control units are positioned at the places suggested by the general criteria, the control and primary fields are out of phase; however, when the general criteria are violated, the control and primary fields are in phase, lowering the active noise barrier's performance.

The repetitive calculation together with the two-step approach can estimate the proper locations of the control sources and error microphones, but this method clearly has some limitations if more parameters should take into account in the optimization procedure. Accordingly, for optimizing more parameters, the model of this work is optimized by the genetic algorithms (GA) based on the genetic optimizer toolbox of Matlab (ga). The parameters were the *X*- and *Z*-coordinates of the transducers locations, as well as the interval of neighboring control source and error microphones, together with their numbers. The optimizations are followed with the two-step and the multi-parameters approaches. In the

Multi-parameters approach, all of the variables are optimized in a single step and simultaneously.

The results show greater insertion loss achieves at the target area when the multi-parameters are employed for the optimization. Furthermore, from the viewpoint of calculation time, this strategy outperforms the two-step approach. The computation time can also decrease more for the problems with asymmetrical geometries. In these problems, the strengths of control sources are symmetrical, and less computation effort is required.

Regarding the pace between the transducers, it is illustrated that the optimum values for the interval of the error microphones increase if a wider target area is considered for the optimization, but the interval of control sources is independent of the size of the target area.

### 6.1.2. Active noise window

In this study, the correct implementation of the active noise control system is investigated for a square aperture in an infinite baffle. In the previous studies, two classical arrangements were proposed for the transducers of an active noise control window, including the planar and the boundary configurations. However, the aperture can be considered as a particular case of the noise barriers as it is the composition of four finite edge barriers, and then based on this consideration a novel arrangement is proposed for the transducers. In the present study, this new proposed configuration met the general criteria previously developed for the active noise barriers.

The suitable positions of control sources and error microphones are selected between different candidate arrangements including the classical setups (planar and boundary control) and the novel arrangement, based on the Two-step approach.

Among those arrangements, the new configuration that follows the proposed general criteria for placement of transducers of the active noise barrier could achieve a higher reduction at the observation points behind the window.

The control sources in this arrangement are placed at two different positions. One set of control sources are located at the same angle as the incident plane wave to suppress the diffracted field, and the other set is placed in front of the window to control the direct field. For each set of control sources there exist a corresponding set of error microphones on the receivers' side.

The results suggest that this arrangement yields promising outcomes as long as the impinging noise has a defined direction, such as road noise or noise propagating from a specific activity with a determined position of the noise source. On the other hand, the boundary and planar arrangements are suitable for the general control situations and the noise arrives from randomly placed sources. Furthermore, it is shown that the planar control is more efficient than the boundary arrangement, but installing the control units on the surface of the opening may reduce the access and the ventilation.

## 6.2. Further work

The present research laid the foundation of performing optimization of active noise control performance for the noise barriers and open windows. However, many potential future projects, will require extending the use of active noise control technologies and improving their effectiveness. Some of them are mentioned in this section.

### 6.2.1. Active noise barrier

The optimizations in this study are done for a fixed noise source or a mobile source moves toward the barrier, however, further investigation is required to study the effect of a moving source along the barrier on the optimal location of transducers. Moreover, to verify the simulation results, experimental validation is necessary.

In terms of implementation of GA optimization, the objective function can be changed in such a manner that it is possible to discover the optimal number of control units as well as their position to be cost-effective for the real applications of active noise barriers. For instance, the cost of control units, as well as the extra attenuation achieves by adding the control unit can be formulated effectively in the objective function. In this way, in addition to the reduction, the GA considers the project cost in the optimization procedure.

### 6.2.2. Active noise window

The positions of transducers are highly important for an active noise window. In this study, the Two-step approach is employed to define the suitable positions of control sources and error microphones, but in order to optimize the performance of the active control system, the parameters should specify simultaneously with optimization methods such as genetic algorithms. Furthermore, experimental validation is required to verify the simulation models. Also, more generic models which include the noise interior of a room, as well as the point noise source instead of plane wave noise, are necessary.

# Appendix A

## Publications

### Journals

#### Accepted manuscripts

- Sohrabi S, Pàmies Gómez T, Romeu Garbí J. Suitability of Active Noise Barriers for Construction Sites. Appl Sci 2020;10:6160. doi:10.3390/app10186160.

#### Manuscripts under review

- Sohrabi S, Pàmies Gómez T, Romeu Garbí J. Proper location of the transducers for an active noise barrier. Journal of Vibration and Control.
- Sohrabi S, Pàmies Gómez T, Romeu Garbí J. Exploring the optimal geometric parameters of an active noise barrier with the genetic. Journal of Sound and Vibration.

### International Conferences

- Sohrabi S, Pàmies Gómez T, Romeu Garbí J. Active noise control for open windows. INTER-NOISE 2021-50th Int. Congr. Expo. 259 (11), 3097-3107. doi:10.3397/IN-2021-2306
- Sohrabi S, Pàmies Gómez T, Romeu Garbí J. Revision of cancellation at the edge approach for active noise barrier. Proceedings of ISMA2020 International Conference on Noise and Vibration Engineering. USD2020 International Conference

on Uncertainty in Structural Dynamics: Leuven, Belgium: 2020, p. 173-181. ISBN 9789082893113.

- Sohrabi S, Pàmies Gómez T, Romeu Garbí J. Investigate the effect of the active noise barrier on the reduction of noise level at the shadow zone and the neighboring building. INTER-NOISE 2020-49th Int. Congr. Expo. 259 (10), 1978-1987.
- Sohrabi S, Pàmies Gómez T, Romeu Garbí J. Evaluation of the effectiveness of control sources' interval on active noise control performance. INTER-NOISE 2019-48th Int. Congr. Expo. 259 (5), 4196-4204.

  Sohrabi S, Pàmies Gómez T, Romeu Garbí J. Numerical study of an active noise barrier. INTER-NOISE 2017- 46th Int. Congr. Expo. 255 (2), 5946-5954

# Bibliography

[1] Castiñeira-Ibañez S, Rubio C, Sánchez-Pérez JV. Environmental noise control during its transmission phase to protect buildings. Design model for acoustic barriers based on arrays of isolated scatterers. Build Environ 2015;93:179–85. doi:10.1016/j.buildenv.2015.07.002.

[2] Lee HM, Wang Z, Lim KM, Lee HP. A Review of Active Noise Control Applications on Noise Barrier in Three-Dimensional/Open Space: Myths and Challenges. Fluct Noise Lett 2019;18:1–21. doi:10.1142/S0219477519300027.

[3] Héroux ME, Babisch W, Belojevic G, Brink M, Janssen S, Lercher P, et al. WHO environmental noise guidelines for the European Region. Euronoise 2015 2020:2589–93.

[4] Zannin PHT, Ferreira AMC, Szerememetta B. Evaluation of noise pollution in urban parks. Environ Monit Assess 2006;118:423–33. doi:10.1007/s10661-006-1506-6.

[5] Broner N. The effects of low frequency noise on people-A review. J Sound Vib 1978;58:483–500. doi:10.1016/0022-460X(78)90354-1.

[6] Ng CF. Effects of building construction noise on residents: A quasi-experiment. J Environ Psychol 2000;20:375–85. doi:10.1006/jevp.2000.0177.

[7] Lee SC, Hong JY, Jeon JY. Effects of acoustic characteristics of combined construction noise on annoyance. Build Environ 2015;92:657–67. doi:10.1016/j.buildenv.2015.05.037.

[8] Li X, Song Z, Wang T, Zheng Y, Ning X. Health impacts of construction noise on workers: A quantitative assessment model based on exposure measurement. J Clean Prod 2016;135:721–31. doi:10.1016/j.jclepro.2016.06.100.

[9] Kłosak AK. Design, simulations and experimental research in the process of development of sound absorbing perforated ceiling tile. Appl Acoust 2020;161. doi:10.1016/j.apacoust.2019.107185.

[10] Zhaomeng W, Kian Meng L, Priyadarshinee P, Pueh LH. Applications of noise barriers with a slanted flat-tip jagged cantilever for noise attenuation on a construction site. JVC/Journal Vib Control 2018. doi:10.1177/1077546317747779.

[11] Godinho L, António J, Tadeu A. 3D sound scattering by rigid barriers in the vicinity of tall buildings. Appl Acoust 2001;62:1229–48. doi:10.1016/S0003-682X(01)00004-4.

[12] Butler GF. A note on improving the attenuation given by a noise barrier. J Sound Vib 1974;32:367–9. doi:10.1016/S0022-460X(74)80092-1.

[13] Lam B, Gan WS, Shi DY, Nishimura M, Elliott S. Ten questions concerning active noise control in the built environment. Build Environ 2021;200:107928. doi:10.1016/j.buildenv.2021.107928.

[14] Li KM, Wong HY. A review of commonly used analytical and empirical formulae for predicting sound diffracted by a thin screen. Appl Acoust 2005;66:45–76. doi:10.1016/j.apacoust.2004.06.004.

[15] CEDR Task Group Road Noise, Vanhooreweder B, Marcocci S, Alberto D. Technical Report 2017-02. State of the art in managing road traffic noise: noise barriers. 2017.

[16] Sharma GS, Sarkar A. Directivity-based passive barrier for local control of low-frequency noise. J Theor Comput Acoust 2018;26:1–18. doi:10.1142/S2591728518500123.

[17] Svensson UP, Calamia PT. Edge-diffraction impulse responses near specular-zone and shadow-zone boundaries. Acta Acust United with Acust 2006;92:501–12. doi:10.1.1.122.2992.

[18] Huang X, Zou H, Qiu X. Effects of the top edge impedance on sound barrier diffraction. Appl Sci 2020;10. doi:10.3390/app10176042.

[19] Duhamel D. Efficient calculation of the three-dimensional sound pressure field around a noise barrier. J Sound Vib 1996;197:547–71. doi:10.1006/jsvi.1996.0548.

[20] Piechowicz J. Sound wave diffraction at the edge of a sound barrier. Acta Phys Pol A 2011;119:1040–5. doi:10.12693/APhysPolA.119.1040.

[21] Biot MA, Tolstoy I. Formulation of Wave Propagation in Infinite Media by Normal Coordinates with an Application to Diffraction. J Acoust Soc Am 1957. doi:10.1121/1.1908899.

[22] Medwin H. Shadowing by finite noise barriers. J Acoust Soc Am 1981;69:1060–4. doi:10.1121/1.385684.

[23] Svensson UP, Fred RI, Vanderkooy J. An analytic secondary source model of edge diffraction impulse responses. J Acoust Soc Am 1999;106:2331–44. doi:10.1121/1.428071.

[24] Pierce AD. Diffraction of sound around corners and over wide barriers. J Acoust Soc Am 1974;55:941–55. doi:10.1121/1.1914668.

[25] Hadden WJ, Pierce AD. Sound diffraction around screens and wedges for arbitrary point source locations. J Acoust Soc Am 1981;69:1266–76. doi:10.1121/1.385809.

[26] Asheim A, Peter Svensson U. An integral equation formulation for the diffraction from convex plates and polyhedra. J Acoust Soc Am 2013;133:3681–91. doi:10.1121/1.4802654.

[27] Kropp W, Svensson PU. Application of the time domain formulation of the method of equivalent sources to radiation and scattering problems. Acta Acust United with Acust 1995;81:528–43.

[28] Svensson UP, Calamia PT, Nakanishi S. Frequency-domain edge diffraction for finite and infinite edges. Acta Acust United with Acust 2009;95:568–72. doi:10.3813/AAA.918181.

[29] Macdonald HM. A class of diffraction problems. Proc London Math Soc 1915;s2-14:410–27. doi:10.1112/plms/s2_14.1.410.

[30] Sommerfeld A. Mathematische Theorie der Diffraction. Math Ann 1896;47:317–74. doi:10.1007/BF01447273.

[31] Xiaojun Q. An Introduction to Virtual Sound Barriers. CRC Press; 2019.

[32] Greiner D, Aznárez JJ, Maeso O, Winter G. Single- and multi-objective shape design of Y-noise barriers using evolutionary computation and boundary elements. Adv Eng Softw 2010;41:368–78. doi:10.1016/j.advengsoft.2009.06.007.

[33] Grubeša S, Jambrošić K, Domitrović H. Noise barriers with varying cross-section optimized by genetic algorithms. Appl Acoust 2012;73:1129–37. doi:10.1016/j.apacoust.2012.05.005.

[34] Wang Y, Jiao Y, Chen Z. Research on the well at the top edge of noise barrier. Appl Acoust 2018;133:118–22. doi:10.1016/j.apacoust.2017.12.018.

[35] Gannoruwa A, Ruwanpura JY. Construction noise prediction and barrier optimization using special purpose simulation. Proc - Winter Simul Conf

2007:2073–81. doi:10.1109/WSC.2007.4419839.

[36] Oldham DJ, Egan CA. A parametric investigation of the performance of T-profiled highway noise barriers and the identification of a potential predictive approach. Appl Acoust 2011;72:803–13. doi:10.1016/j.apacoust.2011.04.012.

[37] Reiter P, Wehr R, Ziegelwanger H. Simulation and measurement of noise barrier sound-reflection properties. Appl Acoust 2017;123:133–42. doi:10.1016/j.apacoust.2017.03.007.

[38] Gilchrist A, Allouche EN, Cowan D. Prediction and mitigation of construction noise in an urban environment. Can J Civ Eng 2003;30:659–72. doi:10.1139/l03-019.

[39] Paul L. Process of silencing sound oscillations 1936.

[40] Elliott SJ, Nelson PA. Models for describing active noise control in ducts. Mdan 1984.

[41] Munjala ML, Eriksson LJ. An analytical, one dimensional, standing wave model of a linear active noise control system in a duct. J Acoust Soc Am 1988;84:1086–93. doi:10.1121/1.396694.

[42] Munjal ML, Eriksson LJ. Analysis of a linear one-dimensional active noise control system by means of block diagrams and transfer functions. J Sound Vib 1989;129:443–55.

[43] Ai Y, Qiu X, Hansen CH. Minimizing wind effects on active control systems for attenuating outdoor transformer noise. Noise Control Eng J 2000. doi:10.3397/1.2827968.

[44] Zou H, Huang X, Hu S, Qiu X. Applying an active noise barrier on a 110 KV power transformer in hunan. INTERNOISE 2014 - 43rd Int Congr Noise Control Eng Improv World Through Noise Control 2014:1–7.

[45] Ohnishi K, Saito T, Teranishi S, Namikawa Y, Mori T, Kimura K, et al. Development of the product-type active soft edge noise barrier. Proc. 18th Int. Congr. Acoust., 2004, p. 1041–4.

[46] Borchi F, Carfagni M, Martelli L, Turchi A, Argenti F. Design and experimental tests of active control barriers for low-frequency stationary noise reduction in urban outdoor environment. Appl Acoust 2016;114:125–35. doi:10.1016/j.apacoust.2016.07.020.

[47] Zhao S, Qiu X, Lacey J, Maisch S. Configuring fixed-coefficient active control systems for traffic noise reduction. Build Environ 2019;149:415–27. doi:10.1016/j.buildenv.2018.12.037.

[48] Francesco B, Monica C, Lorenzo M, Alessio T. An active noise barrier system optimized for reducing outdoor stationary noise. Proc. 22nd Int. Congr. Sound Vib., 2015, p. 12–6.

[49] Omoto A, Takashima K, Fujiwara K, Aoki M, Shimizu Y. Active suppression of sound diffracted by a barrier: An outdoor experiment. J Acoust Soc Am 1997;102:1671–9. doi:10.1121/1.420078.

[50] Pàmies T, Romeu J, Genescà M, Arcos R. Active control of aircraft fly-over sound transmission through an open window. Appl Acoust 2014;84:116–21. doi:10.1016/j.apacoust.2014.02.018.

[51] Lau SK, Tang SK. Sound fields in a rectangular enclosure under active sound transmission control. J Acoust Soc Am 2001;110:925–38. doi:10.1121/1.1387095.

[52] Tang SK. Reduction of sound transmission across plenum windows by incorporating an array of rigid cylinders. J Sound Vib 2018;415:25–40. doi:10.1016/j.jsv.2017.11.027.

[53] Huang X, Zou H, Qiu X. A preliminary study on the performance of indoor active noise barriers based on 2D simulations. Build Environ 2015;94:891–9. doi:10.1016/j.buildenv.2015.06.034.

[54] Lam B, Shi C, Shi D, Gan WS. Active control of sound through full-sized open windows. Build Environ 2018;141:16–27. doi:10.1016/j.buildenv.2018.05.042.

[55] Kanazawa L, Mizutani K. Reduction of construction machinery noise in multiple dominant frequencies using feedforward type active control. INTER-NOISE 2018 - 47th Int. Congr. Expo. Noise Control Eng., 2018.

[56] Thalheimer E. Construction noise control program and mitigation strategy at the Central Artery/Tunnel Project. Noise Control Eng J 2000;48:157–65. doi:10.3397/1.2827963.

[57] Sutton TJ, Elliott SJ, McDonald AM, Saunders TJ. Active control of road noise inside vehicles. Noise Control Eng J 1994;42:137–47. doi:10.3397/1.2828351.

[58] Jung W, Elliott SJ, Cheer J. Local active control of road noise inside a vehicle. Mech

Syst Signal Process 2019;121:144–57. doi:10.1016/J.YMSSP.2018.11.003.

[59] Samarasinghe PN, Zhang W, Abhayapala TD. Recent Advances in Active Noise Control Inside Automobile Cabins: Toward quieter cars. IEEE Signal Process Mag 2016;33:61–73. doi:10.1109/MSP.2016.2601942.

[60] Chen H, Samarasinghe P, Abhayapala TD, Zhang W. Spatial noise cancellation inside cars: Performance analysis and experimental results. 2015 IEEE Work Appl Signal Process to Audio Acoust WASPAA 2015 2015:2–6. doi:10.1109/WASPAA.2015.7336947.

[61] Berge TS. A Feasibility Study of Active Noise Cancellation of Low-Frequency Sound Inside Vehicle Cabs. J Acoust Soc Am 1983;73:699.

[62] Ohnishi H, Uesaka K, Ohnishi K, Nishimura M, Teranishi S. Development of the noise barrier using actively controlled acoustical soft edge - part 2: field test using a loud speaker and a high speed running truck. Proc 29th Int Congr Exhib Noise Control Eng 2000:3–8.

[63] Sohrabi S, Pàmies Gómez T, Romeu Garbí J. Suitability of Active Noise Barriers for Construction Sites. Appl Sci 2020;10:6160. doi:10.3390/app10186160.

[64] Jakob A, Michael M. Active control of double-glazing windows : an experimental comparison between feedback and feedforward controllers Active Control of Double-glazing Windows : an Experimental Comparison between Feedback and Feedforward Controllers 2017.

[65] Moreau D, Cazzolato B, Zander A, Petersen C. A review of virtual sensing algorithms for active noise control. Algorithms 2008;1:69–99. doi:10.3390/a1020069.

[66] Sohrabi S, Pamies T, Romeu J. Numerical study of an active noise barrier. INTER-NOISE 2017 - 46th Int. Congr. Expo. Noise Control Eng. Taming Noise Mov. Quiet, vol. 2017- Janua, 2017.

[67] Fan R, Su Z, Cheng L. Modeling, analysis, and validation of an active T-shaped noise barrier. J Acoust Soc Am 2013;134:1990–2003. doi:10.1121/1.4817887.

[68] Chen W, Rao W, Min H, Qiu X. An active noise barrier with unidirectional secondary sources. Appl Acoust 2011;72:969–74. doi:10.1016/j.apacoust.2011.06.006.

[69] Berkhoff AP. Control strategies for active noise barriers using near-field error sensing. J Acoust Soc Am 2005;118:1469–79. doi:10.1121/1.1992787.

[70] Wang S, Yu J, Qiu X, Pawelczyk M, Shaid A, Wang L. Active sound radiation control with secondary sources at the edge of the opening. Appl Acoust 2017;117:173–9. doi:10.1016/j.apacoust.2016.10.027.

[71] Omoto A, Fujiwara K. A study of an actively controlled noise barrier. J Acoust Soc Am 1993;94:2173–80. doi:10.1121/1.407488.

[72] Guo J, Pan J, Bao C. Actively created quiet zones by multiple control sources in free space. J Acoust Soc Am 1997;101:1492–501. doi:10.1121/1.420362.

[73] Guo J, Pan J. Application of active noise control to noise barriers. Acoust Aust 1997;25:11–6.

[74] Niu F, Zou H, Qiu X, Wu M. Error sensor location optimization for active soft edge noise barrier. J Sound Vib 2007;299:409–17. doi:10.1016/j.jsv.2006.08.005.

[75] Liu JC chun, Niu F. Study on the analogy feedback active soft edge noise barrier. Appl Acoust 2008;69:728–32. doi:10.1016/j.apacoust.2007.02.008.

[76] Han N, Qiu X. A study of sound intensity control for active noise barriers. Appl Acoust 2007;68:1297–306. doi:10.1016/j.apacoust.2006.07.002.

[77] Hart CR, Lau SK. Active noise control with linear control source and sensor arrays for a noise barrier. J Sound Vib 2012;331:15–26. doi:10.1016/j.jsv.2011.08.016.

[78] Wang X, Koba Y, Ishikawa S, Kijimoto S. Hybrid active noise barrier with sound masking in open-plan offices. Noise Control Eng J 2016;64:403–15. doi:10.3397/1/376389.

[79] Duhamel D, Sergent P, Hua C, Cintra D. Measurement of active control efficiency around noise barriers 1998;55.

[80] Nagamatsu H, Ise S, Shikano K. Optimum Arrangement of Secondary Sources and Error Sensors for Active Noise Barrier 2000;1:2–6.

[81] Wang X, Satake T, Koba Y, Ishikawa S, Kijimoto S. Active reduction of the two-way diffraction from a noise barrier by using feedforward control. Proc INTER-NOISE 2016 - 45th Int Congr Expo Noise Control Eng Towar a Quieter Futur 2016:576–86.

[82] Hu S, Chen SY, Zou HS, Li TN. Research on the application of active sound barriers

for the transformer noise abatement system n.d.;59:10–3.

[83] Chen W, Min H, Qiu X. Noise reduction mechanisms of active noise barriers. Noise Control Eng J 2013;61:120–6. doi:10.3397/1.3702011.

[84] Matsui T, Takagi K, Hiramatsu K, Yamamoto T. Outdoor sound propagation from a source having dimensions. J Acoust Soc Japan 1989. doi:10.20697/jasj.45.7_512.

[85] Embleton TFW. Tutorial on sound propagation outdoors. J Acoust Soc Am 1996. doi:https://doi.org/10.1121/1.415879.

[86] Attenborough K. Review of ground effects on outdoor sound propagation from continuous broadband sources. Appl Acoust 1988;24:289–319. doi:10.1016/0003-682X(88)90086-2.

[87] Romeu J, Palacios JI, Balastegui A, Pamies T. Optimization of the Active Control of Turboprop Cabin Noise. J Aircr 2015;52:1386–93. doi:10.2514/1.C032431.

[88] Palacios JI, Romeu J, Balastegui A. Two Step Optimization of Transducer Locations in Single Input Single Output Tonal Global Active Noise Control in Enclosures. J Vib Acoust 2010;132:061011. doi:10.1115/1.4002122.

[89] Elliott SJ, Nelson PA. The active control of sound. Electron Commun Eng J 2009;2:127. doi:10.1049/ecej:19900032.

[90] Shao J, Sha JZ, Zhang ZL. The method of the minimum sum of squared acoustic pressures in an actively controlled noise barrier. J Sound Vib 1997;204:381–5. doi:10.1006/jsvi.1997.0909.

[91] Elliott SJ, Cheer J, Bhan L, Shi C, Gan WS. A wavenumber approach to analysing the active control of plane waves with arrays of secondary sources. J Sound Vib 2018;419:405–19. doi:10.1016/j.jsv.2018.01.028.

[92] Guo J, Pan J. Increasing the insertion loss of noise barriers using an active-control system. J Acoust Soc Am 1998;104:3408–16. doi:10.1121/1.423924.

[93] Lee SC, Kim JH, Hong JY. Characterizing perceived aspects of adverse impact of noise on construction managers on construction sites. Build Environ 2019;152:17–27. doi:10.1016/j.buildenv.2019.02.005.

[94] Liu Y, Xia B, Cui C, Skitmore M. Community response to construction noise in three central cities of Zhejiang province, China. Environ Pollut 2017;230:1009–17. doi:10.1016/j.envpol.2017.07.058.

[95] Kwon N, Song K, Lee HS, Kim J, Park M. Construction Noise Risk Assessment Model Focusing on Construction Equipment. J Constr Eng Manag 2018;144:1–12. doi:10.1061/(ASCE)CO.1943-7862.0001480.

[96] Ballesteros MJ, Fernández MD, Quintana S, Ballesteros JA, González I. Noise emission evolution on construction sites. Measurement for controlling and assessing its impact on the people and on the environment. Build Environ 2010;45:711–7. doi:10.1016/j.buildenv.2009.08.011.

[97] Cheng KW, Law CW, Wong CL. Quiet construction: State-of-the-art methods and mitigation measures. INTERNOISE 2014 - 43rd Int. Congr. Noise Control Eng. Improv. World Through Noise Control, Melbourne: 2014, p. 1–10.

[98] Kwon N, Park M, Lee H-SS, Ahn J, Shin M. Construction Noise Management Using Active Noise Control Techniques. J Constr Eng Manag 2016;142:04016014. doi:10.1061/(asce)co.1943-7862.0001121.

[99] Ireland TI, Centre PB, Street P. Noise management during the construction of a light rail scheme through Dublin city centre. INTER-NOISE 2019, 2019.

[100] Wilson PM. Innovations that make infrastructure and construction noise control more effective. Proc. INTER-NOISE 2016 - 45th Int. Congr. Expo. Noise Control Eng., 2016.

[101] Lee HP, Tan L Bin, Lim KM. Assessment of the performance of sonic crystal noise barriers for the mitigation of construction noise. Proc INTER-NOISE 2016 - 45th Int Congr Expo Noise Control Eng 2016:4220–6.

[102] Monson BB, Sommerfeldt SD, Gee KL. Improving compactness for active noise control of a small axial cooling fan. Noise Control Eng J 2007;55:397–407. doi:10.3397/1.2762207.

[103] Martin V, Gronier C. Sensor configuration efficiency and robustness against spatial error in the primary field for active sound control. J Sound Vib 2001;246:679–704. doi:10.1006/jsvi.2001.3669.

[104] Sjösten P, Johansson S, Persson P, Claesson I. Considerations on Large Applications of Active Noise Control. Part II: Experimental Results. Acta Acust 2003;89:834–43.

[105] Ise S, Yano H, Tachiban H. Basic study on active noise barrier. J Acoust Soc Japan 1991;12:299–306.

[106] Marler RT, Arora JS. Survey of multi-objective optimization methods for engineering. Struct Multidiscip Optim 2004;26:369–95. doi:10.1007/s00158-003-0368-6.

[107] Duhamel D. Shape optimization of noise barriers using genetic algorithms. J Sound Vib 2006;297:432–43. doi:10.1016/j.jsv.2006.04.004.

[108] Baulac M, Defrance J, Jean P. Optimisation with genetic algorithm of the acoustic performance of T-shaped noise barriers with a reactive top surface. Appl Acoust 2006;69:332–42. doi:10.1016/j.apacoust.2006.11.002.

[109] Gounot YJR, Musafir RE. Genetic algorithms: A global search tool to find optimal equivalent source sets. J Sound Vib 2009;322:282–98. doi:10.1016/j.jsv.2008.11.001.

[110] Tao J, Wang S, Qiu X, Pan J. Performance of a multichannel active sound radiation control system near a reflecting surface. Appl Acoust 2017;123:1–8. doi:10.1016/j.apacoust.2017.02.020.

[111] Toledo R, Aznárez JJ, Maeso O, Greiner D. Optimization of thin noise barrier designs using Evolutionary Algorithms and a Dual BEM Formulation. J Sound Vib 2015;334:219–38. doi:10.1016/j.jsv.2014.08.032.

[112] Montazeri A, Poshtan J, Kahaei MH, A. Montazeri, J. Poshtan MHK. Optimal placement of loudspeakers and microphones in an enclosure using genetic algorithm. 2003 IEEE Conf., IEEE; 2003, p. 135–9. doi:10.1109/CCA.2003.1223278.

[113] Manolas DA, Borchers I, Tsahalis DT. Simultaneous optimization of the sensor and actuator positions for an active noise and/or vibration control system using genetic algorithms, applied in a Dornier aircraft. Eng Comput 2002;17:620–30. doi:10.1108/02644400010339806.

[114] Fabrizio Russo. Genetic Optimization in Nonlinear Systems for Active Noise Control: Accuracy and Performance Evaluation 2006:1512–7. doi:10.1109/imtc.2006.236682.

[115] Russo F, Sicuranza GL. Accuracy and performance evaluation in the genetic optimization of nonlinear systems for active noise control. IEEE Trans Instrum Meas 2007;56:1443–50. doi:10.1109/TIM.2007.899911.

[116] Shor NZ. Minimization methods for non-differentiable functions. vol. 3. Springer

Science & Business Media; 2012.

[117] Schwefel H-P. Numerical optimization of computer models. John Wiley & Sons, Inc.; 1981.

[118] Fogel DB. Evolutionary computation: toward a new philosophy of machine intelligence. vol. 1. John Wiley & Sons; 2006.

[119] Back T. Evolutionary algorithms in theory and practice: evolution strategies, evolutionary programming, genetic algorithms. Oxford university press; 1996.

[120] Bagavathi C, Saraniya O. Evolutionary Mapping Techniques for Systolic Computing System. Deep Learn. Parallel Comput. Environ. Bioeng. Syst., 2019. doi:10.1016/b978-0-12-816718-2.00020-8.

[121] Sivanandam SN, Deepa SN. Introduction to genetic algorithms. 2008. doi:10.1007/978-3-540-73190-0.

[122] Holland JH. Genetic Algorithms. Sci Am 1992;267:66–73.

[123] Tarabini M, Roure A, Pinhede C. Active control of noise on the source side of a partition to increase its sound isolation. J Sound Vib 2009;320:726–43. doi:10.1016/j.jsv.2008.09.004.

[124] Jakob A, Möser M. Active control of double-glazed windows. Part I: Feedforward control. Appl Acoust 2003;64:163–82. doi:10.1016/S0003-682X(02)00070-1.

[125] Jakob A, Möser M. Active control of double-glazed windows. Part II: Feedback control. Appl Acoust 2003;64:183–96. doi:10.1016/S0003-682X(02)00071-3.

[126] Tong YG, Tang SK. Acoustical Benefits of Plenum Window as Facade Device - A Parametric Study. MATEC Web Conf 2017;103. doi:10.1051/matecconf/201710303021.

[127] Tong YG, Tang SK, Kang J, Fung A, Yeung MKL. Full scale field study of sound transmission across plenum windows. Appl Acoust 2015;89:244–53. doi:10.1016/j.apacoust.2014.10.003.

[128] Tong YG, Tang SK. Plenum window insertion loss in the presence of a line source—A scale model study. J Acoust Soc Am 2013;133:1458–67. doi:10.1121/1.4788996.

[129] Moore JA, Lyon RH. Resonant porous material absorbers. J Acoust Soc Am 1982;72:1989–99. doi:10.1121/1.388630.

[130] García-Chocano VM, Cabrera S, Sánchez-Dehesa J. Broadband sound absorption by

lattices of microperforated cylindrical shells. Appl Phys Lett 2012;101. doi:10.1063/1.4764560.

[131] Fenech B, Keith GM, Jacobsen F. The use of microperforated plates to attenuate cavity resonances. J Acoust Soc Am 2006;120:1851–8. doi:10.1121/1.2258438.

[132] Huang H, Qiu X, Kang J. Active noise attenuation in ventilation windows. J Acoust Soc Am 2011;130:176–88. doi:10.1121/1.3596457.

[133] Kwon B, Park Y. Interior noise control with an active window system. Appl Acoust 2013;74:647–52. doi:10.1016/j.apacoust.2012.11.005.

[134] Wang S, Tao J, Qiu X. Controlling sound radiation through an opening with secondary loudspeakers along its boundaries. Sci Rep 2017;7:1–6. doi:10.1038/s41598-017-13546-2.

[135] Wang S, Tao J, Qiu X, Pan J. Mechanisms of active control of sound radiation from an opening with boundary installed secondary sources. J Acoust Soc Am 2018;143:3345–51. doi:10.1121/1.5040139.

[136] Wang K, Tao J, Qiu X. Boundary control of sound transmission into a cavity through its opening. J Sound Vib 2019;442:350–65. doi:10.1016/j.jsv.2018.11.006.

[137] Shi C, Murao T, Shi D, Lam B, Gan WS. Open loop active control of noise through open windows. Proc Meet Acoust 2016;29. doi:10.1121/2.0000461.

[138] Elliott S, Cheer J, Lam B, Shi C, Gan WS. Controlling incident sound fields with source arrays in free space and through apertures. 24th Int Congr Sound Vib ICSV 2017 2017:1–7.

[139] Lam B, Elliott S, Cheer J, Gan WS. Physical limits on the performance of active noise control through open windows. Appl Acoust 2018;137:9–17. doi:10.1016/j.apacoust.2018.02.024.

[140] Carme C, Schevin O, Romerowski C, Clavard J. Active noise control applied to open windows. Proc INTER-NOISE 2016 - 45th Int Congr Expo Noise Control Eng 2016:3058–64.

[141] Carme C, Schevin O, Romerowski C, Clavard J. Active opening windows. ICSV 2016 - 23rd Int. Congr. Sound Vib. From Anc. to Mod. Acoust., 2016.

[142] Murao T, Nishimura M, He J, Lam B, Ranjan R, Shi C, et al. Feasibility study on decentralized control system for active acoustic shielding. Proc INTER-NOISE 2016

- 45th Int Congr Expo Noise Control Eng 2016:462–71.

[143] Murao T, Shi C, Gan WS, Nishimura M. Mixed-error approach for multi-channel active noise control of open windows. Appl Acoust 2017;127:305–15. doi:10.1016/j.apacoust.2017.06.024.

[144] Hansen CN. Understanding active noise cancellation. CRC Press; 2002.

[145] Lam B, Shi C, Gan WS. Active noise control systems for open windows: Current updates and future perspectives. 24th Int Congr Sound Vib ICSV 2017 2017.

[146] Thomasson SI. Diffraction by a screen above an impedance boundary. J Acoust Soc Am 1978;63:1768–81. doi:10.1121/1.381905.

[147] Svensson UP. Edge diffraction toolbox. https://github.com/upsvensson/Edge-diffraction-Matlab-toolbox 2020.

[148] Martin SR, Svensson UP, Slechta J, Smith JO. A hybrid method combining the edge source integral equation and the boundary element method for scattering problems. Proc Meet Acoust 2016;26. doi:10.1121/2.0000226.

[149] Rakhmanov EA, Saff EB, Zhou YM. Minimal Discrete Energy on the Sphere. Math Res Lett 1994;1:647–62. doi:10.4310/mrl.1994.v1.n6.a3.

[150] Poletti MA, Svensson UP. Beamforming synthesis of binaural responses from computer simulations of acoustic spaces. J Acoust Soc Am 2008;124:301–15. doi:10.1121/1.2924206.

[151] Lam B, Shi D, Belyi V, Wen S, Gan WS, Li K, et al. Active control of low-frequency noise through a single top-hung window in a full-sized room. Appl Sci 2020;10. doi:10.3390/app10196817.

[152] Murao T, Nishimura M, Gan WS. A hybrid approach to active and passive noise control for open windows. Appl Acoust 2019;155:338–45. doi:10.1016/j.apacoust.2019.05.028.

[153] MURAO T, NISHIMURA M. Basic Study on Active Acoustic Shielding. J Environ Eng 2012;7:76–91. doi:10.1299/jee.7.76.

[154] Wang S, Tao J, Qiu X. Performance of a planar virtual sound barrier at the baffled opening of a rectangular cavity. J Acoust Soc Am 2015;138:2836–47. doi:10.1121/1.4934267.

[155] Wang S, Tao J, Qiu X, Pan J. A boundary error sensing arrangement for virtual

sound barriers to reduce noise radiation through openings. J Acoust Soc Am 2019;145:3695–702. doi:10.1121/1.5112502.

[156] Zhang C, Qin M, Zou H, Qiu X. Secondary source and error sensing strategies for the active control of sound transmission through a small opening. J Sound Vib 2020;464:114973. doi:10.1016/j.jsv.2019.114973.